C149-738

[redacted] John O. Windham
MAIL STOP 123

ENGINEERING DEPARTMENT

TECHNICAL NOTE

TN-AE-65-97

GPO PRICE $ ______

CFSTI PRICE(S) $ ______

Hard copy (HC) 3.00

Microfiche (MF) .75

ff 653 July 65

STATIC STABILITY AND AXIAL FORCE CHARACTERISTICS OF A 1.32% SCALE MODEL OF THE SATURN IB/APOLLO, ITS COMPONENTS, AND THE SATURN IB/APOLLO/MINUTEMAN LAUNCH VEHICLE, DETERMINED BY WIND TUNNEL TEST

SPACE DIVISION CHRYSLER CORPORATION

SPACE DIVISION CHRYSLER CORPORATION

TECHNICAL NOTE TN-AE-65-97

STATIC STABILITY AND AXIAL FORCE CHARACTERISTICS OF A 1.32% SCALE MODEL OF THE SATURN IB/APOLLO, ITS COMPONENTS, AND THE SATURN IB/APOLLO/MINUTEMAN LAUNCH VEHICLE, DETERMINED BY WIND TUNNEL TEST

September 9, 1965

Prepared by: Frank Chianese
F. Chianese, Project Engineer
Aerodynamics Group

GB 20

Approved by: R H Ross
R. H. Ross, Manager
Aerospace Physics Section

Approved by: D N Buell
D. N. Buell, Chief Engineer
Advance Engineering Branch

CHRYSLER CORPORATION SPACE DIVISION
NEW ORLEANS, LOUISIANA

TABLE OF CONTENTS

LIST OF ILLUSTRATIONS

LIST OF ILLUSTRATIONS (CONT.)

LIST OF ILLUSTRATIONS (CONT.)

LIST OF ILLUSTRATIONS (CONT.)

Section 1

INTRODUCTION

1.1 Summary

A wind tunnel test was conducted at Ling-Temco-Vought, (LTV) High Speed Wind Tunnel during December 1964 to determine the static stability and axial force characteristics of a 1.32 percent scale model of the current Saturn IB/Apollo launch vehicle. This test and analysis was performed under NASA contract NAS8-4016, Part III-b, Task Assignment No. R-AERO-SAT-I/IB-1-65, Work Assignments Aero/AD-13 and Aero/AU-3. LTV has designated this test as HSWT 182. The basic data from this test can be obtained from reference 1.

Static stability and axial force characteristics are presented for the Saturn IB/Apollo and Saturn IB/Apollo/Minuteman configurations for Mach numbers of 0.7 to 4.75 and angles of attack of 0 to 15 degrees. Stability parameters of the Saturn IB/Apollo components (command module, service module, etc.) with, and without, protuberances are also presented. Data for components with protuberances are presented, where possible, at Mach numbers of 0.7 to 4.75. Protuberance-off component data is presented, where possible, for Mach numbers of 0.8 to 1.6.

Test data obtained show that the break between the S-IB and S-IVB stages has no effect on the complete model stability characteristics at Mach numbers of 0.7, 1.0, and 1.6 and angles of attack up to 15 degrees.

Test data was obtained at Reynolds numbers per foot of approximately 5 to 9 x 10^6 at Mach numbers of 0.8 to 1.6 for Saturn IB/Apollo without protuberances. Data for the total model and components forward of the S-IVB stage showed a change of 1 percent or less due to Reynolds number in stability parameters at angles of attack up to 15 degrees.

At Mach numbers of 2 and 3 the Reynolds number per foot was varied from 6.5 x 10^6 to 12.4 x 10^6 and 9.2 x 10^6 to 29 x 10^6 respectively for the Saturn IB/Apollo with fins and protuberances. An evaluation of data at $\alpha = 13°$ indicated a 2 percent to 3 percent increase of total model normal force but a 6 percent to 16 percent decrease of upper stage (forward of S-IB stage) normal force for the Reynolds number increase shown above.

1.2 Nomenclature

All moments are referenced to vehicle station 100 (engine gimbal station) as shown in figure 1.

α	Angle of attack, degrees
A_b	Model S-IB stage base area including base area of engine skirts, 10.97 sq. in.

AC_{1-4}	Cross-sectional area of each of the Saturn IB/Apollo components forward of the S-IB stage. Subscript refers to component: 1. S-IVB stage, 2. LEM adaptor, 3. S/M, and 4. C/M.
C/M	Command module
C_{ℓ}	Rolling moment coefficient, rolling moment/qSD
C_m	Pitching moment coefficient, pitching moment/qSD
C_n	Yawing moment coefficient, yawing moment/qSD
CX_B	Base axial force coefficient, $(P_\infty - P_b)A_b/qS$
CX_f	Forebody axial force coefficient, $CX_T - CX_B$
CX_T	Total axial force coefficient, total axial force/qS
C_Y	Side force coefficient, side force/qS
C_Z	Normal force coefficient, normal force/qS
$\Delta C_{Z,m}$	Change in normal force or pitching moment coefficients
D	Reference diameter, 3.3924 inches, model scale
LEM	Lunar excursion module adaptor
LTV	Ling-Temco-Vought, Inc.
LRC	Langley Research Center
M	Mach Number
P	Pressure, psi or psf
q	Dynamic pressure ($\frac{\gamma}{2}$ PM2), psi or psf
R_N	Reynolds number VD/ν
RCS	Reaction control system
S	Reference area, 9.03865 sq. in.
S/M	Service module
TED	Turbine exhaust ducts
V	Freestream velocity
ψ	Angle of yaw, degrees

γ	Ratio of specific heats (1.4 for air)
σ	Standard deviation
ν	Kinematic viscosity of air

Subscripts

∞	Freestream or undisturbed wind tunnel test section conditions
b	Base conditions
S	Static conditions

Section 2

DISCUSSION

2.1 Description of Test Model and Instrumentation

Data presented in this report were obtained from a 1.32 percent dimensionally scaled model of the Saturn IB/Apollo launch vehicle, with and without Minuteman strap-ons, which was instrumented to measure forces, moments, and base pressures. Pertinent details of this model are shown in figures 2 and 3 and are completely defined by reference 2. The model was designed to measure simultaneously the loads on the complete model and all or part of the major model components from the C/M through the S-IVB stage, i.e., C/M with LES, C/M with LES + S/M, etc. Each upper stage configuration is denoted by a "break point" and a number as shown in figure 2. For example: break point 4 designates the model gapped between the C/M and S/M with C/M loads being measured by the forward balance. Two six component strain gauge balances supplied by LTV were used to measure all force and moment data, except base axial forces. The six components measured by the balances are normal force, pitching moment, side force, yawing moment, rolling moment and total axial force. Loads on the complete model were measured by LTV balance VB-17. The various upper stage configuration forces and moments were measured by LTV balance VB-11B. Pressures were sampled at two locations in the model base and at various locations inside the upper stages of the model. In the base region pressures were sampled on the top and bottom of the model sting about one inch forward of the base, with the pressure tubing facing forward along the longitudinal axis. Inside the model, the upper stage pressures were sampled at two locations, one near the break point being tested, and the other several inches away. All pressures were measured by a scanivalve unit mounted in a cavity at the rear of the model cart. Electrical wiring for the VB-11B balance and nylon pressure tubing jumped the VB-17 balance inside the base of the model. Several checks were made throughout the test to insure that the wiring and tubing were not inducing an erroneous load or hysteresis effect on the VB-17 balance.

All fins and protuberances were removable to permit desired configuration changes.

To determine the effects of gapped tanks, a solid S-IB stage tank section was simulated by filling in between the scaled 70-inch diameter tanks with red wax and forming the wax with a template of a previous ungapped model tank section (references 4 and 5).

2.2 Data Reduction

All test data were recorded on magnetic tape during a test run, after which the tape was played back and the raw data punched out on IBM cards. These data cards were then put into a computer program which converted the raw data to useable aerodynamic coefficients as defined in the nomenclature. Balance calibrations performed prior to testing were used in this operation. The model - balance deflection calibration information obtained prior to the test was used to correct the indicated angle of attack to the true model angle of attack.

2.3 Data Accuracy

Overall accuracy of the data is difficult to define because certain factors affecting the accuracy cannot be determined. A general indication of the data accuracy can be obtained from the Mach number and force balance accuracies. Tests made to determine the Mach number accuracy (reference 3) indicated the Mach number is known with $\pm\frac{1}{2}$ percent of the stated value. Accuracy of the force balance was established from the calibration performed prior to the test. Uncertainty of the measurement of each component from both balances is summarized in the following table. These uncertainties are expressed as coefficients based on a dynamic pressure of 11.6 psi and represent a 2σ (95.5 percent) probability of occurrence.

Balance	CZ	C_m	C_y	C_n	C_ℓ	CX
VB-17	±0.20	±0.20	±0.12	±.012	±.012	±.008
VB-11B	±.002	±.002	±.008	±.011	±.008	±.022

The following table presents specific values of dynamic pressure for each test Mach number and Reynolds number.

Mach No.	Dynamic Pressure, psi	
	Max R_N	Min R_N
0.7	8.8	—
0.8	9.8	5.8
0.84	10.0	—
0.9	10.6	6.8
0.94	11.0	—
1.0	11.1	7.5
1.05	11.9	—
1.1	12.9	—

Mach No.	Dynamic Pressure, psi	
	Max R_N	Min R_N
1.2	12.9	8.8
1.4	13.9	—
1.6	13.9	11.0
2.0	17.3	9.5
2.4	21.8	9.21
3.0	32.0	10.4
3.4	22.4	—
4.0	—	10.6
4.8	—	10.5

All component loads except those for the S-IB stage were obtained from the VB-11B balance. The S-IB stage loads were obtained from data measured by the VB-17 and VB-11B balances.

2.4 Test Results

The basic data used in this report were obtained from reference 1. In general, all data were obtained with the model having gaps between the S-IB stage tanks. The exception is the run series where the gaps were filled in to simulate other test models. All data presented are for the high Reynolds number condition except as noted.

Data were obtained at Mach numbers of .70, .79, .84, .89, .94, .99, 1.04, 1.1, 1.2, 1.42, 1.61, 2.01, 2.41, 2.99, 3.39, 3.98, and 4.75 for the various configurations tested. Mach numbers at which specific configurations were tested varied to suit the particular requirements. Angle of attack was varied continuously from -4 to +16 degrees with data being sampled at a rate which yielded a minimum of two data points per degree of angle of attack.

2.4.1 Saturn IB/Apollo Static Stability

Static longitudinal stability derivatives and centers of pressure of the Saturn IB Apollo launch vehicle at zero angle of attack and Mach numbers of 0.7 to 4.75 are presented in figures 4 and 5. Also shown on these figures are data for a similar model obtained from other wind tunnel tests conducted at LTV and LRC (references 4 and 5). The models used in these other tests differed from the model used in this test as follows: LEM adapter angle of 8°37', wider auxiliary propulsion system units, and no gaps between the S-IB stage tanks. Reynolds numbers for the previous LTV test are the same as the present, however, the Langley data (Reference 5) was obtained at Reynolds numbers lower than the present test, or about 1.1 x 10^6. There is generally good agreement of all data from Mach number 0.7 to 2.0. Above Mach 2.0, however, the latest stability derivatives are lower than the previous data and the centers of pressure deviate from the previous data by as much as +.2 to -.5 calibers depending on Mach number.

At the beginning of the test a series of runs were made to evaluate the effect of the break between the S-IVB and S-IB stages on the total model stability characteristics at Mach numbers of 0.7, 1.0, and 1.6. As shown in figures 6 and 7 there is no change in normal force coefficients or pitching moment coefficients of the model when the model is broken between the S-IB and S-IVB stage, at Mach 1.6. This same conclusion was drawn after evaluating similar data comparisons at Mach numbers of 0.7 and 1.0.

A comparison of the static longitudinal stability derivatives and centers of pressure of the Saturn IB/Apollo launch vehicle with and without gaps between the S-IB stage tanks is shown in figure 8. These data show there is no change in the stability derivatives or C.P. location by changing the simulation of the S-IB stage tank section. For purposes of simplification the S-IB stage tank section with gaps is referred to as the "gapped tank" configuration and the S-IB stage tank section without gaps is referred to as the "solid tank" configuration. A comparison was made of normal force coefficient, pitching moment coefficient, and C.P. of the Saturn IB/Apollo launch vehicle solid and gapped tank at angles of attack of 6, 8, 10, and 16 degrees and Mach numbers of .8 to 4.75. These data, presented in figures 9 and 10, show the gapped tank normal force coefficients to be greater than the solid tank data but that the pitching moment coefficients for the gapped tank model are generally less than solid tank data. The center of pressure is not affected appreciably up to a Mach number of 1.2. Above Mach 1.2, however, the C.P. of the gapped tank model moves aft of that of the solid tank model by as much as .2 calibers. In general the deviation of the gapped tank model data from the solid tank model data increases with angle of attack. The change in normal force coefficient and C.P. location of the gapped tank model is not as great as was estimated prior to the test, Figures 11 and 12 . Even though these increments are very close to the balance estimated accuracy levels, the data are believed indicative.

Static longitudinal stability derivatives and centers of pressure for the Saturn IB/Apollo with 8, 4, and 0 fins are compared in figures 13 and 14. The pitching moment derivatives show little or no change while the normal force derivative for both the 4 and 0 fin configuration are approximately 20% and 50% less than the 8 fin configuration in the transonic Mach number region (M = .8 to 1.2). Data for the 4 fin configuration were obtained at Mach numbers of 0.8 to 1.2. The 0 fin configuration normal force derivative has little change for Mach numbers of 0.8 to 3.4. Centers of pressure move forward about half a caliber when 4 fins are removed and about 2 calibers when all fins are removed when compared to the 8 fin configuration.

Static lateral and longitudinal stability derivatives and specific characteristics of the Saturn IB/Apollo model are compared in figures 13 and 15. Both the stability derivatives and the force and moment coefficients at Mach numbers of 0.8, 1.0, and 1.6 and angles of attack of -4 to +7 degrees indicate no difference between the lateral and longitudinal stability characteristics.

Data were obtained at Reynolds numbers lower than the general test Reynolds number for several Saturn IB/Apollo configurations. For the Saturn IB/Apollo launch vehicle without protuberances, low Reynolds number data were obtained at Mach numbers of 0.8 to 1.6. Figures 16 and 17 present a comparison of normal force and pitching moment coefficient at M = 0.9 which is representative of the other Mach numbers. This comparison indicates a decrease of about 1% of the measured value at 15° angle of attack for the Reynolds number per foot change from 8.6×10^6 to 5.5×10^6. This change is negligible and may be neglected. A low Reynolds number test run was made for the Saturn IB/Apollo launch vehicle at Mach

numbers of 2.0, 2.4, and 3.0. These data indicate approximately a 3% decrease in measured normal force and pitching moment coefficients for changes in Reynolds number per foot from 6.5 - 12.4 x 10^6 and 9 - 29 x 10^6 at Mach numbers of 2.0 to 3.0 respectively.

2.4.2 Saturn IB/Apollo Component Static Stability

Evaluation of data with and without the break between the S-IB and S-IVB stages indicated there was no effect on the stability characteristics of the Saturn IB/Apollo launch vehicle at Mach numbers of 0.7 to 1.6. It was concluded from this evaluation that this break would not effect the measurement of the upper stage component data.

Data were obtained at Reynolds numbers per foot of approximately 5.5 x 10^6 to 8.6 x 10^6 for the upper stage configuration which includes the components from the C/M with LES through the LEM adaptor without protuberances at Mach numbers from 0.8 to 1.6. The variation of normal force and pitching moment coefficients with angle of attack for this configuration at M = 0.9 and for both Reynolds number cases are shown in figures 18 and 19. There is essentially no change in the stability characteristics for the Reynolds number change tested. The results presented for M = 0.9 are similar for the other Mach numbers investigated.

Static lateral and longitudinal stability parameters of the upper stages forward of the S-IB stage are compared at Mach numbers of 0.8, 1.0, and 1.6 and angles of attack from -4 to +7 degrees in figure 20. These data indicate there are no differences between the lateral and longitudinal stability characteristics.

Normal force coefficients and pitching moment coefficients of the Saturn IB/Apollo components are presented for protuberances on (figures 21 through 32) and protuberances off (figures 33 through 40). Components included in the protuberance on plots are the C/M, C/M with LES, S/M, LEM adaptor, S-IVB stage, and S-IB stage with fins. Plots for the protuberance off components include the S/M, LEM adaptor, S-IVB stage and S-IB stage with fins. All component loads data except for the C/M were obtained by subtracting data from a particular "break point" from the data obtained for the next lower numbered break point at the same condition (**M**, α , etc.). For example, the LEM adaptor data were obtained by subtracting data for break point 3 from break point 2 data. C/M data were measured directly by the VB-11B balance.

Data for all angles of attack at Mach 3 for a number of configurations were not available, either because of model fouling or balance overload. On figure 40, data for some of the angles of attack at Mach 1.04 and 1.2 were eliminated because the trends of these data were significantly different from data at adjacent Mach numbers and therefore were considered erroneous.

A comparison of component loads with and without protuberances (figures 25 through 40) and the C/M with and without the LES (figures 21 through 24)

was made for Mach numbers from 0.8 to 1.2. Addition of the LES to the C/M increases the stability derivatives by a factor of approximately 2.5. A part of this increased load is due to the LES but the LES loads cannot be determined from this test data. Data for the LES obtained from reference 6 indicates the LES would contribute about 15% of the C/M with LES stability derivatives. This increase in normal force and pitching moment coefficients is attributed to the large wake induced by the LES flare and tower. A 10% increase in normal force and pitching moment derivatives occurred on the LEM adaptor when the RCS motors were put on the S/M. These changes are considered to result from the wakes off the RCS motors.

The RCS motors had little effect on the normal force of the S/M (figure 25 and 33) with a ΔC_Z of about $\pm.004$, but had a greater effect on pitching moment ($\Delta C_m = \pm.09$) figures 26 and 34. Trends of the changes (magnitude and senses) were random at particular angles of attack throughout the Mach number range.

Removal of the protuberances on the S-IVB stage resulted in a reduction of normal force and pitching moment (figures 29, 30, 37, and 38). The change in normal force coefficient is about 0.05 to 0.08 and the pitching moment coefficient change is about 0.1 to 0.4 at $\alpha = 15$ degrees.

Protuberances had little effect on the stability characteristics of the S-IB stage with fins, (figures 31, 32, 39, and 40). Data obtained for the low Reynolds number cases at Mach 2, 2.4, and 3 showed a reduction in normal force and pitching moment coefficients. Evaluation of the data at 15° angle of attack indicated about a 15% reduction of the normal force and pitching moment. Most of this change occurred in the upper stage data but did not occur in the total model loads. The reason for this change in loads with a change in Reynolds number has not yet been determined.

The change in model normal force coefficient due to the addition of 8 fins and 4 TED's is presented in figure 41. Data were presented for 0, 2, 4, 6, 8, 10, 12, 14, and 15 degrees angle of attack and at Mach numbers from 0.7 to 3.4. These data were obtained by subtracting Saturn IB/Apollo without fins from the fin-on configuration. Due to the manner in which the fin normal force coefficient increment was determined it includes a load due to change in normal force on the engines skirts. The magnitude and sense of this change cannot be determined from these test data.

The change in vehicle pitching moment due to the addition of the fins and TED's are not presented. This change is very small and cannot be accurately determined.

2.4.3 Saturn IB/Apollo/Minuteman Static Longitudinal Stability

Static longitudinal stability derivatives and centers of pressure are presented for the Saturn IB/Apollo/Minuteman and the Saturn IB/Apollo in figures 42 and 43. The Minuteman increases the basic Saturn IB/Apollo derivatives 15% to 25% and moves the C.P. aft up to 0.5 calibers. The variations of normal force and pitching moment with angle of attack for the Saturn IB/Apollo and Saturn IB/Apollo/Minuteman at Mach numbers of 0.8 to 4.75 are shown in figures 44 and 45. In general the launch vehicle with the Minuteman becomes non-linear at lower angles of attack than the Saturn IB/Apollo and does not exhibit the same trends with angle of attack.

2.4.4 Axial Force

Axial force coefficients for the Saturn IB/Apollo launch vehicle at $\alpha = 0°$ are presented in figure 46. Included in this figure are the following:

1. total and base axial force coefficients obtained from HSWT 182 runs at constant Mach number for both the solid and gapped tank configuration

2. a HSWT 182 run in which the angle of attack was held constant at 0° and the Mach number varied from 0.7 to 1.15

3. total and base axial force coefficients from a previous LTV test, HSWT 135 (reference 4).

In all cases the total axial force was measured by a force balance and the base axial force was determined from pressures measured on the sting in the base region. Forebody axial force is considered to be the difference between the total and base axial force. The HSWT 182 data generally seems valid, however, both the base and total axial force coefficients between Mach 1.0 and 1.2 appear to be low in comparison to the adjacent data. Examination of the data indicated that the base axial force coefficient is actually lower than it should be (higher base pressure) and might result from the sting flare affecting the base pressure. The 10° half angle flare in the sting starts about 4 model base diameters aft of the base. Information presented in Reference 7 indicates the sting should be at least 5.2 base diameters long to minimize sting effects. There is generally good agreement between the HSWT 182 and HSWT 135 axial force coefficient data, the variation being no more than 2% of the HSWT 182 data.

Forebody axial force coefficients at α = 0 degrees for the total vehicle and components is presented for protuberances on in figure 47 and protuberances off in figure 48. Included in figure 47 are data for the total vehicle, C/M with and without the LES, S/M, LEM adaptor, S-IVB stage, and the S-IB stage with fins and turbine exhaust ducts. Figure 48 presents forebody axial forces for the total vehicle at two Reynolds numbers, S/M, LEM adaptor, S-IVB stage and S-IB stage with fins. All data for a given configuration have been shown on these plots. In figure 47, data for the total vehicle and S-IVB stage indicate poor repeatability at M = 1.61 and low values at M = 1.42 (no repeat runs). The cause of the problems noted for these Mach numbers could not be determined. Axial force of the fin could not be accurately determined and therefore is not presented. Removing protuberances from the S/M and S-IVB stage resulted in a reduction of forebody axial force on both components of 95% and 50% respectively of the protuberance on data, but increased the forebody axial force coefficient of the LEM adaptor approximately 20 percent. These C_{X_F} changes are within the estimated balance accuracy but are still considered as reasonable indications of the trends. The reduction in forebody axial force coefficient of the LEM adaptor when the protuberances are added may be the result of the wakes set up by the RCS on the S/M. This assumption concerning the forebody axial force coefficient reduction of the LEM is supported by the fact that the forebody axial force coefficient of the C/M is reduced significantly (greater than 50%) by adding the LES. Protuberances on the S-IB stage (antenna pannels and turbine exhaust ducts) have essentially no effect on forebody axial force coefficients. Forebody axial force coefficients were determined by subtracting the measured base axial force coefficients from the total axial force measured by the force balance. The forebody axial force coefficient of the total vehicle without protuberances is presented at two Reynolds number conditions. Axial force for the lower Reynolds number is generally greater than the high Reynolds number case. It could not be determined whether this change in forebody axial force coefficient was real because the change in forebody axial force coefficient is within the balance accuracy, and similar data for the complete upper stages were not obtained to either verify or disprove the total vehicle results.

Total, forebody, and base axial force coefficients for the Saturn IB/Apollo/Minuteman configurations are shown in figure 49. The base axial force at M = 1.1 is low, in comparison to the data at M = 1.0 and 1.2 and therefore was not used in fairing a curve through the data. The low base axial force could be the result of sting flare interference.

2.5 Conclusions

Analysis of the data from HSWT 182 presented in this report indicates the following:

1. The S-IB stage tank section configuration, i.e., with or without gaps between the tanks, has no effect on the stability derivatives at $\alpha = 0$ degrees. At angles of attack greater than 6 degrees the gapped tank model has slightly greater normal force and a more aft C.P.; however, these changes are no greater than the differences between test data obtained with a similar Saturn IB model in several test facilities.

2. Complete vehicle static lateral stability characteristics are the same as the static longitudinal stability characteristics for Mach numbers of 0.7 to 1.6 and angles of attack from -4 to +7 degrees. There is also no difference between static lateral and longitudinal stability characteristics of Saturn IB/Apollo upper stages at Mach numbers of 0.8 to 1.6.

3. Varying Reynolds number per foot from 5.5 to 8.5 x 10^6 has no effect on the normal force and pitching moment coefficients of the Saturn IB/Apollo upper stages.

4. Addition of the LES to the C/M results in a decrease in forebody axial force coefficient and an increase in the normal force and pitching moment derivatives of the C/M.

5. Addition of the RCS to the S/M causes a decrease in forebody axial force coefficient and an increase in normal force and pitching moment derivatives of the LEM adaptor.

6. Normal force and pitching moment coefficients of the S/M and S-IVB stage with protuberances were greater than the protuberance off configurations.

7. Protuberances on the S-IB stage have little or no effect on its normal force and pitching moment coefficients.

Section 3

REFERENCES

1. Felber, M.L., "A Force Test in the LTV High Speed Wind Tunnel to Determine the Stability and Axial Force Characteristics of a 1.32% Saturn IB Launch Vehicle Model in the Mach Number Range of 0.7 to 4.8 (U)", LTV Report No. HSWT 182, March 25, 1965.

2. Chrysler Corporation Space Division drawing numbers R-112-00A and 112-001 through 112-029.

3. Simon, E. H., "Mach Number Calibration Tests of the CVC High Speed Wind Tunnel", Ling-Temco-Vought, Inc. Report No. AER-EIR-13493, June 15, 1961.

4. Ziegler, C. E., "Static Stability Tests on a .0132 Scale Model of the Saturn IB/Apollo In the Mach Number Range of 0.6 to 4.8", Ling-Temco-Vought, Inc. Report Number HSWT 135, January 1964.

5. Johnson, J., "Static Longitudinal Stability and Axial Force Characteristics of the Saturn IB/Apollo Launch Vehicle as Determined from Tests of a 1.32 Percent Scale Model at Langley Research Center", NASA Memo No. R-AERO-AD-64-94, October 15, 1964.

6. "Set of Charts on Component and Interface Airloads for the Apollo C-1 Payload" transmitted to NASA George C. Marshall Space Flight Center by the North American Aviation Co. Letter No. 64MA 2748, February 25, 1964.

7. Pope, A., "Wind Tunnel Testing", John A. Wiley & Sons, 1954.

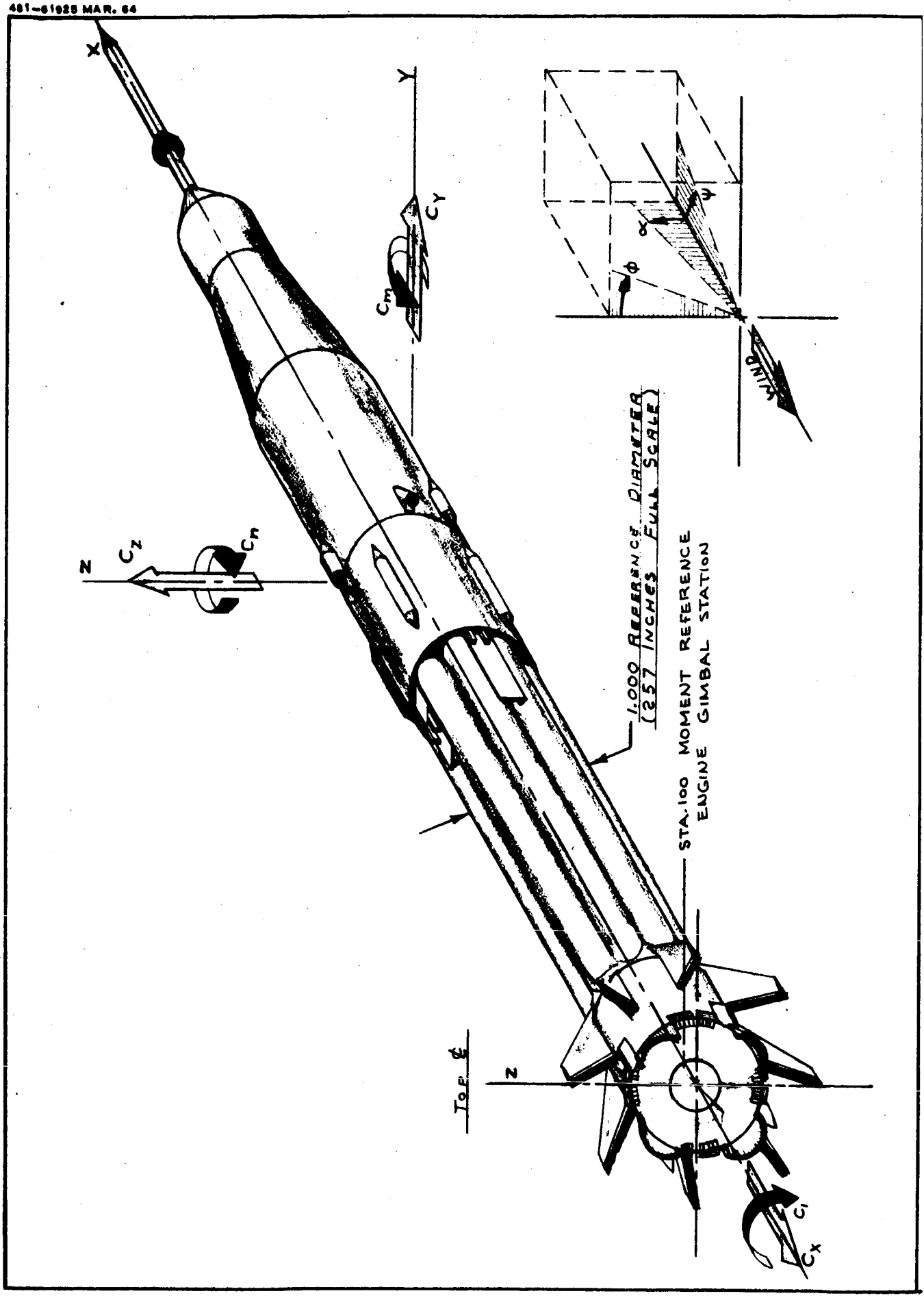

Figure 1 - SATURN IB AXIS SYSTEM

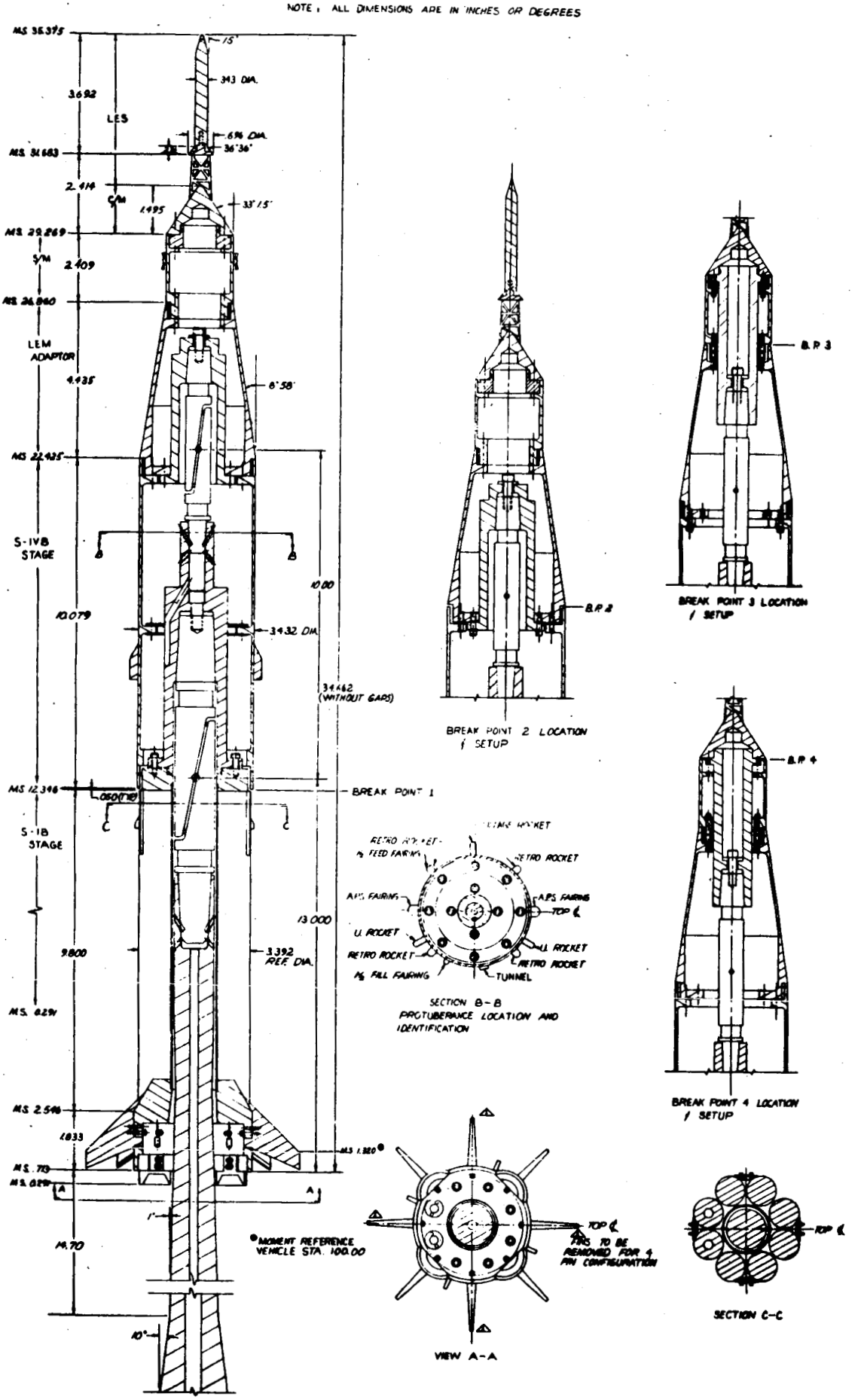

Figure 2 - SATURN IB/APOLLO MODEL DETAILS

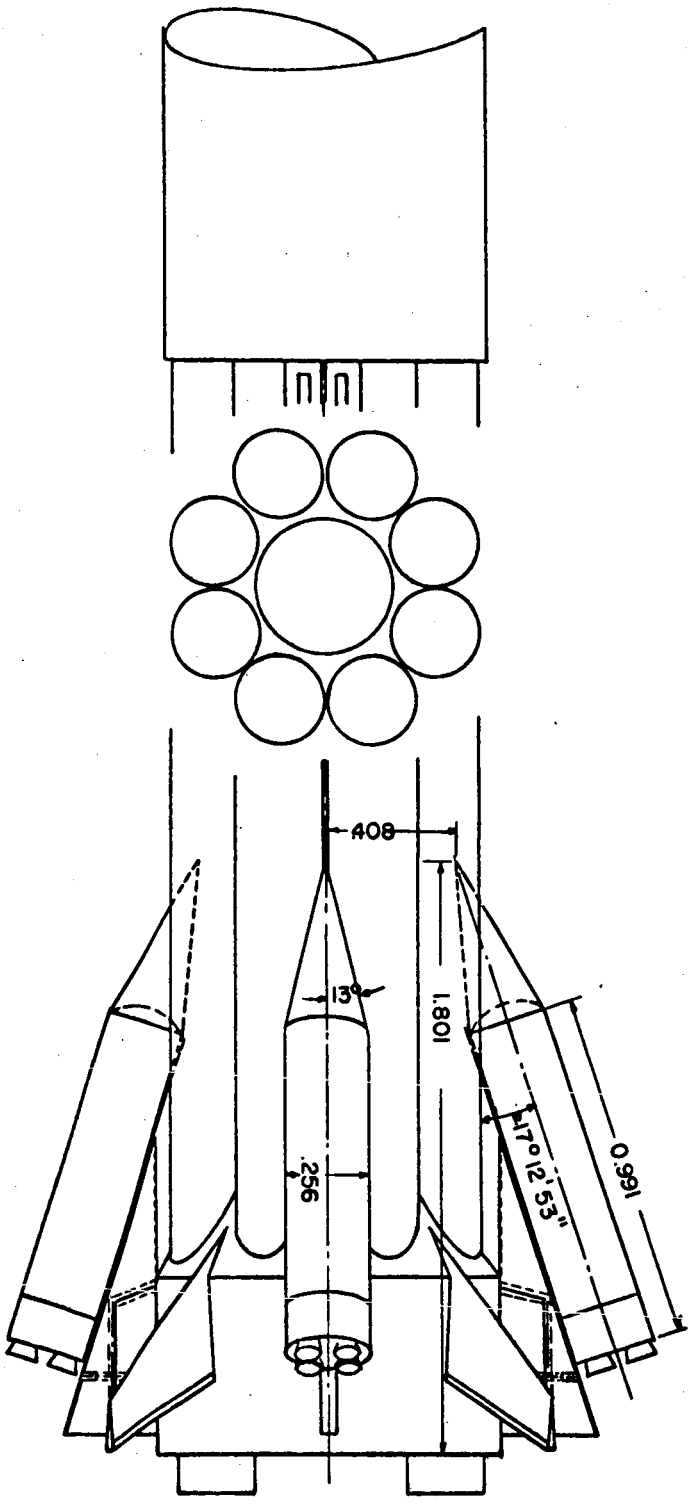

Figure 3 - MINUTEMAN DETAILS AND INSTALLATION

REVISED 5-25-65
2-4-65

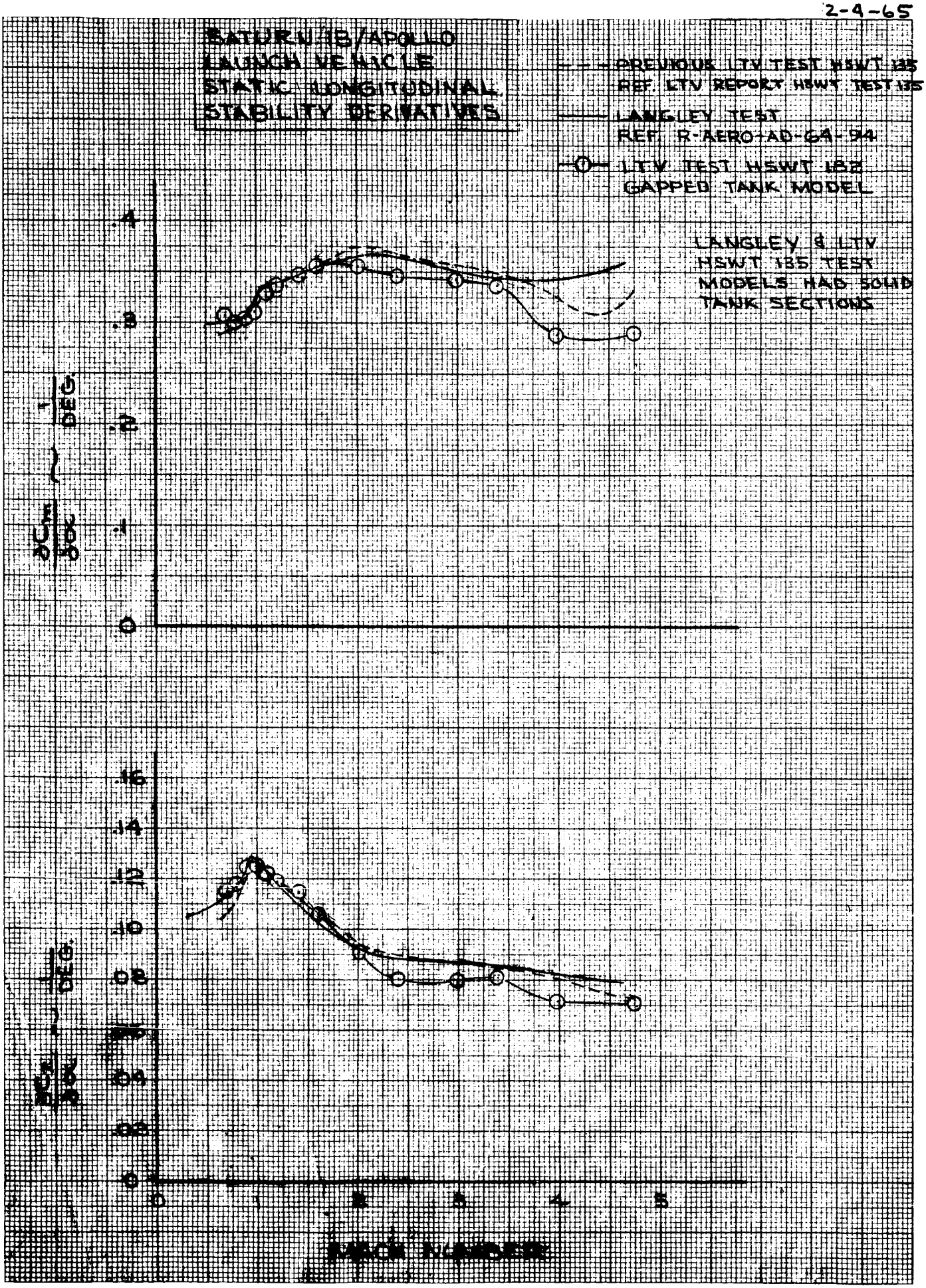

FIGURE 4

REVISED 5-25-65
2-4-65

SATURN IB/APOLLO LAUNCH VEHICLE CENTERS OF PRESSURE

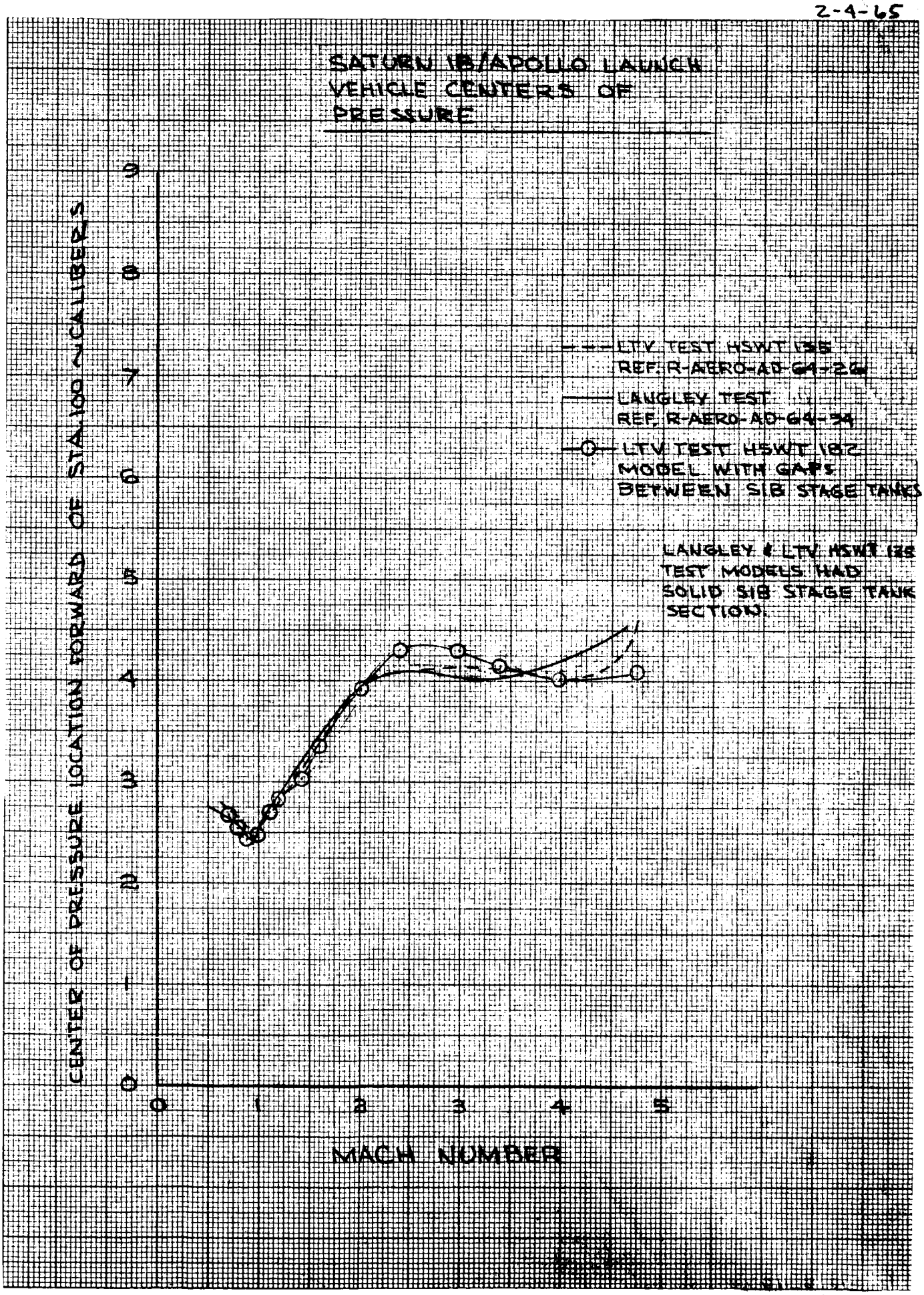

FIGURE 5

EFFECT OF THE GAP BETWEEN THE S-IB & S-IVB STAGES ON SATURN IB/APOLLO NORMAL FORCE COEFFICIENT AT M=1.6
NORMAL FORCE COEFFICIENT ~ C_N
2.8
2.4
2.0
1.6
1.2
.8
.4
0
-.4
-4
0
4
8
12
16
20
ANGLE OF ATTACK ~ DEGREES
O MODEL WITHOUT BREAK POINTS
Δ MODEL WITH BREAK BETWEEN S-IB & S-IVB STAGES

FIGURE 6

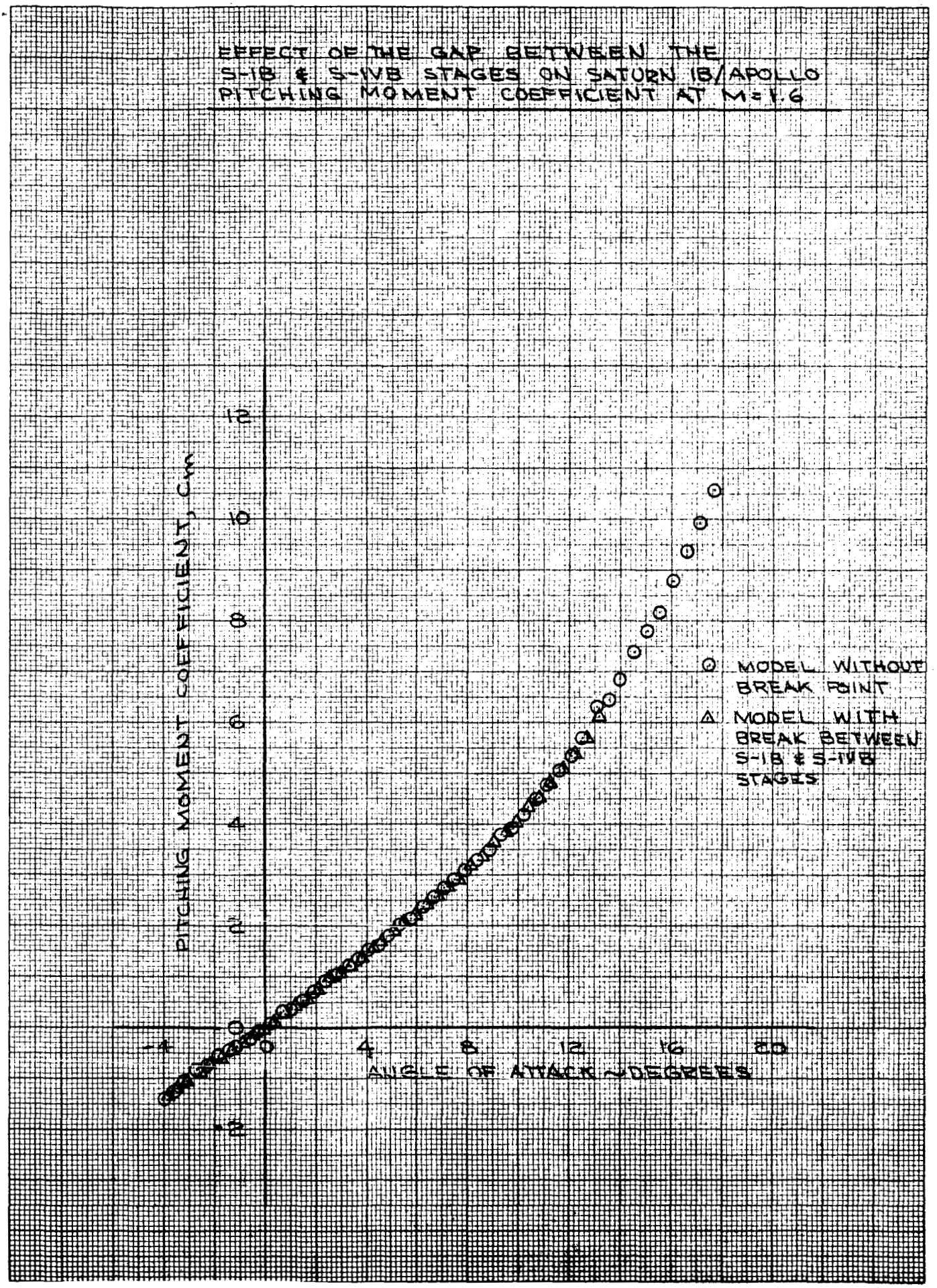
EFFECT OF THE GAP BETWEEN THE S-IB & S-IVB STAGES ON SATURN IB/APOLLO PITCHING MOMENT COEFFICIENT AT M = 1.6
PITCHING MOMENT COEFFICIENT, C_m
12
10
8
6
4
2
0
-2
-4
0
4
8
12
16
20
ANGLE OF ATTACK ~ DEGREES
MODEL WITHOUT BREAK POINT
MODEL WITH BREAK BETWEEN S-IB & S-IVB STAGES

FIGURE 7

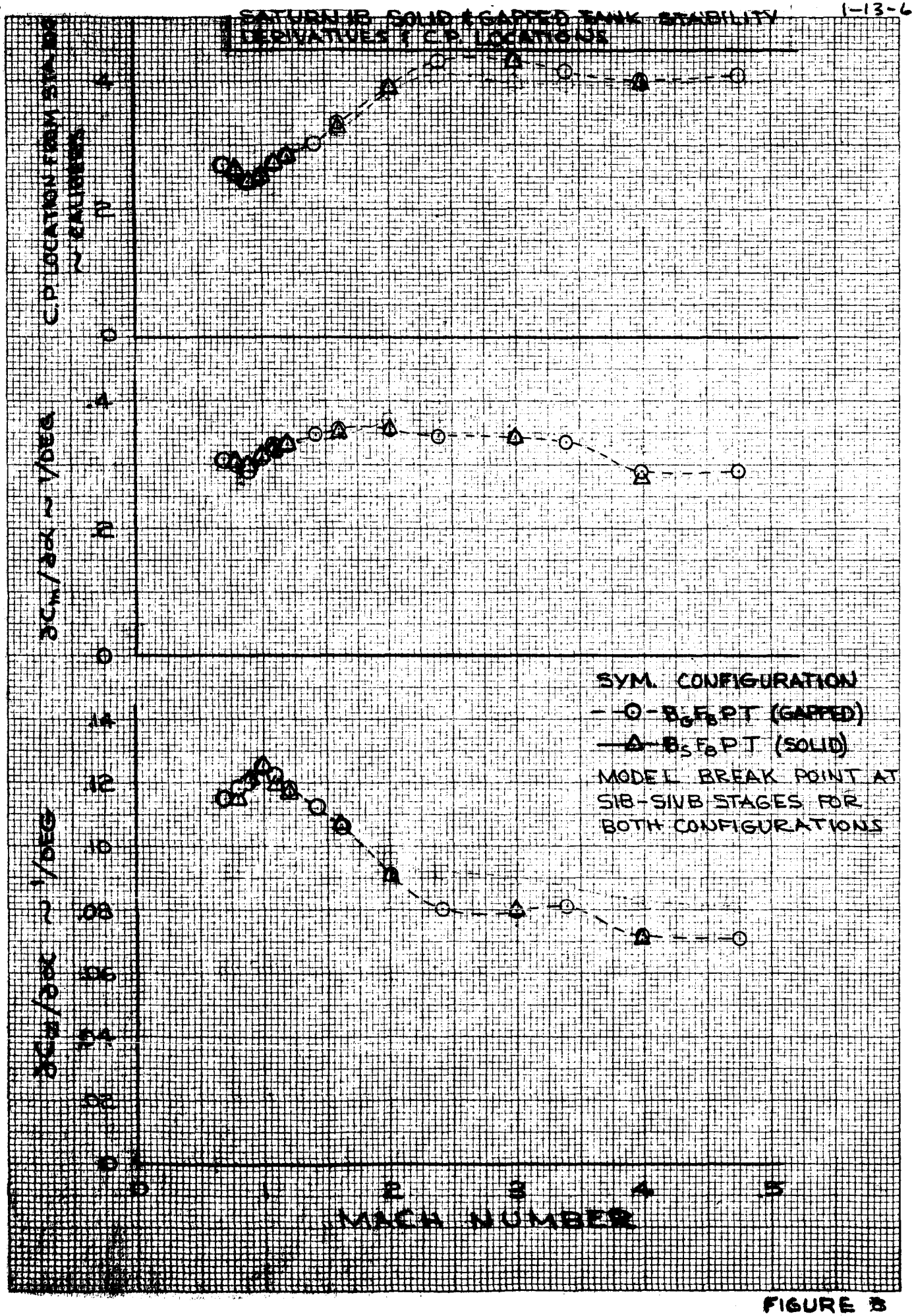
SATURN IB SOLID & GAPPED TANK STABILITY DERIVATIVES & C.P. LOCATIONS
C.P. LOCATION FROM STA 0.0 - INCHES
$\partial C_m/\partial \alpha$ - 1/DEG
$\partial C_N/\partial \alpha$ - 1/DEG
MACH NUMBER
SYM. CONFIGURATION
$B_G F_B$ PT (GAPPED)
$B_S F_B$ PT (SOLID)
MODEL BREAK POINT AT SIB-SIVB STAGES FOR BOTH CONFIGURATIONS

FIGURE 8

1-14-65

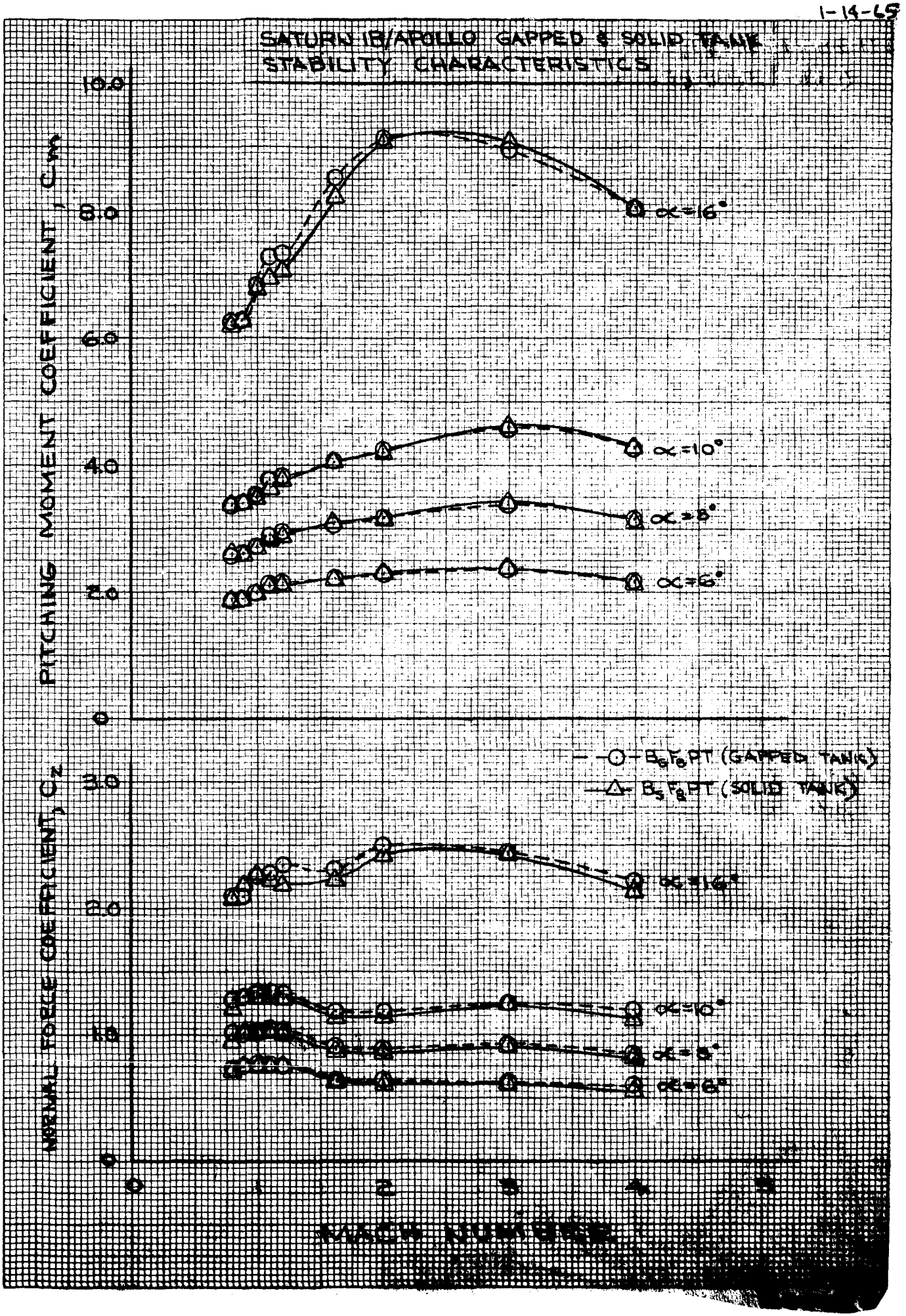
SATURN IB/APOLLO GAPPED & SOLID TANK STABILITY CHARACTERISTICS
PITCHING MOMENT COEFFICIENT, C_m
NORMAL FORCE COEFFICIENT, C_N
MACH NUMBER
B_6F_6 PT (GAPPED TANK)
B_5F_5 PT (SOLID TANK)
$\alpha = 16°$
$\alpha = 10°$
$\alpha = 5°$
$\alpha = 6°$
10.0
8.0
6.0
4.0
2.0
0
3.0
2.0
1.0
0
1
2
3
4

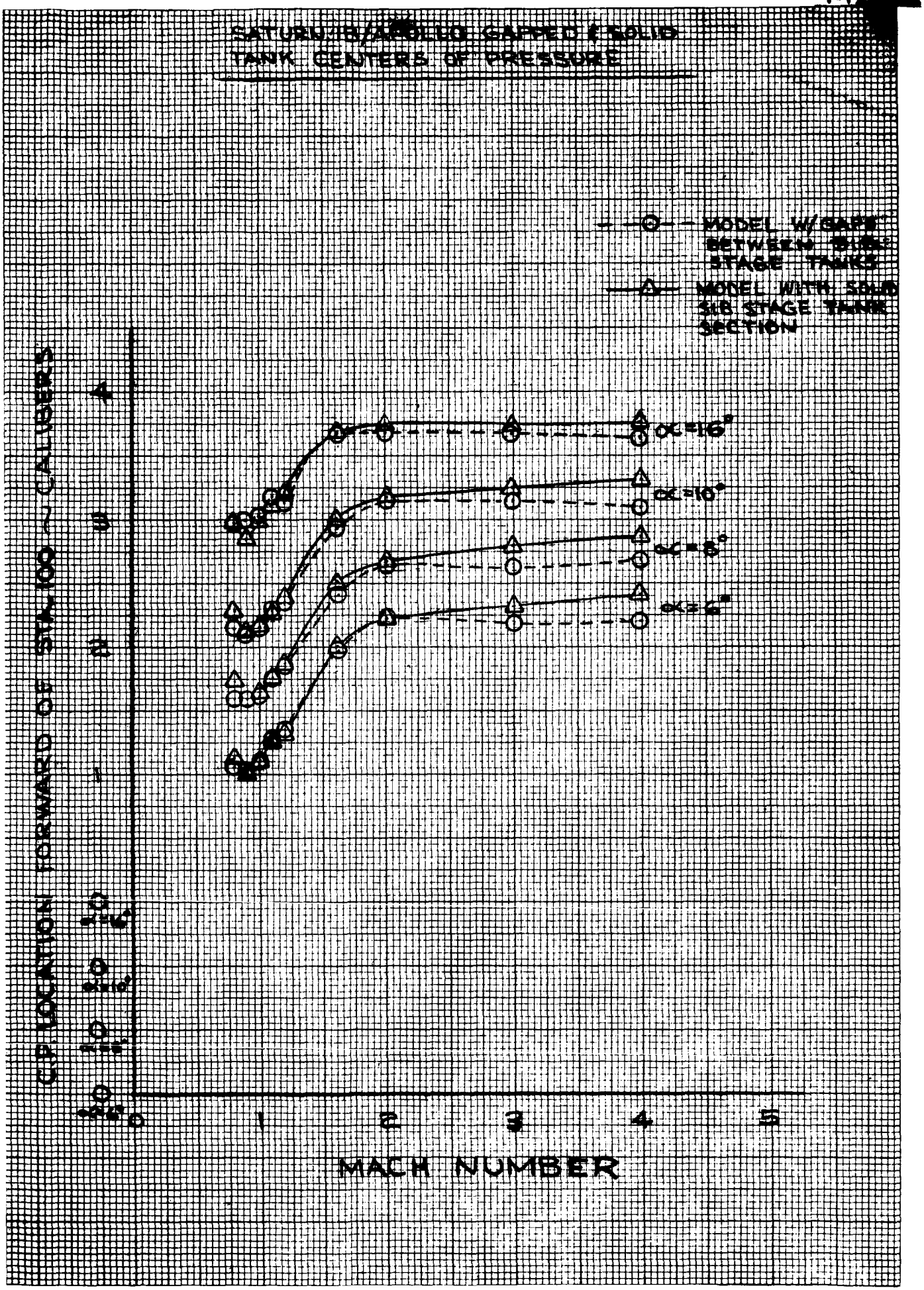
SATURN IB/AROLOX FUELED & SOLID TANK CENTERS OF PRESSURE
MODEL W/GAPS BETWEEN S-IB STAGE TANKS
MODEL WITH SOLID S-IB STAGE TANK SECTION
α=16°
α=10°
α=6°
α=2°
LOCATION FORWARD OF BASE (CALIBERS)
MACH NUMBER
0
1
2
3
4
5

FIGURE 10

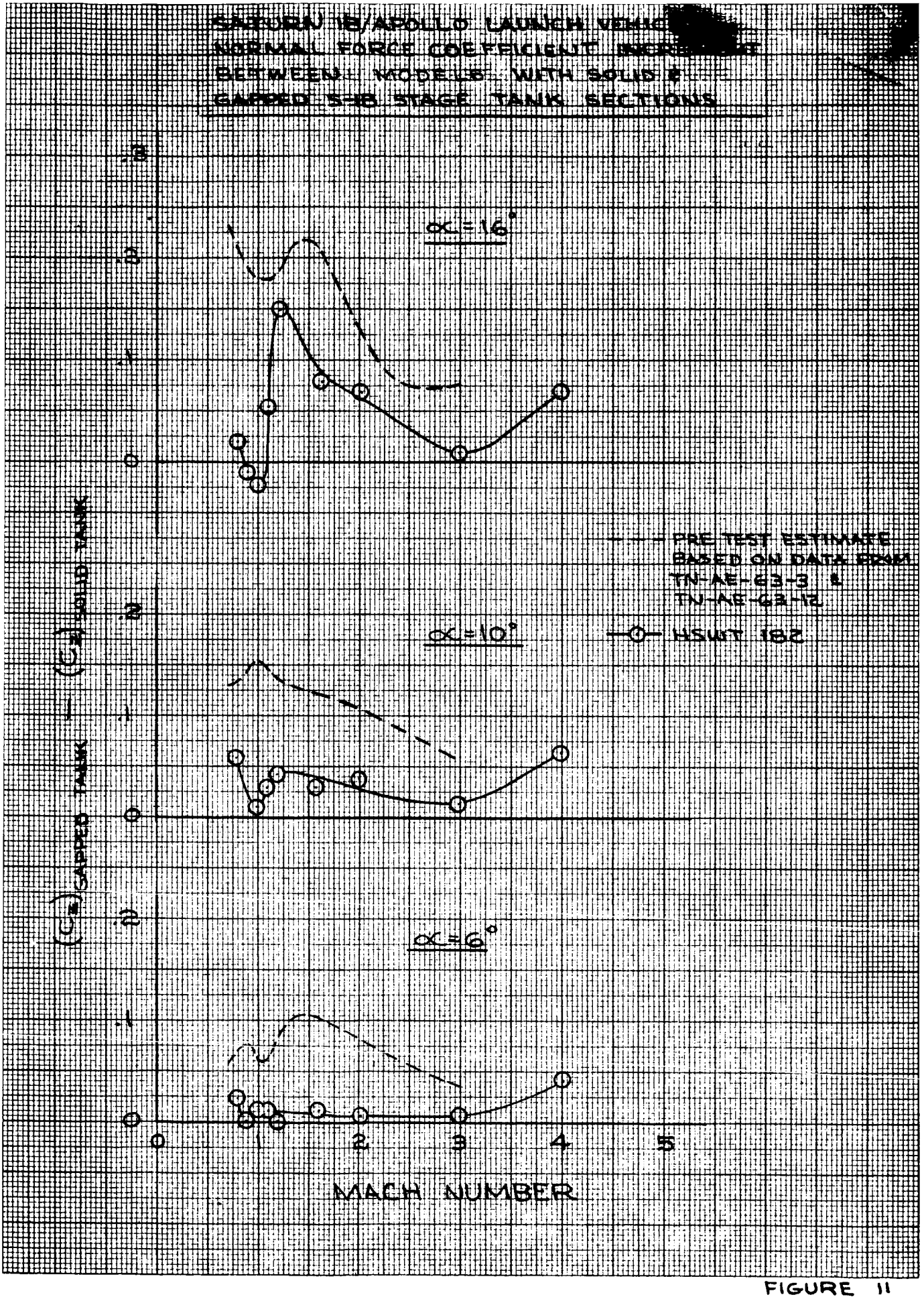
SATURN IB/APOLLO LAUNCH VEHICLE
NORMAL FORCE COEFFICIENT INCREMENT
BETWEEN MODELS WITH SOLID &
GAPPED S-IB STAGE TANK SECTIONS
α = 16°
α = 10°
α = 6°
PRE TEST ESTIMATE BASED ON DATA FROM TN-AE-63-3 & TN-AE-63-12
HSWT 182
$(C_N)_{SOLID\ TANK} - (C_N)_{GAPPED\ TANK}$
-.3
-.2
-.1
0
.1
.2
0
1
2
3
4
5
MACH NUMBER

FIGURE 11

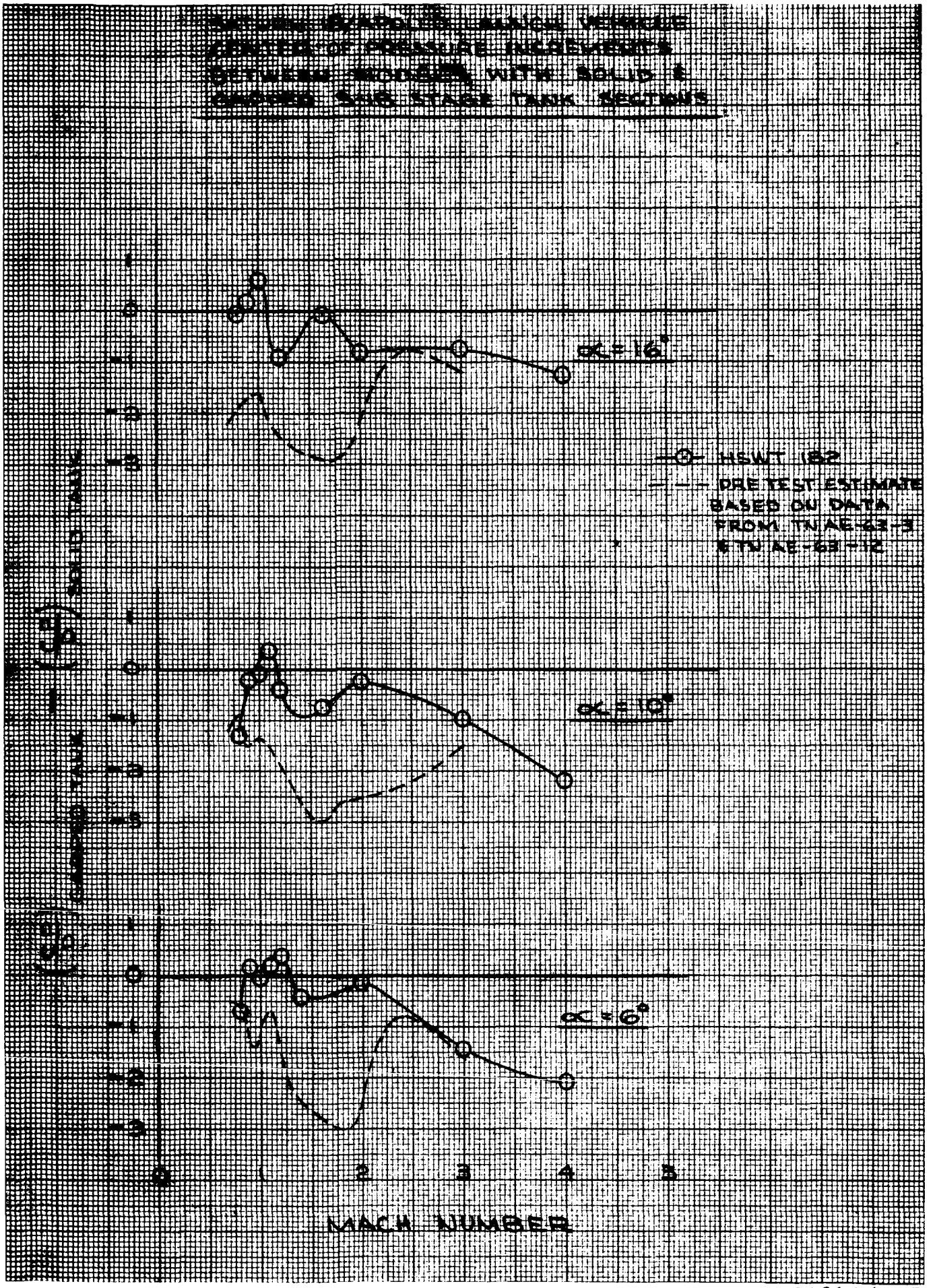
SATURN S-IVB/IB/V LAUNCH VEHICLE
CENTER OF PRESSURE INCREMENTS
BETWEEN MODELS WITH SOLID &
VENTED S-IVB STAGE TANK SECTIONS
α = 16°
α = 10°
α = 6°
HSWT 162
DRE TEST ESTIMATE
BASED ON DATA
FROM TN AE-63-3
& TN AE-63-12
MACH NUMBER

FIGURE 12

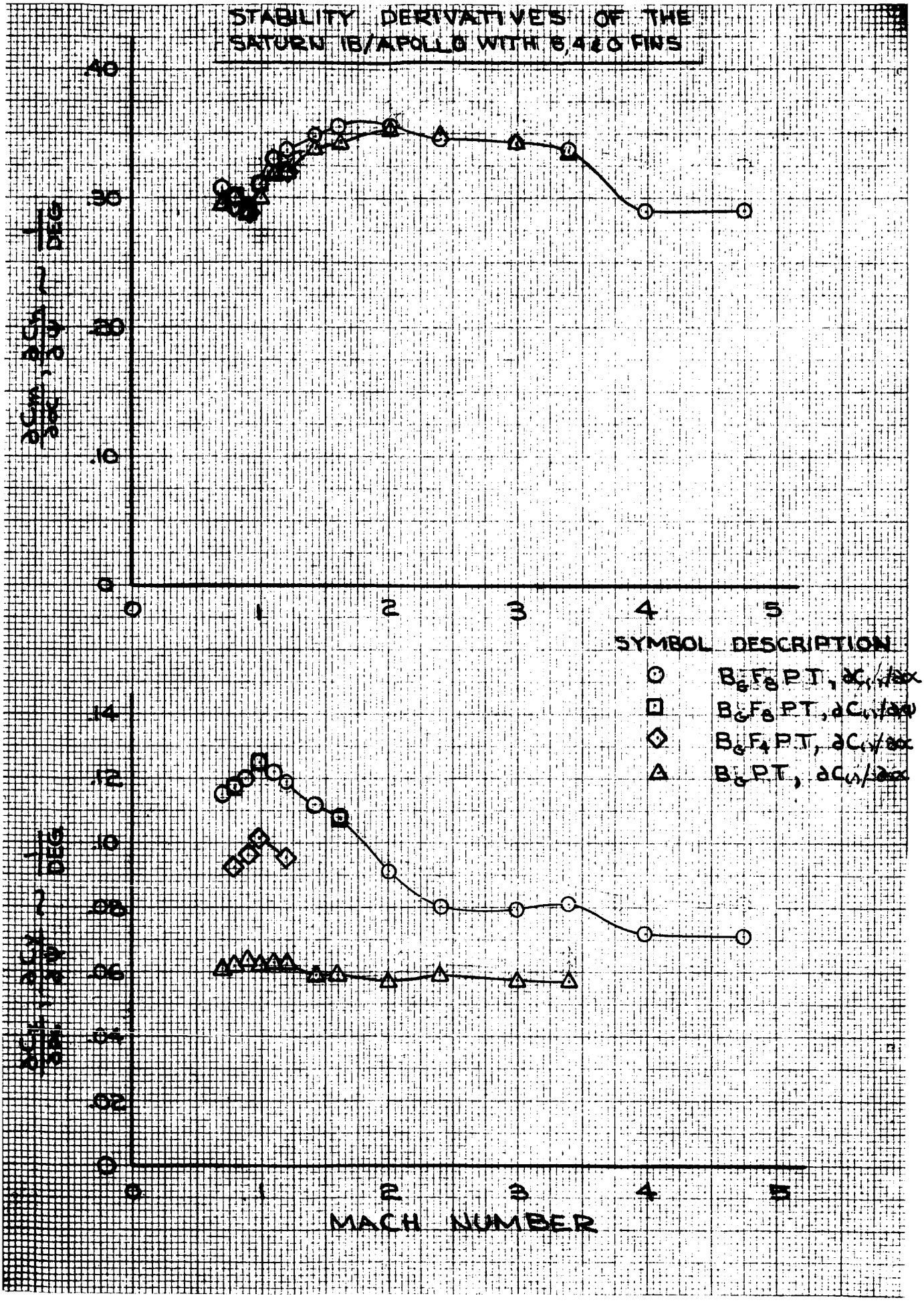
STABILITY DERIVATIVES OF THE SATURN IB/APOLLO WITH 5,4 & 0 FINS
40
30
20
10
0
0
1
2
3
4
5
SYMBOL DESCRIPTION
B_6F_8PT, $\partial C_{n_\alpha}/\partial\alpha$
B_6F_8PT, $\partial C_{n_\alpha}/\partial\alpha$
B_6F_4PT, $\partial C_{n_\alpha}/\partial\alpha$
B_6PT, $\partial C_{n_\alpha}/\partial\alpha$
.14
.12
.10
.08
.06
.04
.02
0
MACH NUMBER

FIGURE 13

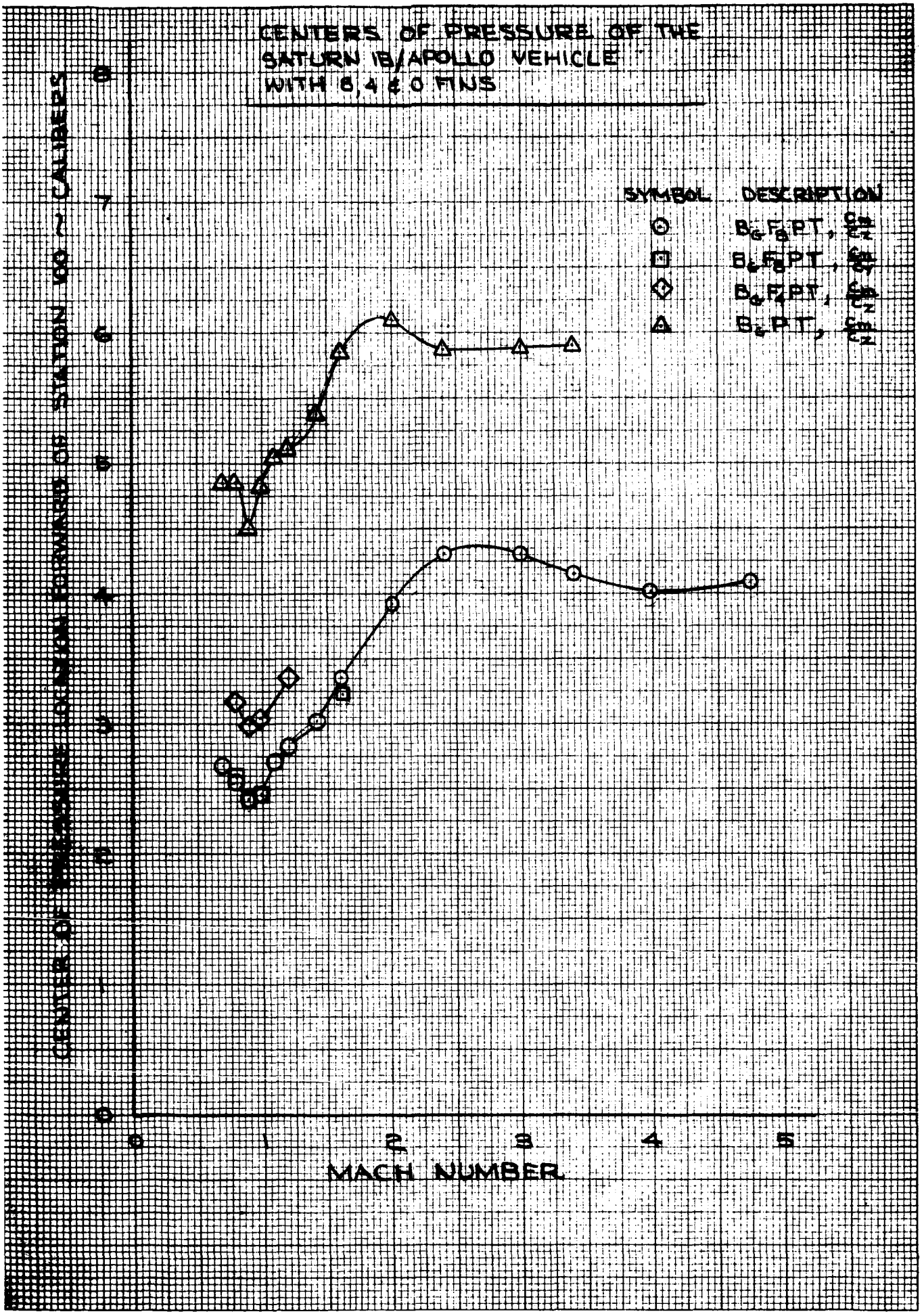
CENTERS OF PRESSURE OF THE SATURN IB/APOLLO VEHICLE WITH 8,4 & 0 FINS
SYMBOL
DESCRIPTION
B_6F_8PT, $\frac{C_m}{C_z}$
B_6F_8PT, $\frac{C_m}{C_y}$
B_6F_4PT, $\frac{C_m}{C_z}$
B_6PT, $\frac{C_m}{C_z}$
CENTER OF PRESSURE, CALIBERS FROM STATION 0.0 COMPUTED ABOVE BASE
0
1
2
3
4
5
6
7
8
MACH NUMBER

FIGURE 1A

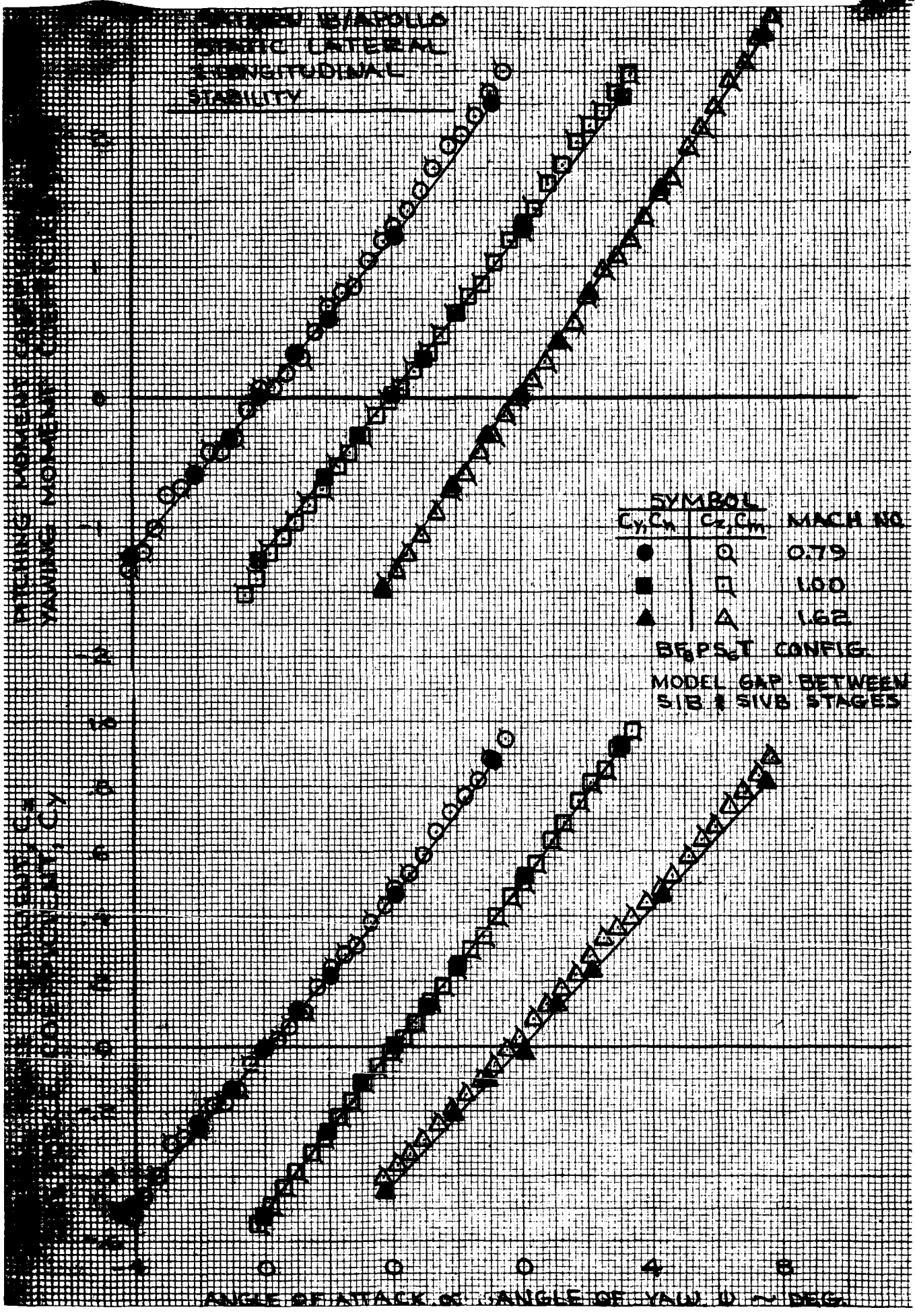
SATURN IB/APOLLO
STATIC LATERAL
& LONGITUDINAL
STABILITY
SYMBOL
C_{y_β} C_{n_β}
C_{z_α} C_{m_α}
MACH NO.
0.79
1.00
1.62
BF$_8$PS$_6$T CONFIG.
MODEL GAP BETWEEN
S1B & S1VB STAGES
C_{y_β}, C_{n_β}
C_{z_α}, C_{m_α}
ANGLE OF ATTACK α, ANGLE OF YAW ψ — DEG.

FIGURE 15

EFFECT OF REYNOLDS NUMBER ON NORMAL FORCE COEFFICIENTS OF THE SATURN IB LAUNCH VEHICLE AT 0.69 MACH NO.
PROTUBERANCES OFF
SYMBOL R_N/FT.
○ 5.47-5.54 x 10^6
△ 8.52-8.64 x 10^6
NORMAL FORCE COEFFICIENT, C_N
ANGLE OF ATTACK - DEGREES
2.4
2.0
1.6
1.2
.8
.4
-.4
-2
2
4
6
8
10
12
14
16
18

FIGURE 16

EFFECT OF REYNOLDS NUMBER
ON PITCHING MOMENT COEFFICIENTS
OF THE SATURN IB LAUNCH VEHICLE
AT 0.82 MACH NO
PROTUBERANCES OFF
SYMBOL
R_N/FT.
5.47 - 5.54 x 10^6
8.52 - 8.64 x 10^6
PITCHING MOMENT COEFFICIENT, C_m
ANGLE OF ATTACK, α, DEGREES
7
6
5
4
3
2
1
-1
-2
-4
2
4
6
8
10
12
14
16
18

FIGURE 17

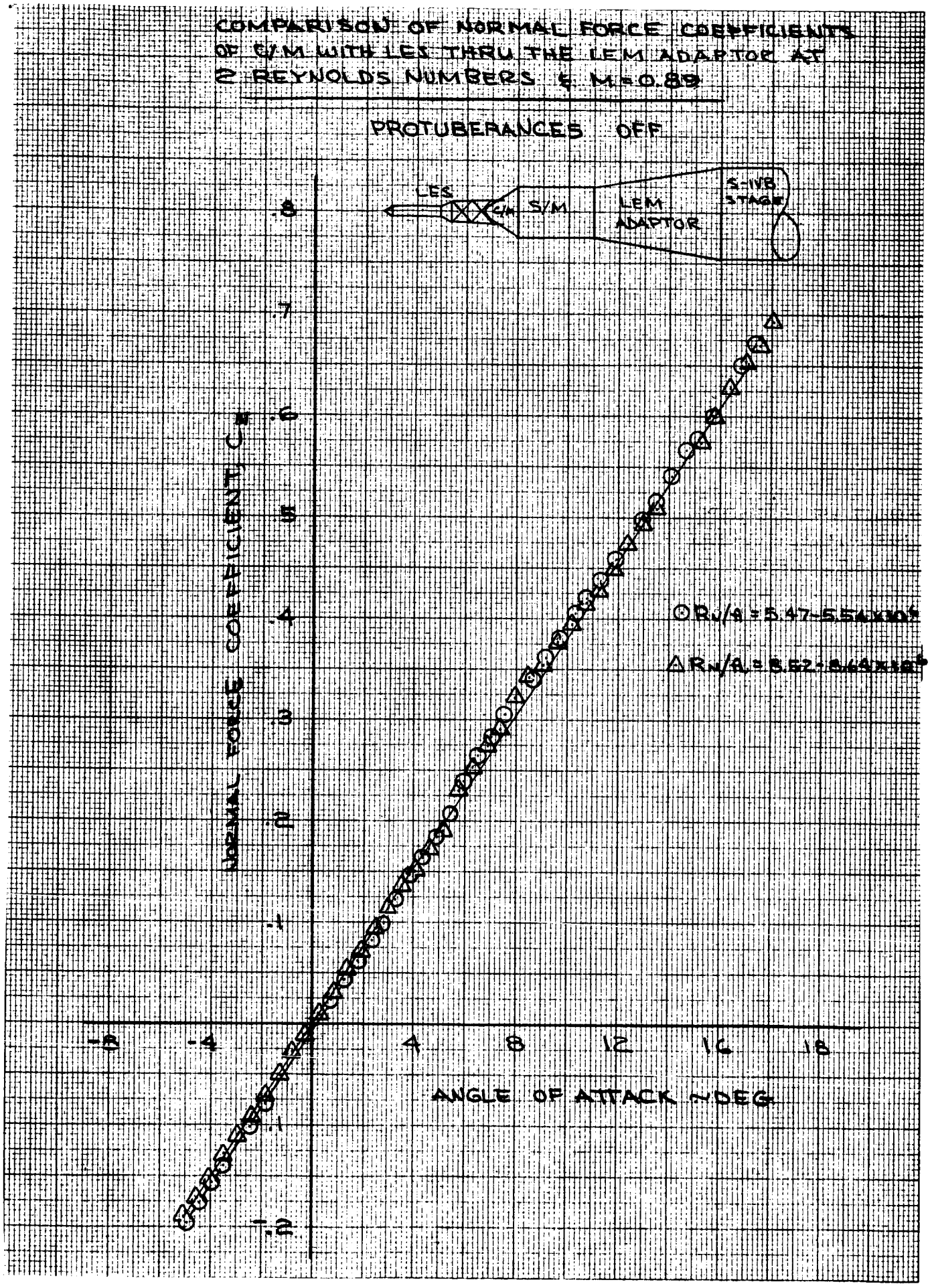
COMPARISON OF NORMAL FORCE COEFFICIENTS OF C/M WITH LES THRU THE LEM ADAPTOR AT 2 REYNOLDS NUMBERS & M=0.89
PROTUBERANCES OFF
LES
C/M
S/M
LEM ADAPTOR
S-IVB STAGE
NORMAL FORCE COEFFICIENT, C_N
ANGLE OF ATTACK - DEG
⊙ $R_N/ft = 5.47-5.54 \times 10^6$
△ $R_N/ft = 8.52-8.64 \times 10^6$
.8
.7
.6
.5
.4
.3
.2
.1
-.2
-8
-4
4
8
12
16
18

FIGURE 18

COMPARISON OF PITCHING MOMENT COEFFICIENTS OF C/M WITH LES THRU THE LEM ADAPTOR AT ≈ REYNOLDS NUMBERS & M=0.89

PROTUBERANCES OFF

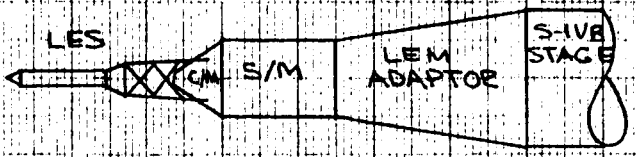

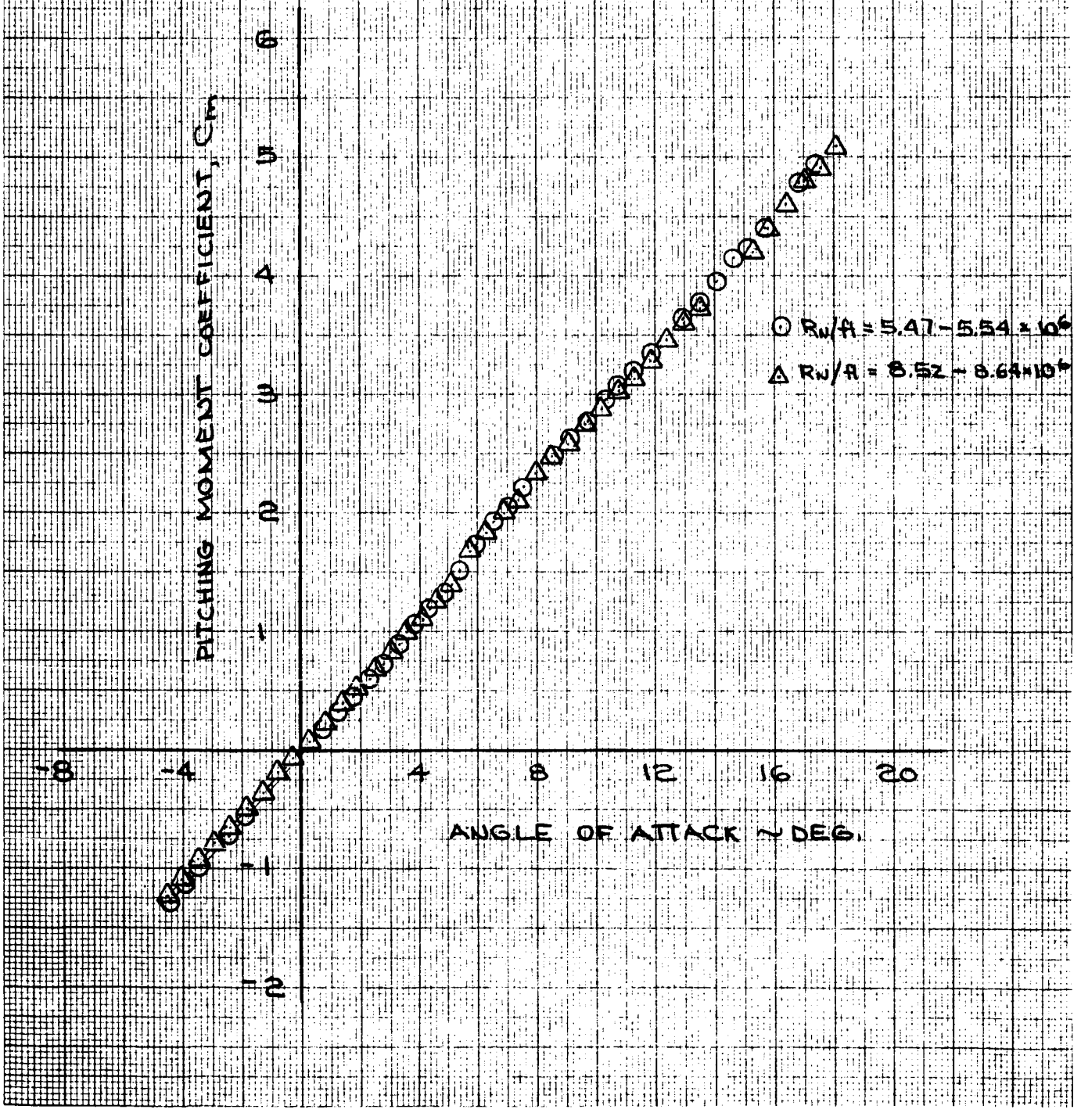

FIGURE 19

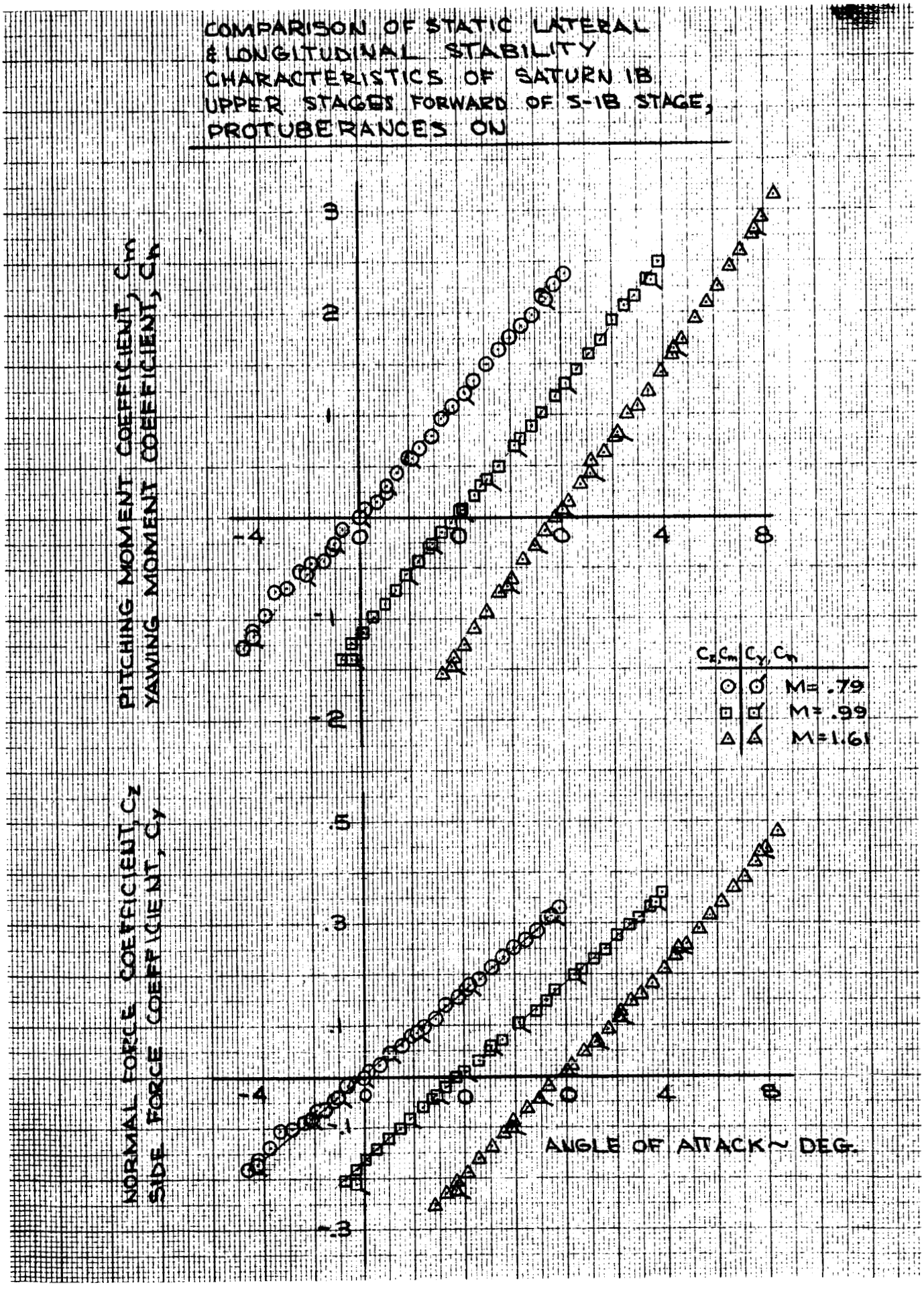
COMPARISON OF STATIC LATERAL & LONGITUDINAL STABILITY CHARACTERISTICS OF SATURN IB UPPER STAGES FORWARD OF S-IB STAGE, PROTUBERANCES ON
NORMAL FORCE COEFFICIENT, C_z PITCHING MOMENT COEFFICIENT, C_m
SIDE FORCE COEFFICIENT, C_y YAWING MOMENT COEFFICIENT, C_n
C_z, C_m C_y, C_n
M= .79
M= .99
M=1.61
ANGLE OF ATTACK ~ DEG.

FIGURE 20

NORMAL FORCE COEFFICIENT -
COMMAND MODULE WITHOUT
LAUNCH ESCAPE SYSTEM
CM | S/M
NORMAL FORCE COEFFICIENT, C_N
.20
.16
.12
.08
.04
0
0.6
0.8
1.0
1.2
1.4
1.6
1.8
MACH NUMBER
0
4
8
12
16
ANGLE OF ATTACK - DEGREES
$\alpha = 15°$
$\alpha = 10°$
$\alpha = 5°$

FIGURE 21

PITCHING MOMENT COEFFICIENT -
COMMAND MODULE WITHOUT
LAUNCH ESCAPE SYSTEM
C/M | S/M
PITCHING MOMENT COEFFICIENT, C_m
2.0
1.6
1.2
.8
.4
0
MACH NUMBER
.6
.8
1.0
1.2
1.4
1.6
1.8
ANGLE OF ATTACK, DEGREES
-4
0
4
8
12
16
$\alpha = 15°$
$\alpha = 10°$
$\alpha = 5°$

FIGURE 22

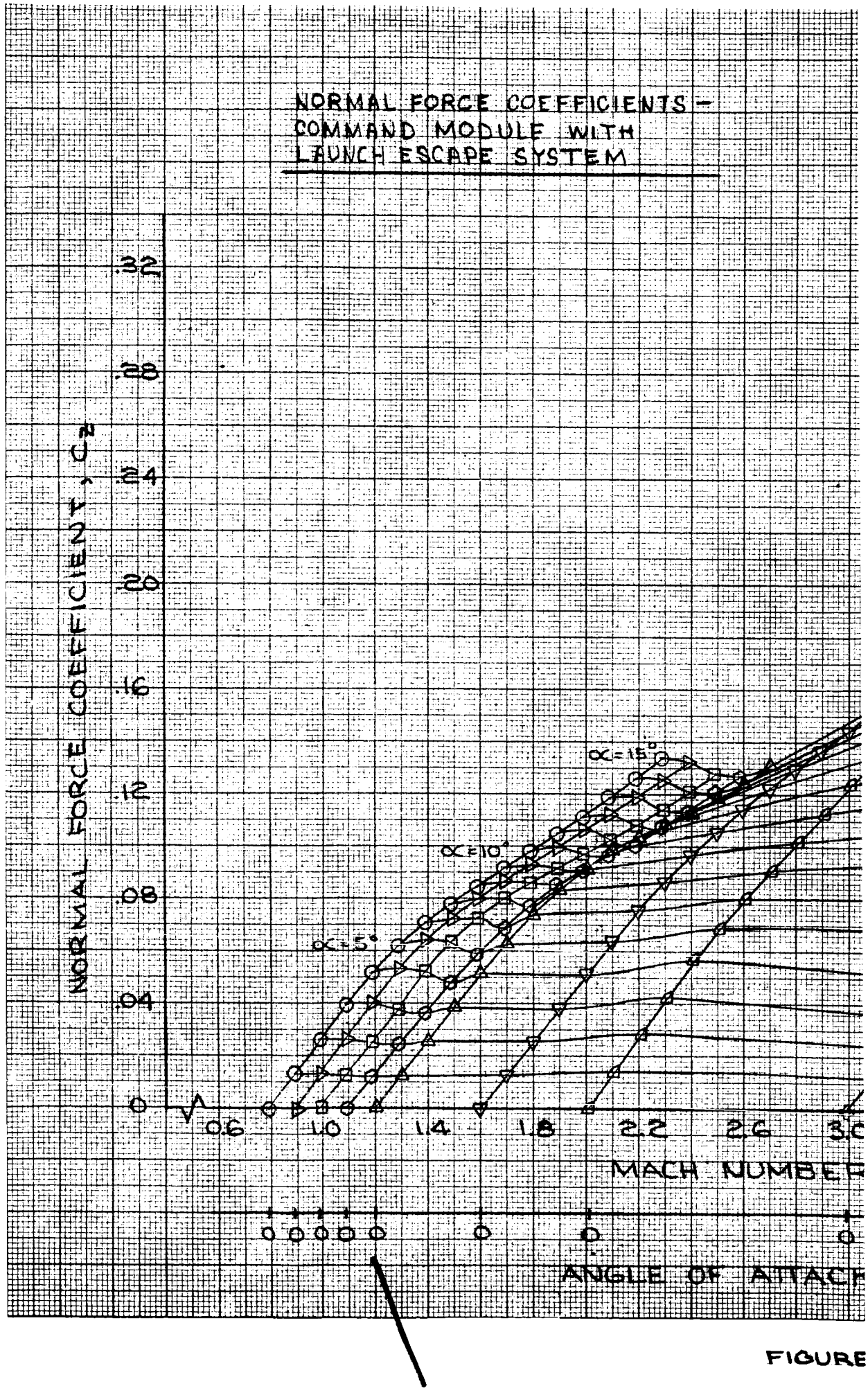
NORMAL FORCE COEFFICIENTS -
COMMAND MODULE WITH
LAUNCH ESCAPE SYSTEM
NORMAL FORCE COEFFICIENT, C_N
.32
.28
.24
.20
.16
.12
.08
.04
0
α=15°
α=10°
α=5°
0.6
1.0
1.4
1.8
2.2
2.6
MACH NUMBER
0
0
0
0
0
0
ANGLE OF ATTACK

FIGURE

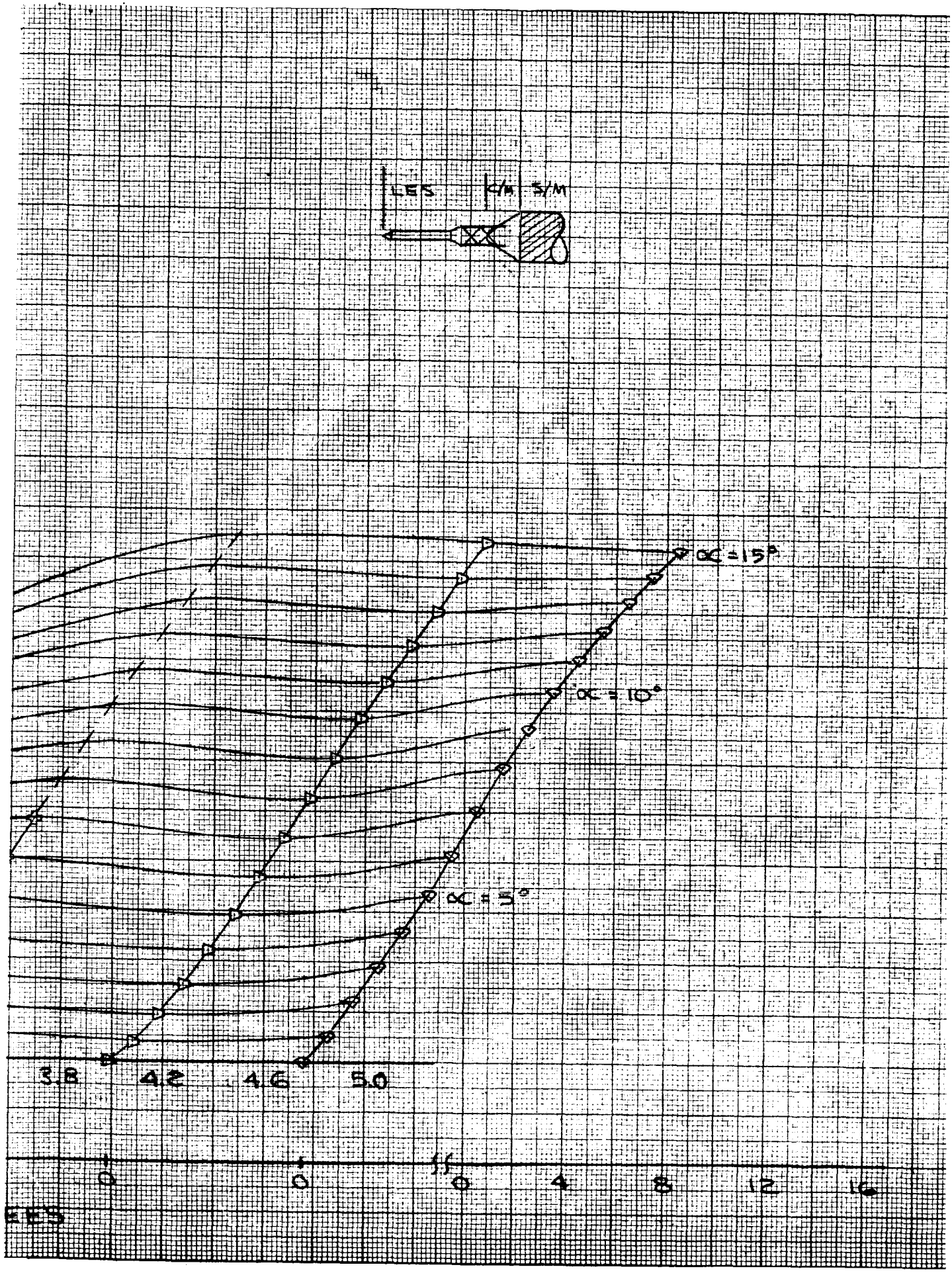
LES
C/M
S/M
α = 15°
α = 10°
α = 5°
3.8
4.2
4.6
5.0
0
5
10
0
4
8
12
16
LES

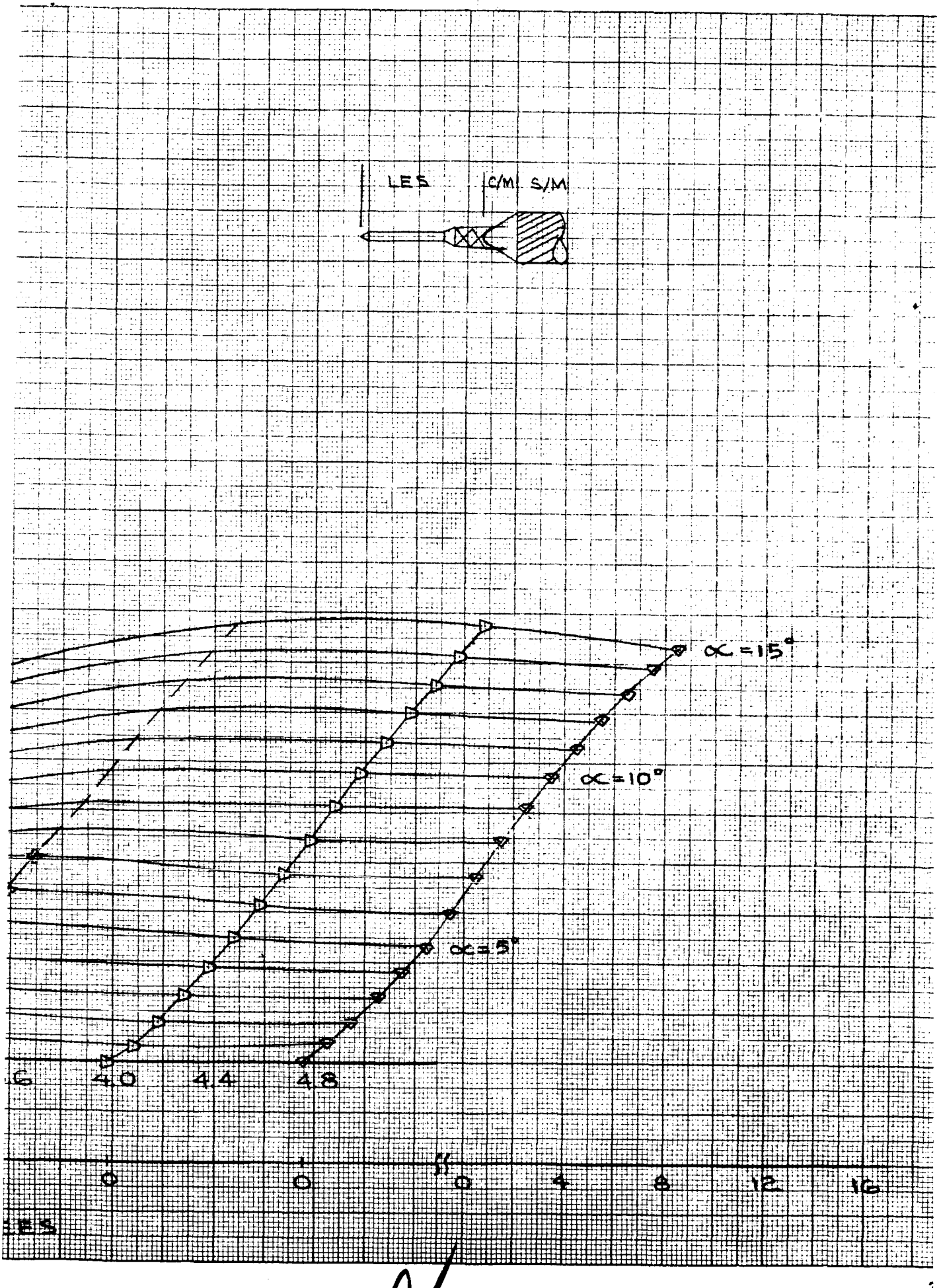
LES
C/M
S/M
α=15°
α=10°
α=5°
4.0
4.4
4.8
0
0
4
8
12
16
LES

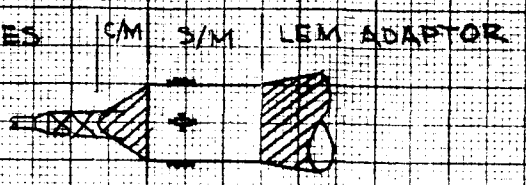
LES
C/M
S/M
LEM ADAPTOR

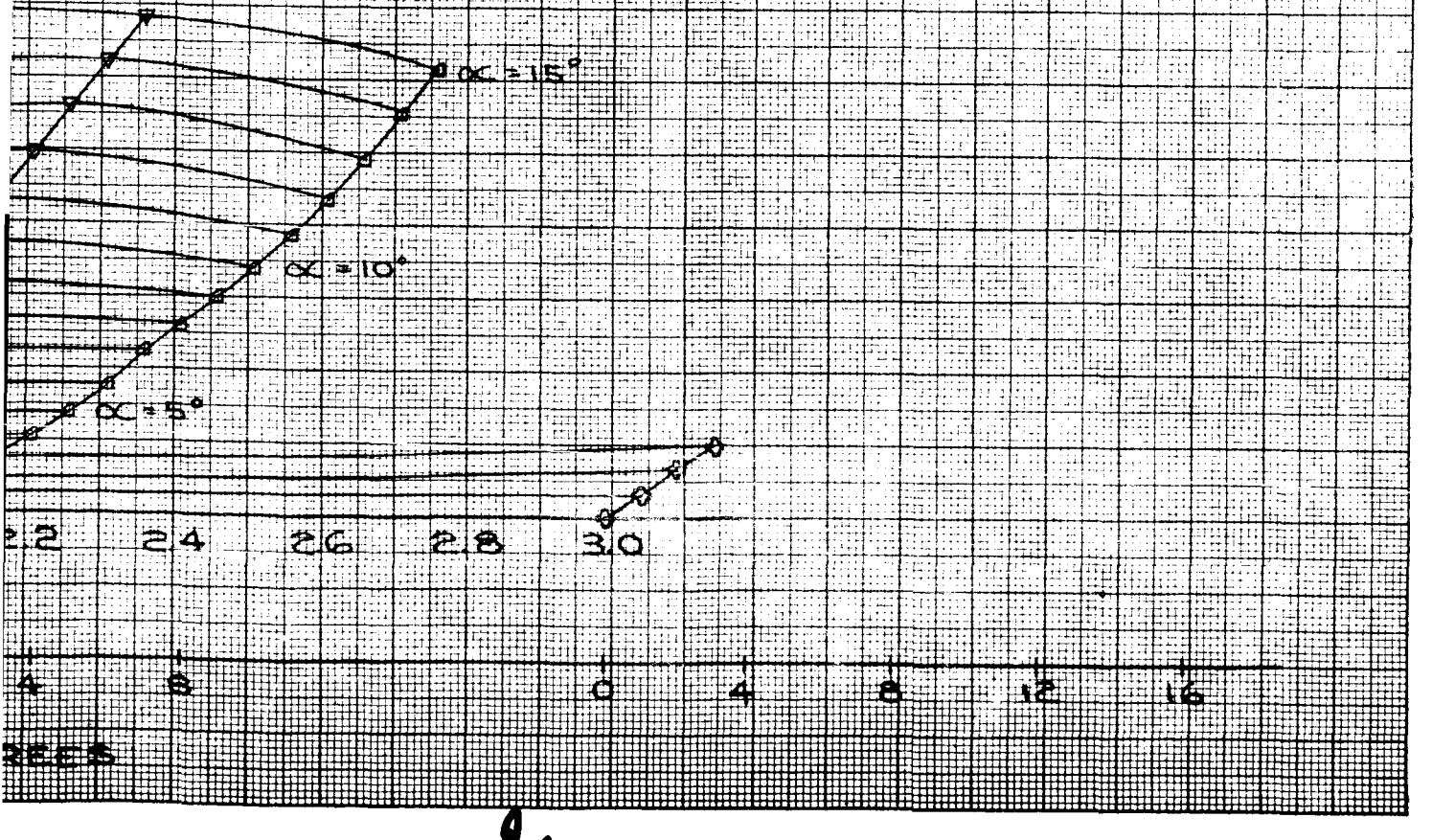
α = 15°
α = 10°
α = 5°
2.2
2.4
2.6
2.8
3.0
4
8
0
4
8
12
16
DEGS

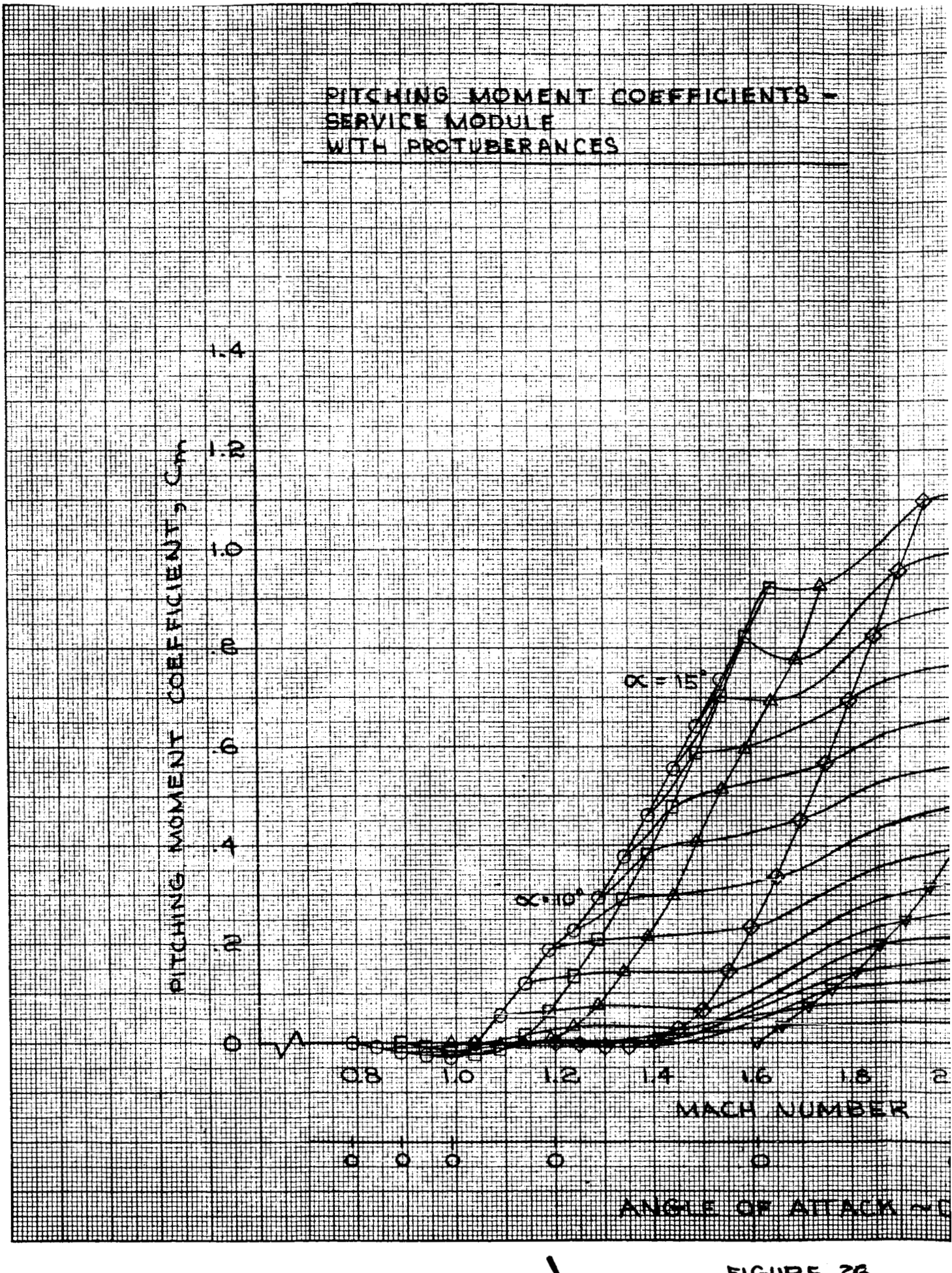
PITCHING MOMENT COEFFICIENTS -
SERVICE MODULE
WITH PROTUBERANCES
PITCHING MOMENT COEFFICIENT, C_m
1.4
1.2
1.0
.8
.6
.4
.2
0
$\alpha = 15°$
$\alpha = 10°$
0.8
1.0
1.2
1.4
1.6
1.8
MACH NUMBER
ANGLE OF ATTACK

FIGURE 26

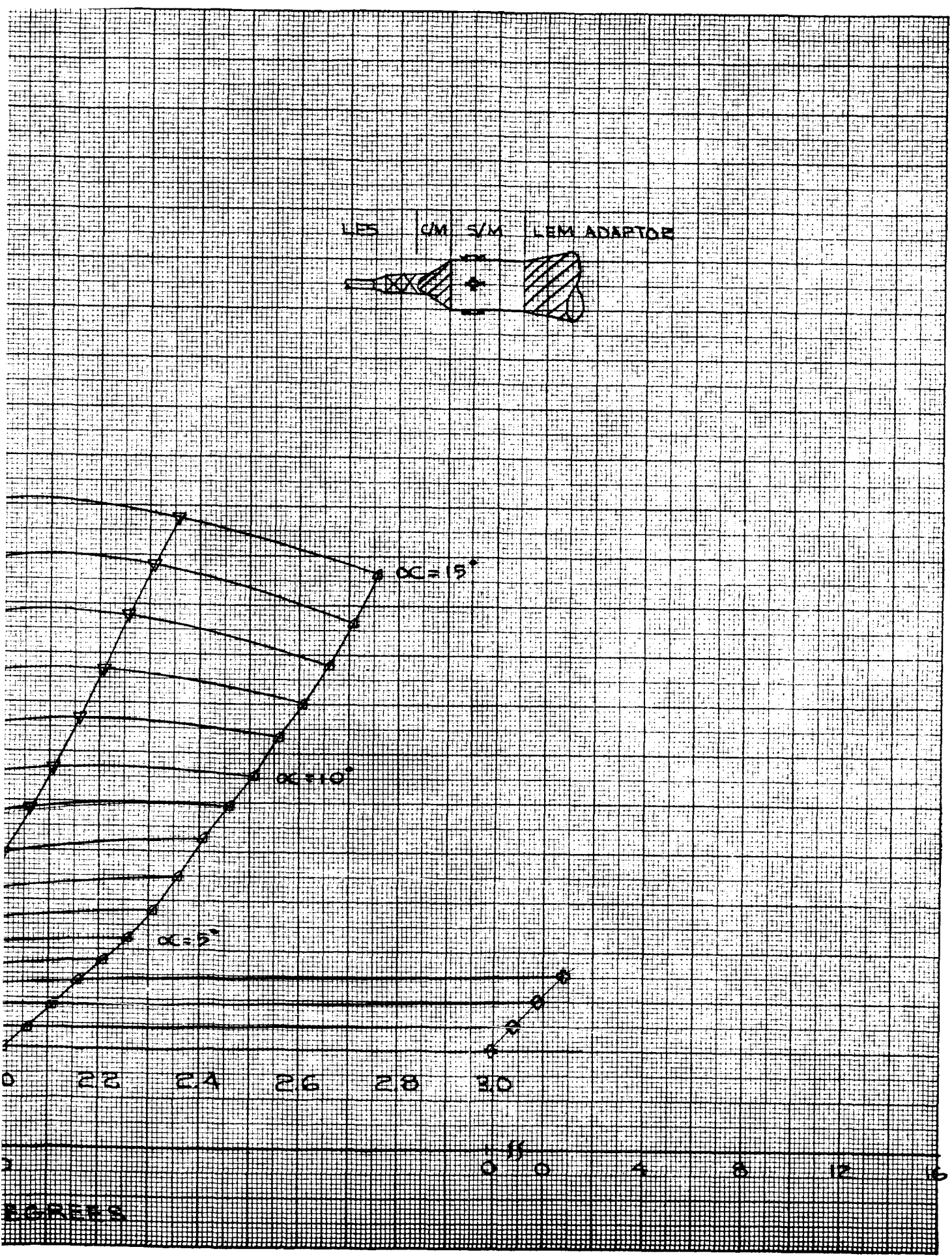
LES
C/M
S/M
LEM ADAPTOR
α = 15°
α = 10°
α = 5°
22
24
26
28
30
0
4
8
12
16
EGREES

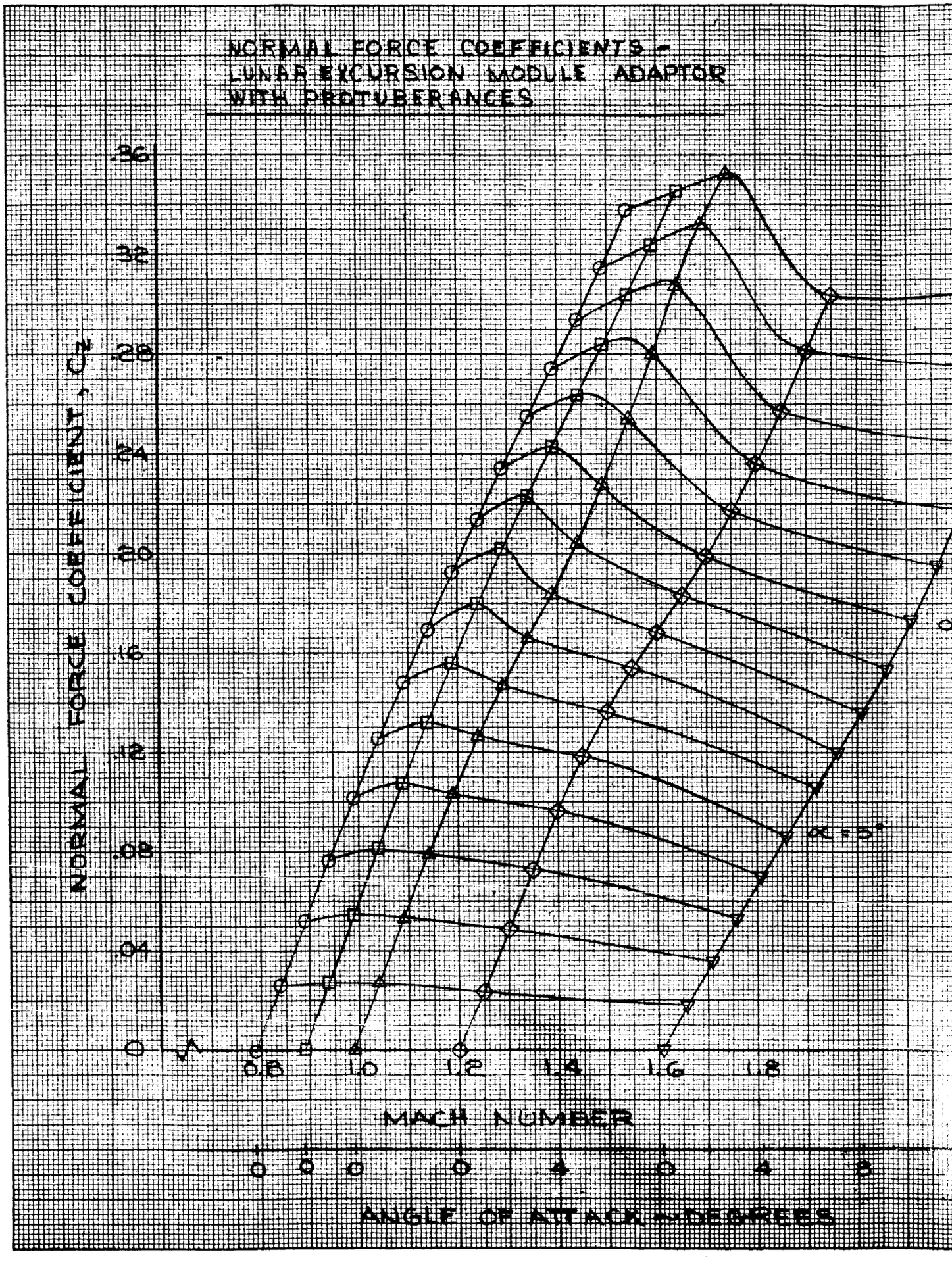
NORMAL FORCE COEFFICIENTS -
LUNAR EXCURSION MODULE ADAPTOR
WITH PROTUBERANCES
NORMAL FORCE COEFFICIENT, C_N
.36
.32
.28
.24
.20
.16
.12
.08
.04
0
0.8
1.0
1.2
1.4
1.6
1.8
MACH NUMBER
0
0
0
0
4
0
4
8
ANGLE OF ATTACK - DEGREES
α = 5°

FIGURE 27

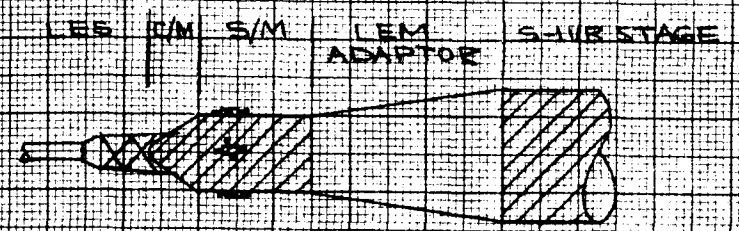

$\alpha = 15°$

$= 10°$

2 16

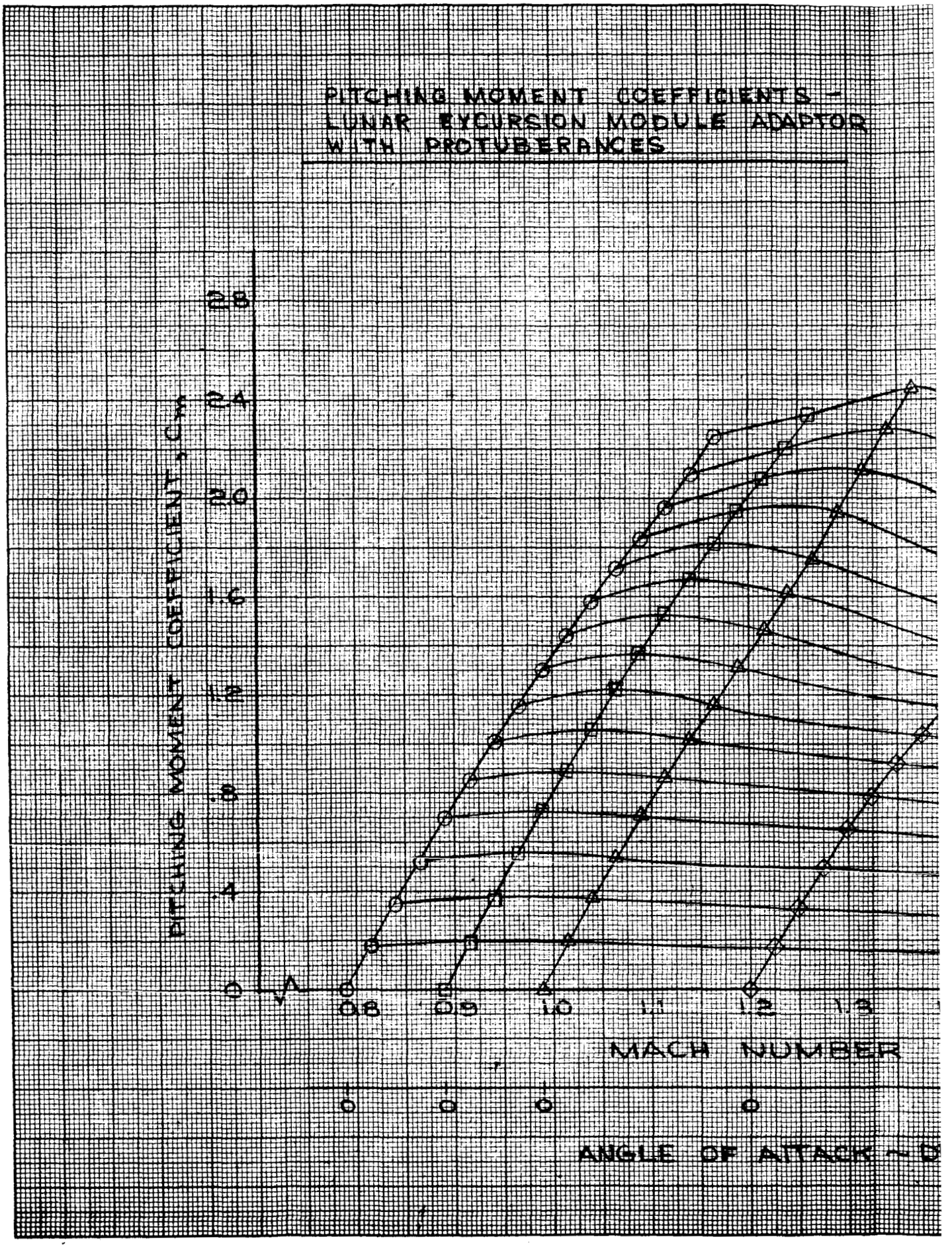
PITCHING MOMENT COEFFICIENTS -
LUNAR EXCURSION MODULE ADAPTOR
WITH PROTUBERANCES
PITCHING MOMENT COEFFICIENT, C_m
2.8
2.4
2.0
1.6
1.2
.8
.4
0
.8
.9
1.0
1.1
1.2
1.3
MACH NUMBER
0
0
0
0
ANGLE OF ATTACK - D

FIGURE 2

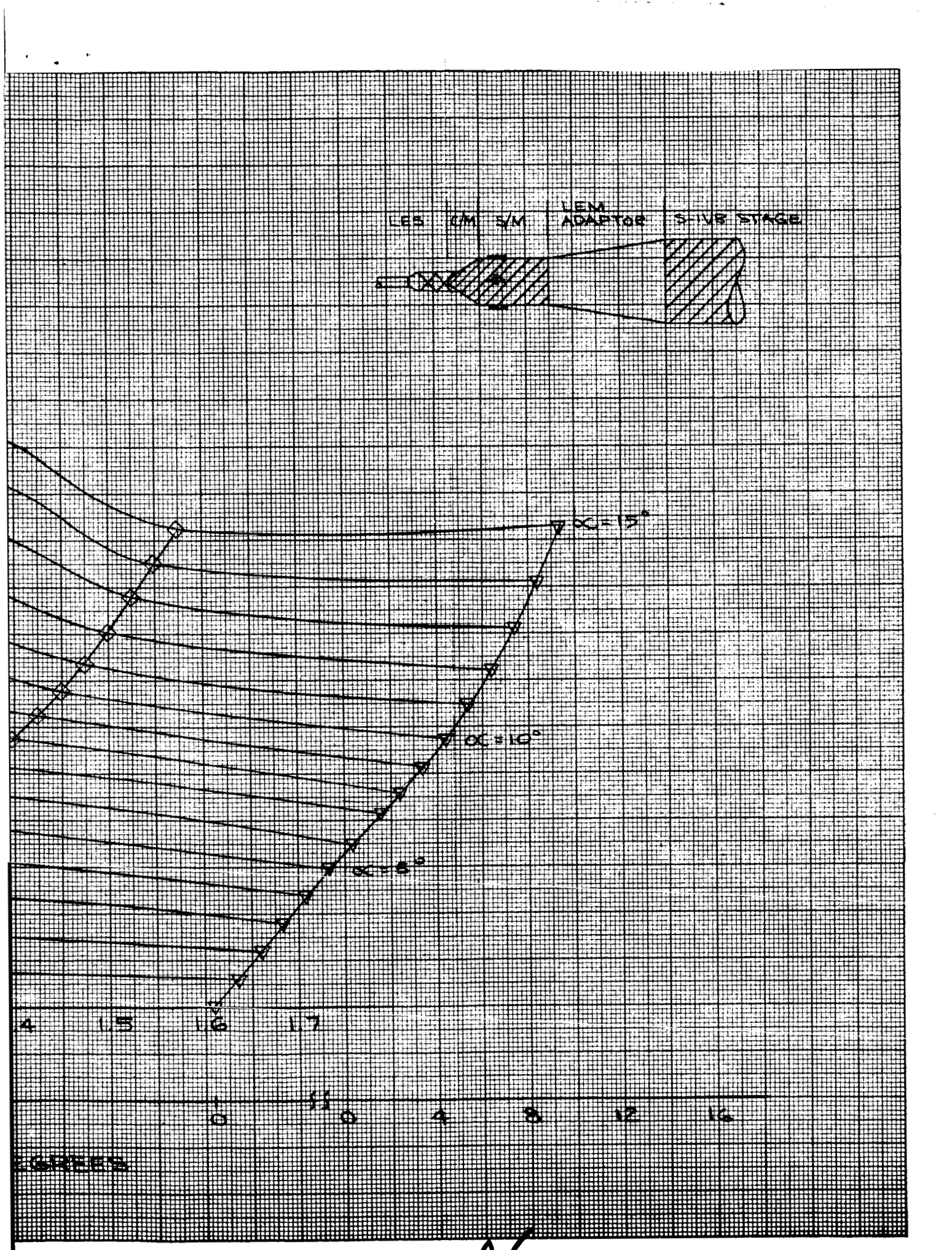
LES
C/M
S/M
LEM ADAPTOR
S-IVB STAGE
α = 15°
α = 10°
α = 5°
1.4
1.5
1.6
1.7
0
4
8
12
16
DEGREES

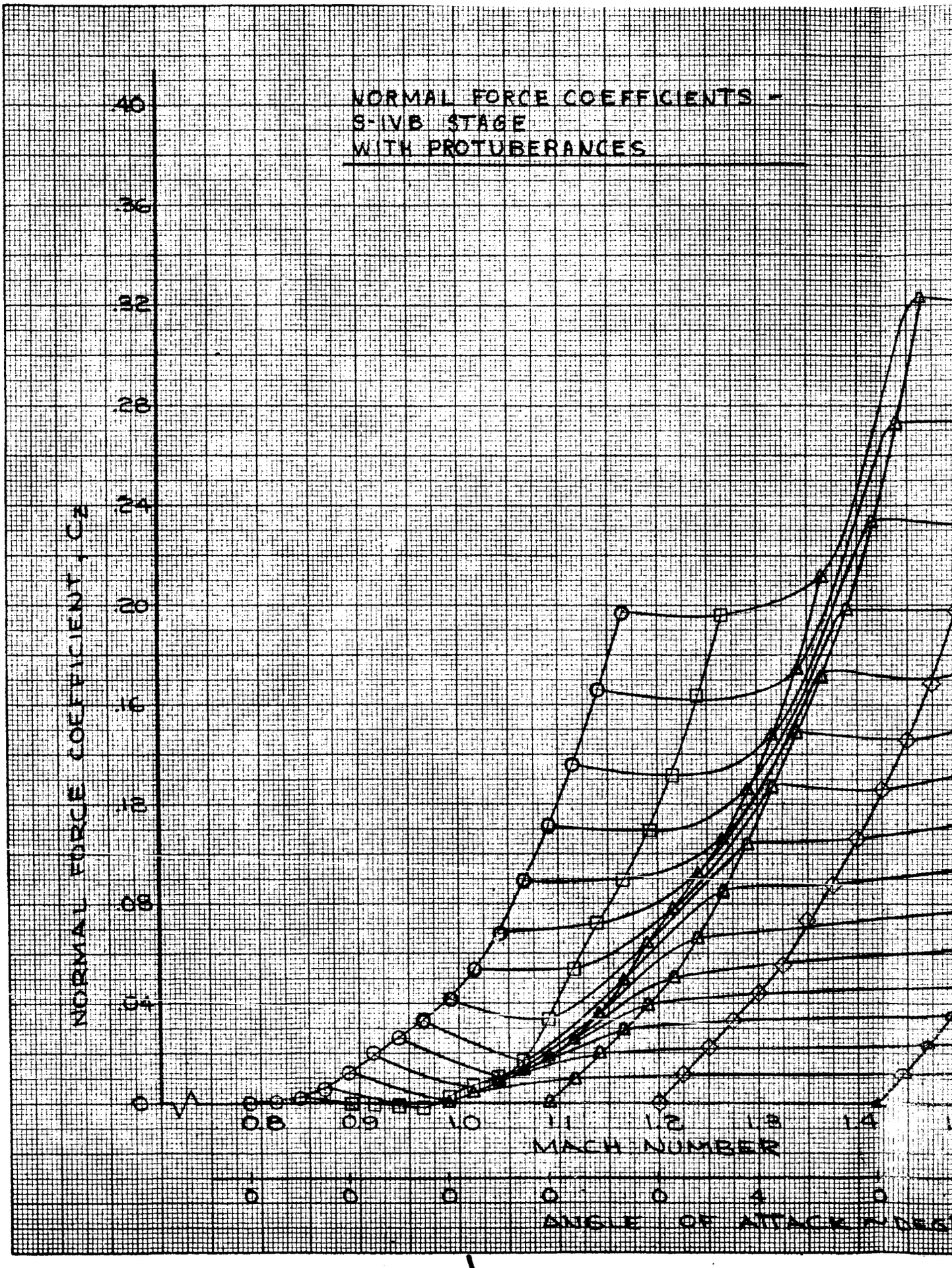
NORMAL FORCE COEFFICIENTS -
S-IVB STAGE
WITH PROTUBERANCES
NORMAL FORCE COEFFICIENT, C_N
.40
.36
.32
.28
.24
.20
.16
.12
.08
.04
0
0.8
0.9
1.0
1.1
1.2
1.3
1.4
MACH NUMBER
ANGLE OF ATTACK IN DEG

FIGURE 29

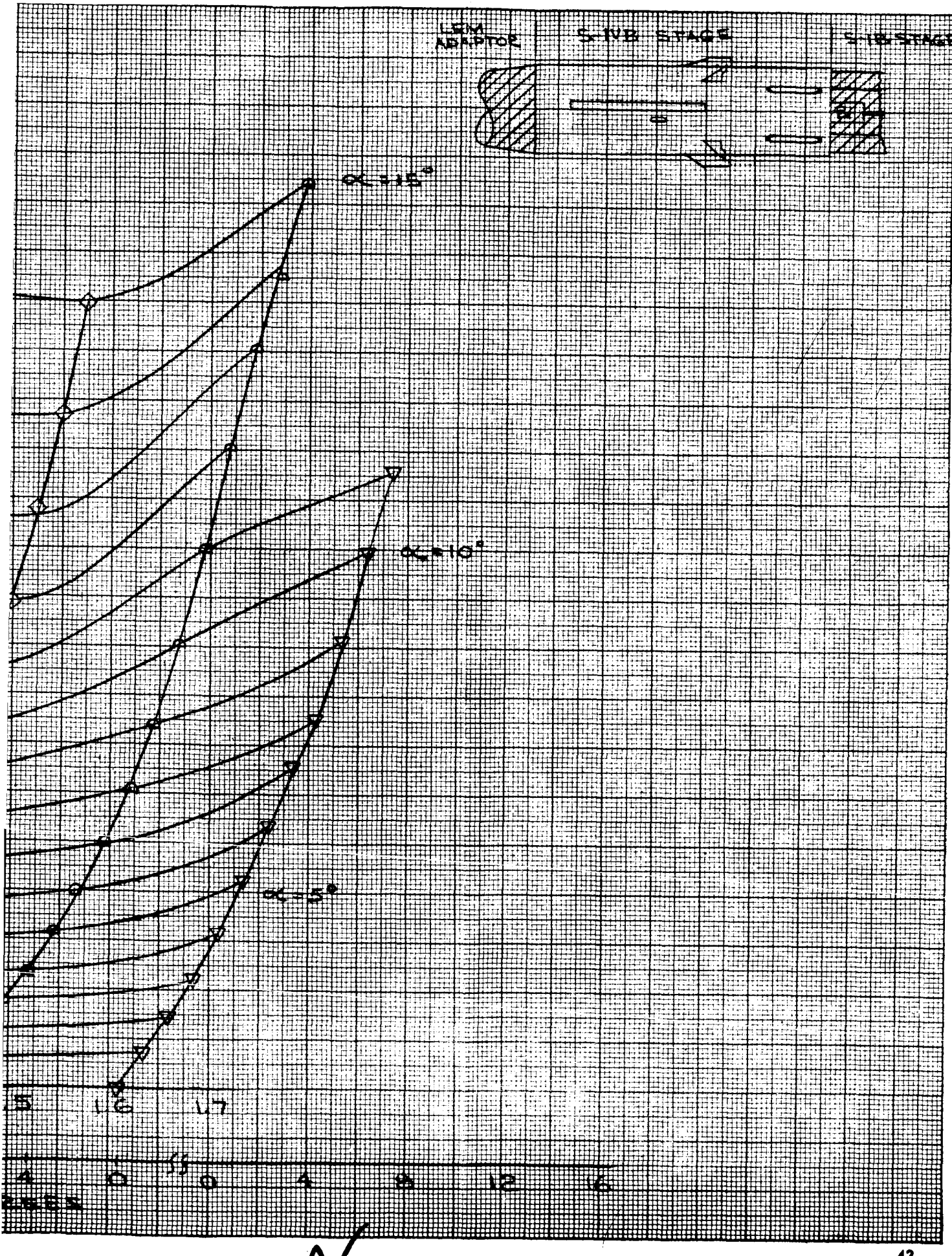
LEM ADAPTOR
S-IVB STAGE
S-IB STAGE
α = 15°
α = 10°
α = 5°
.5
1.6
1.7
4
0
4
8
12
6
ACCS

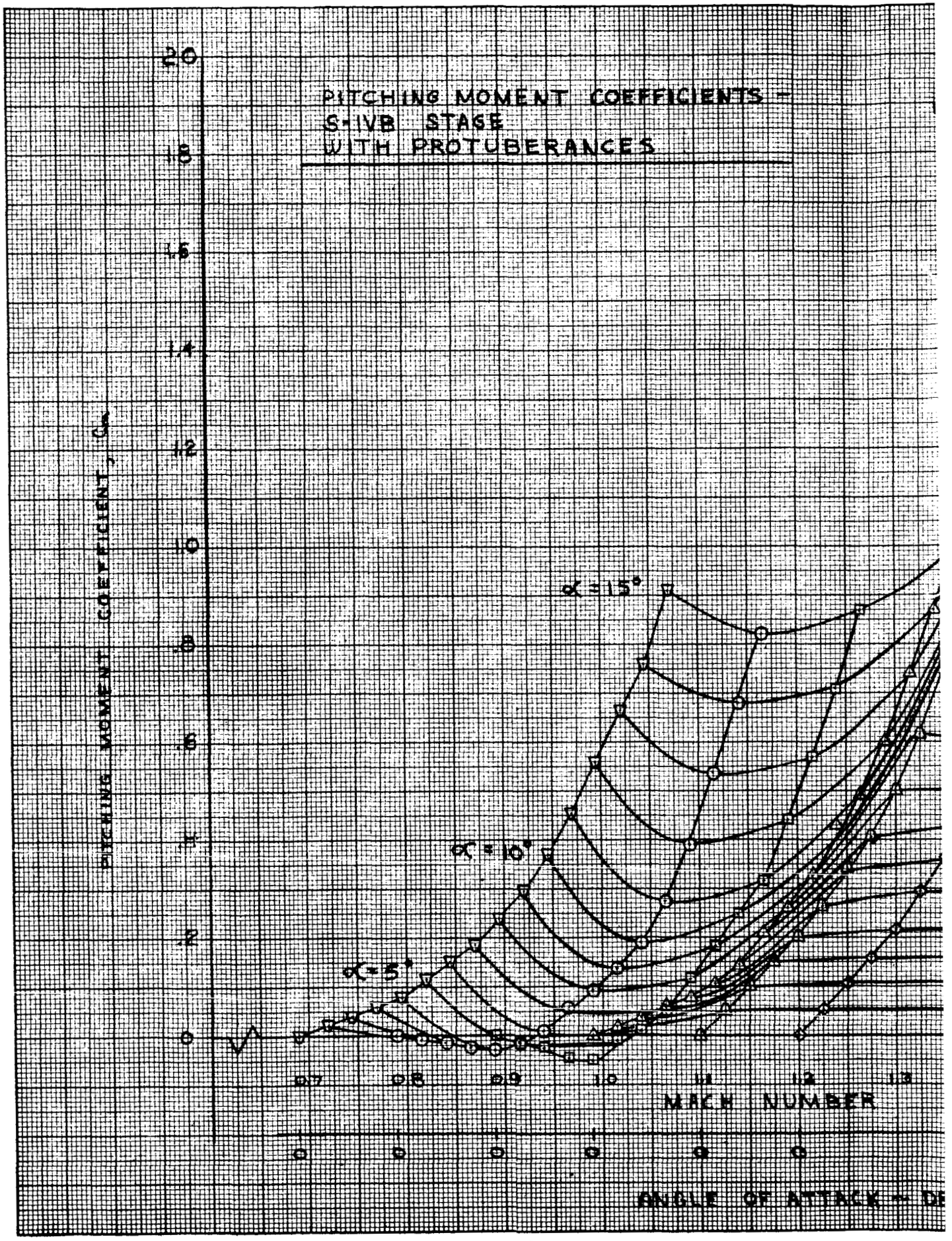
PITCHING MOMENT COEFFICIENTS -
S-IVB STAGE
WITH PROTUBERANCES
PITCHING MOMENT COEFFICIENT, C_m
2.0
1.8
1.6
1.4
1.2
1.0
.8
.6
.4
.2
0
$\alpha = 15°$
$\alpha = 10°$
$\alpha = 5°$
0.7
0.8
0.9
1.0
1.1
1.2
1.3
MACH NUMBER
ANGLE OF ATTACK - DE

FIGURE 30

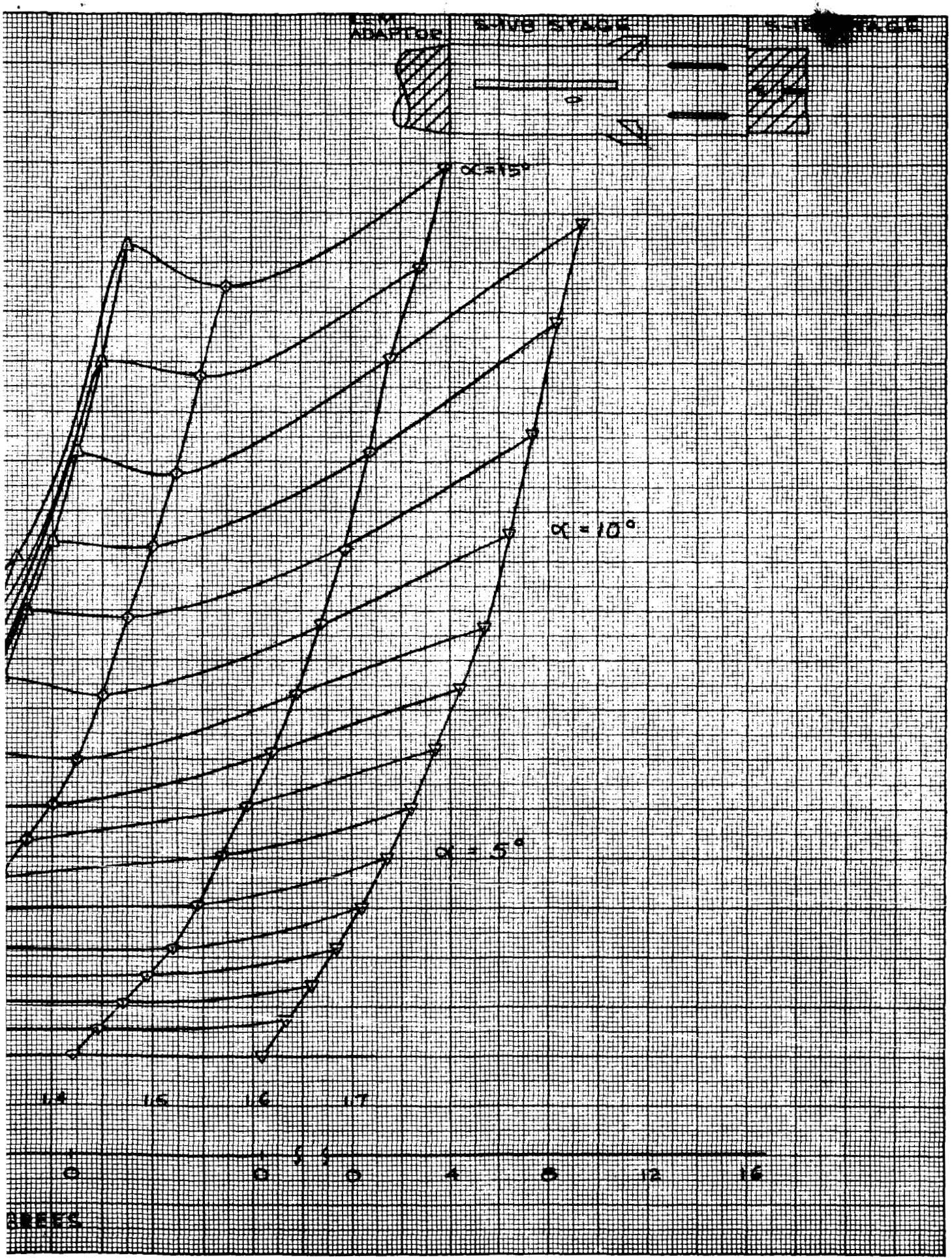

γ

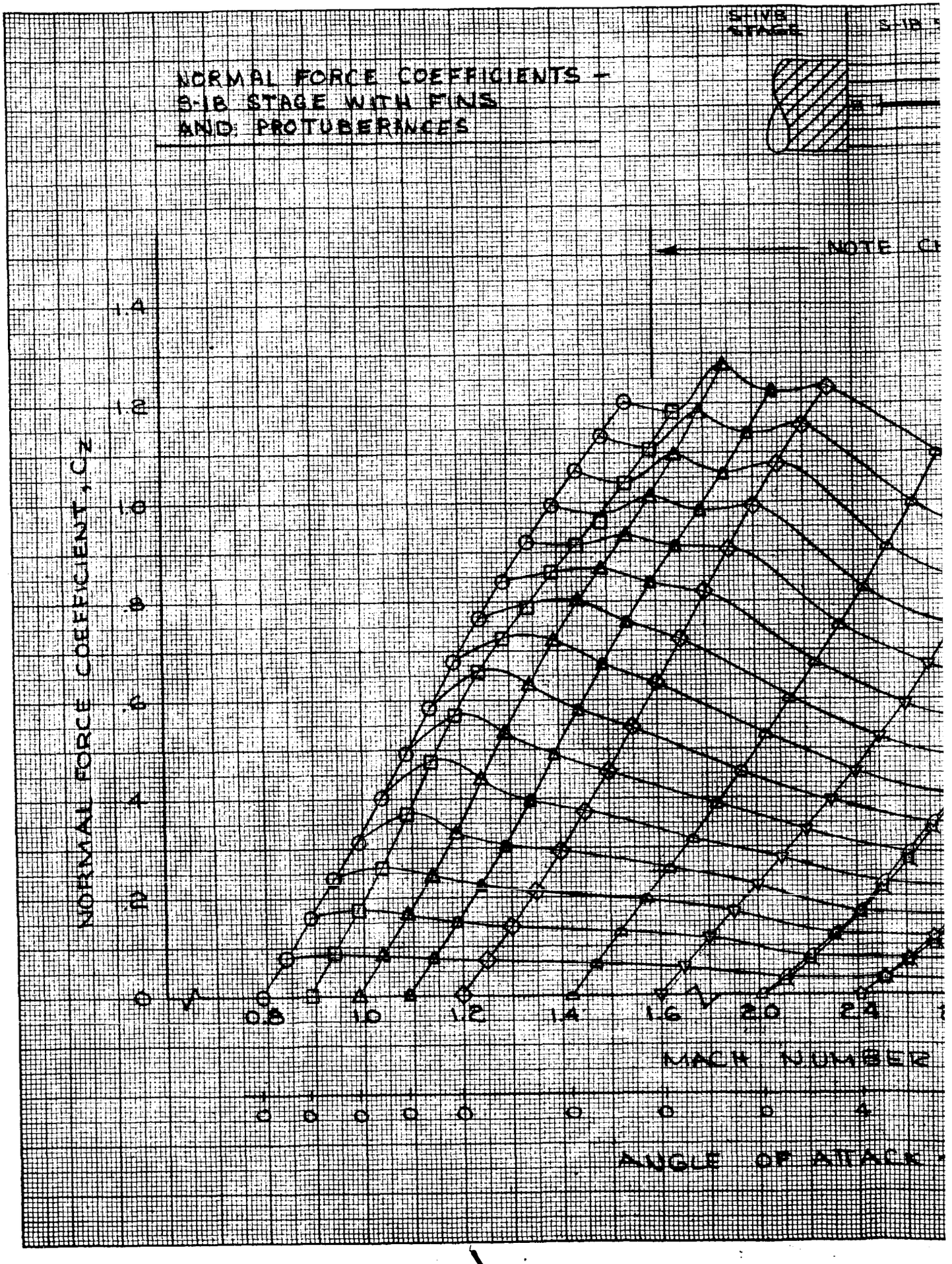
NORMAL FORCE COEFFICIENTS -
S-IB STAGE WITH FINS
AND PROTUBERANCES
S-IVB STAGE
S-IB
NOTE C
NORMAL FORCE COEFFICIENT, CN
1.4
1.2
1.0
.8
.6
.4
.2
0
0.8
1.0
1.2
1.4
1.6
2.0
2.4
MACH NUMBER
ANGLE OF ATTACK

FIGURE 31

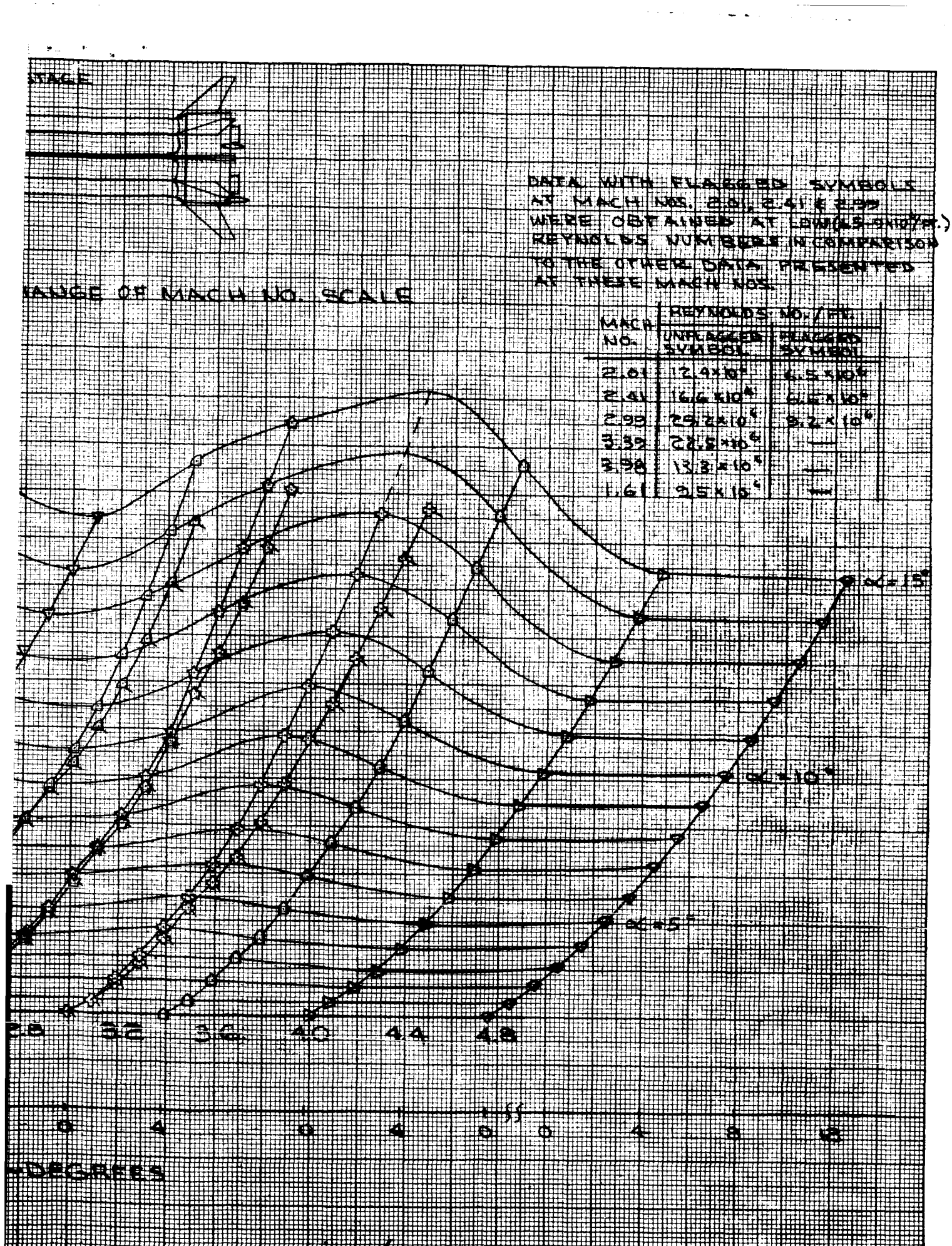
STAGE
RANGE OF MACH NO. SCALE
DATA WITH FLAGGED SYMBOLS AT MACH NOS. 2.81, 2.41 & 2.93 WERE OBTAINED AT LOW REYNOLDS NUMBERS IN COMPARISON TO THE OTHER DATA PRESENTED AT THESE MACH NOS.
MACH NO. | REYNOLDS NO./FT. UNFLAGGED SYMBOL | FLAGGED SYMBOL
2.81 | 12.9×10⁶ | 4.5×10⁶
2.41 | 16.6×10⁶ | 6.6×10⁶
2.93 | 29.2×10⁶ | 9.2×10⁶
3.39 | 22.5×10⁶ | —
3.98 | 13.3×10⁶ | —
1.61 | 9.5×10⁶ | —
α = 15°
α = 10°
α = 5°
3.0
3.5
4.0
4.4
4.8
DEGREES

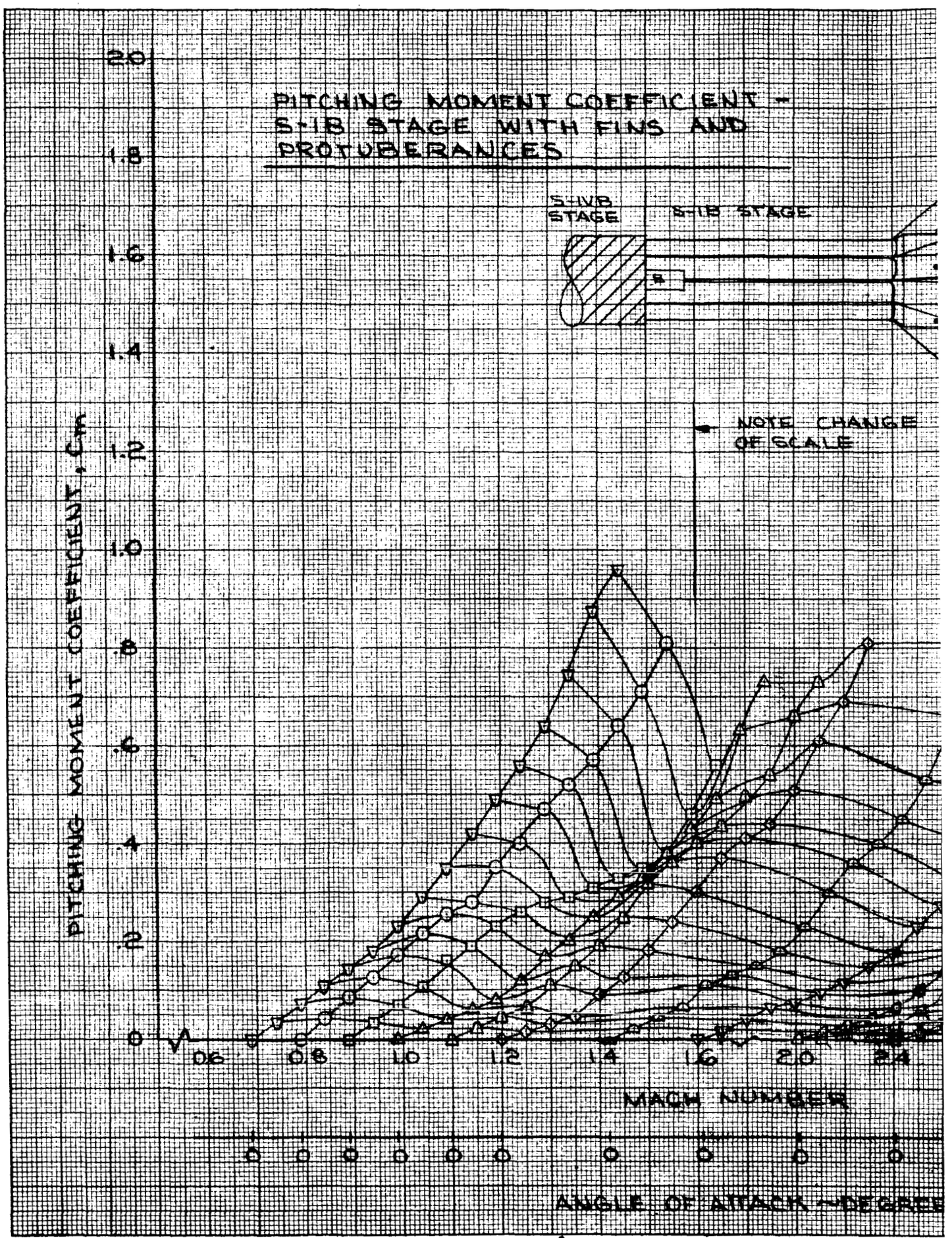
PITCHING MOMENT COEFFICIENT - S-IB STAGE WITH FINS AND PROTUBERANCES
S-IVB STAGE
S-IB STAGE
NOTE CHANGE OF SCALE
PITCHING MOMENT COEFFICIENT, C_m
2.0
1.8
1.6
1.4
1.2
1.0
.8
.6
.4
.2
0
.6
.8
1.0
1.2
1.4
1.6
2.0
2.4
MACH NUMBER
ANGLE OF ATTACK - DEGREES

FIGURE 32

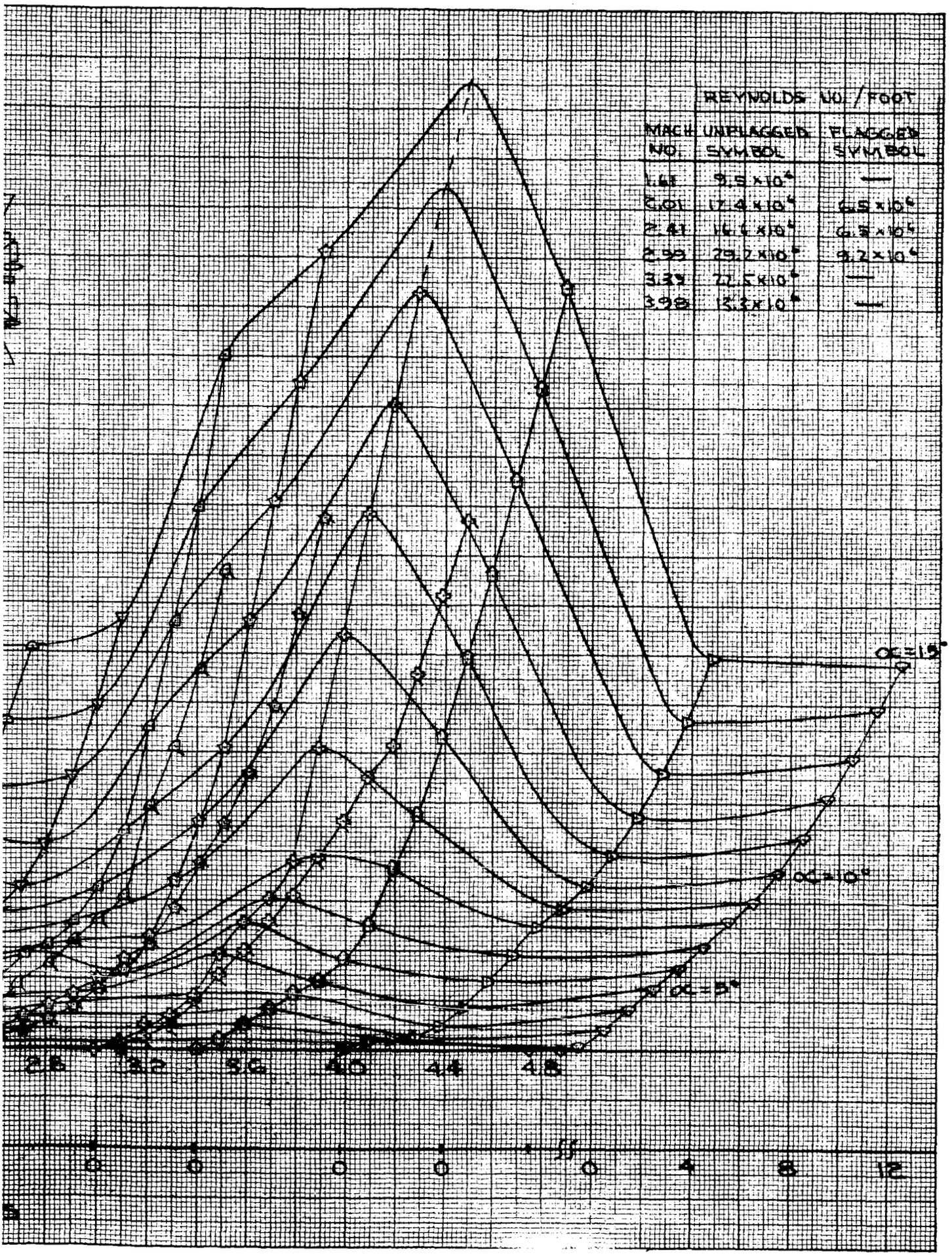
REYNOLDS NO. / FOOT
MACH NO.
UNFLAGGED SYMBOL
FLAGGED SYMBOL
1.68
9.5 x 10^6
—
2.01
12.4 x 10^6
6.5 x 10^6
2.41
16.6 x 10^6
6.5 x 10^6
2.93
29.2 x 10^6
9.2 x 10^6
3.39
22.5 x 10^6
—
3.98
15.3 x 10^6
—
α = 15°
α = 10°
α = 5°
2.8
3.2
3.6
4.0
4.4
4.8
0
0
0
0
0
4
8
12

NORMAL FORCE COEFFICIENTS -
SERVICE MODULE,
PROTUBERANCES OFF
NORMAL FORCE COEFFICIENT, C_N
.24
.20
.16
.12
.08
.04
0
-.04
α = 15°
α = 10°
α = -5°
0.8
0.9
1.0
1.1
1.2
1.3
1.4
MACH NUMBER
0
0
0
0
0
0
0
0
4
8
ANGLE OF ATTACK - DEGREES

FIGURE 33


LES
CM
S/M
LEM
ABORTOE

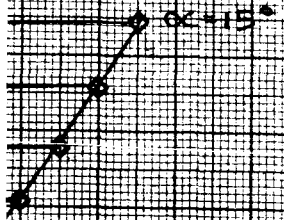
α=+15°

PITCHING MOMENT COEFFICIENTS -
SERVICE MODULE,
PROTUBERANCES OFF

FIGURE 34

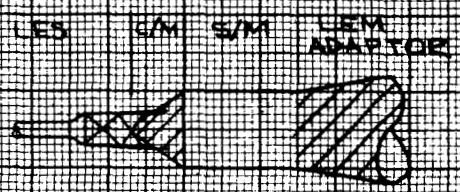
LES
C/M
S/M
LEM ADAPTOR

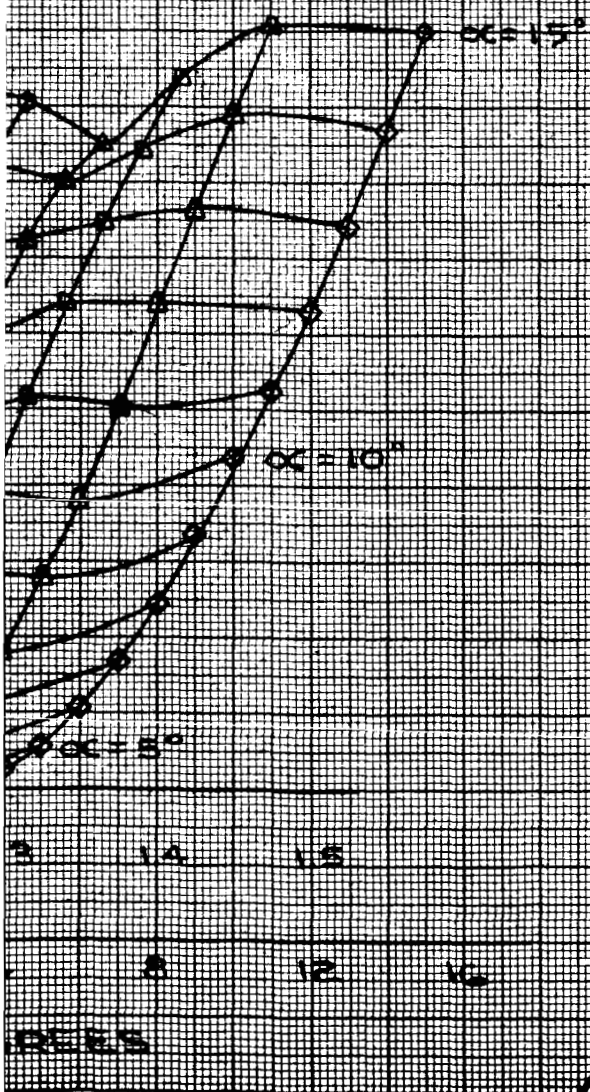
α = 15°
α = 10°
α = 5°

NORMAL FORCE COEFFICIENTS -
LONG EXCURSION MODULE ADAPTOR,
PROTUBERANCES OFF
.32
.28
.24
.20
.16
.12
.08
.04
0
NORMAL FORCE COEFFICIENT, C_N
-.4
-.2
.0
.2
.4
.6
.8
1.0
1.2
1.3
1.4
MACH NUMBER
-6
-4
-2
0
2
4
6
8
ANGLE OF ATTACK - DEGREES
α = 5°

FIGURE 36

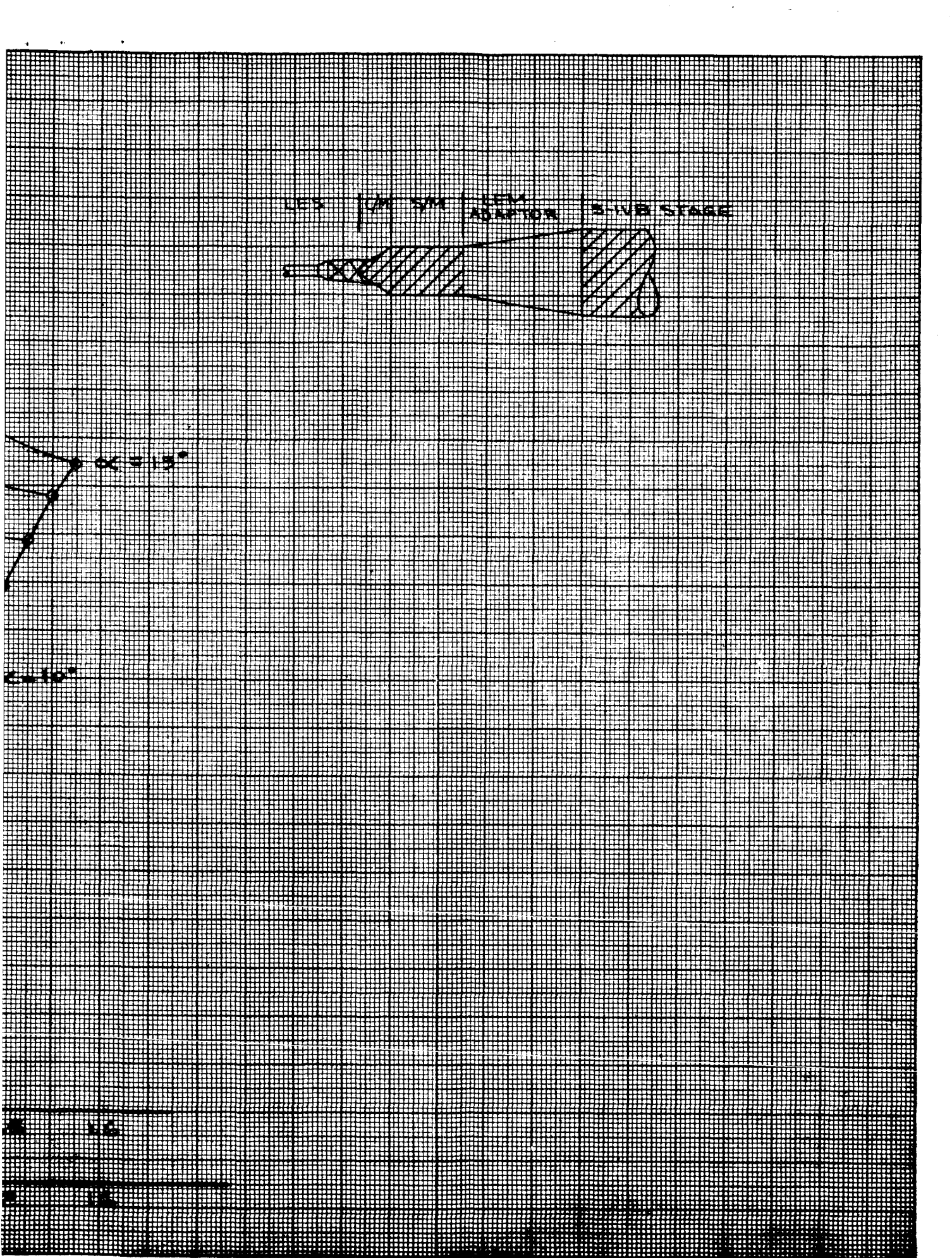
LES
CM
SM
LEM ADAPTOR
S-IVB STAGE
α = 15°
c = 10°

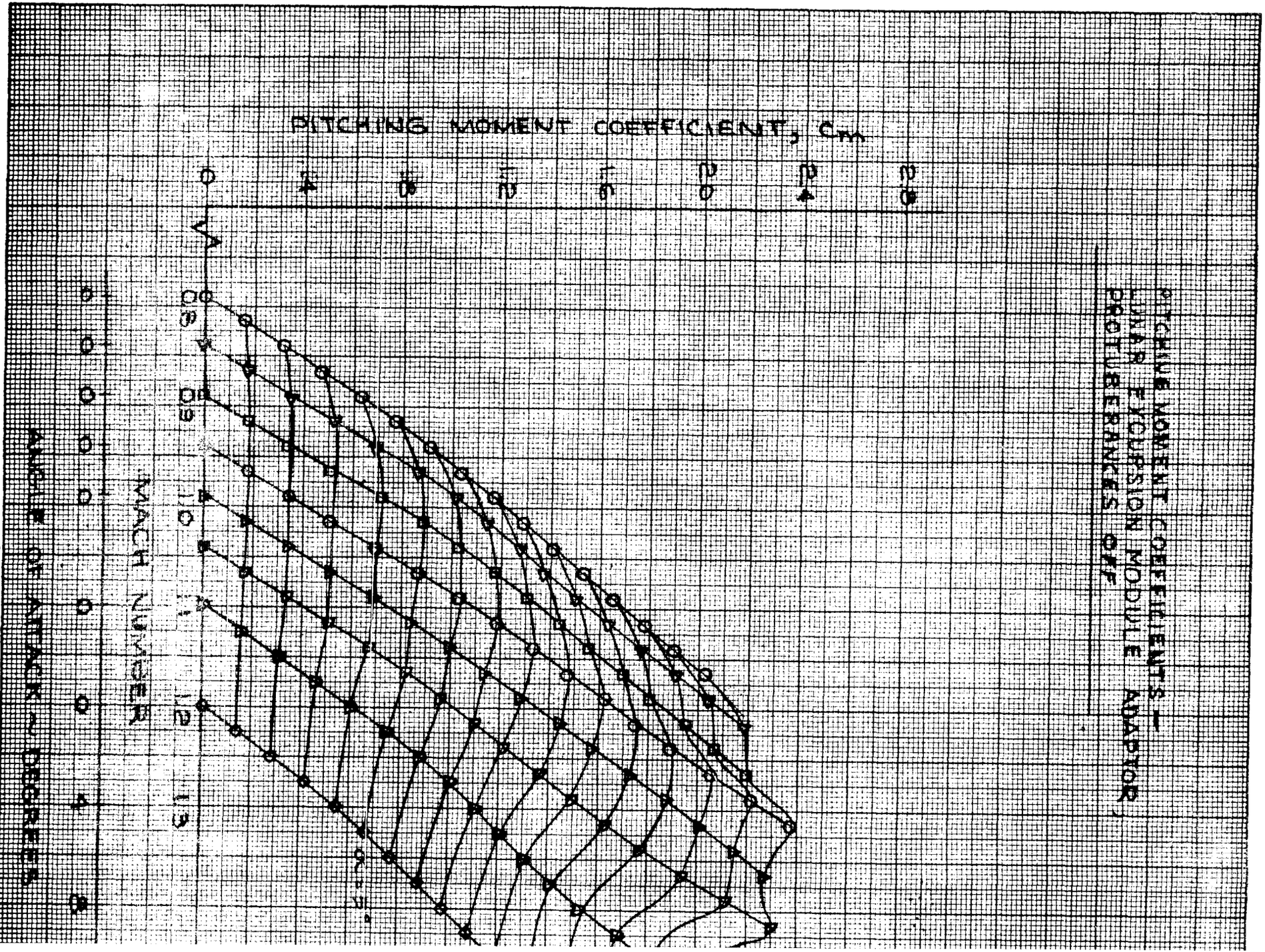
PITCHING MOMENT COEFFICIENT, C_m
MACH NUMBER
ANGLE OF ATTACK, DEGREES
PITCHING MOMENT COEFFICIENTS FOR
FLIGHT EXCURSION MODULE ADAPTOR
PROTUBERANCES OFF

FIGURE 38

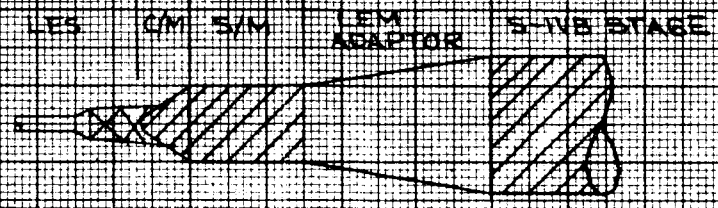

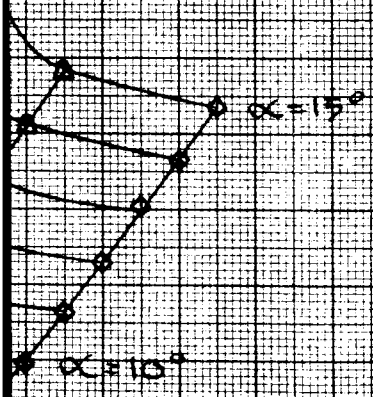

12 16

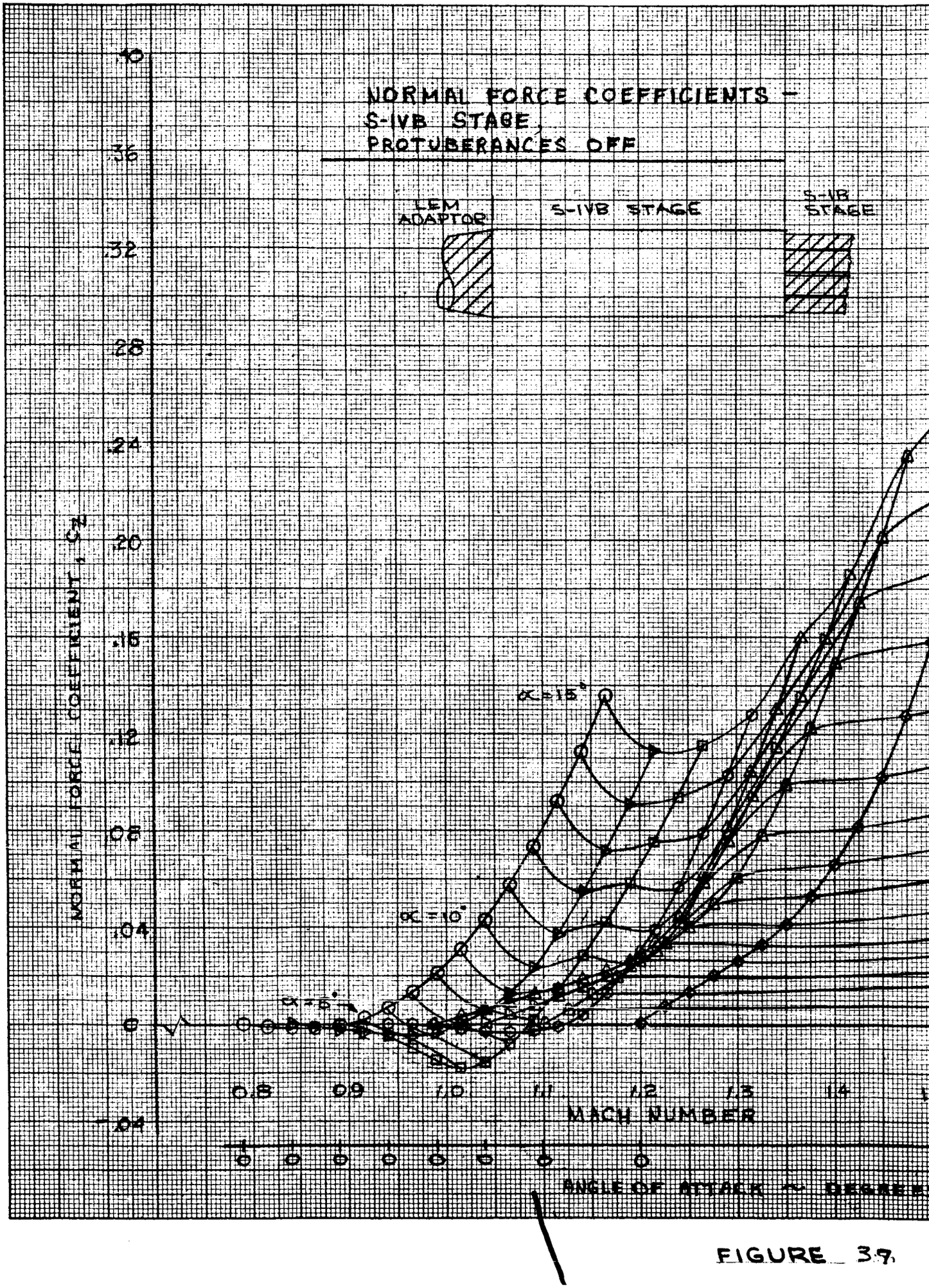
NORMAL FORCE COEFFICIENTS –
S-IVB STAGE,
PROTUBERANCES OFF
LEM ADAPTOR
S-IVB STAGE
S-IVB STAGE
NORMAL FORCE COEFFICIENT, C_N
.40
.36
.32
.28
.24
.20
.16
.12
.08
.04
0
-.04
$\alpha = 15°$
$\alpha = 10°$
$\alpha = 5°$
0.8
0.9
1.0
1.1
1.2
1.3
1.4
MACH NUMBER
ANGLE OF ATTACK – DEGREES

FIGURE 39.

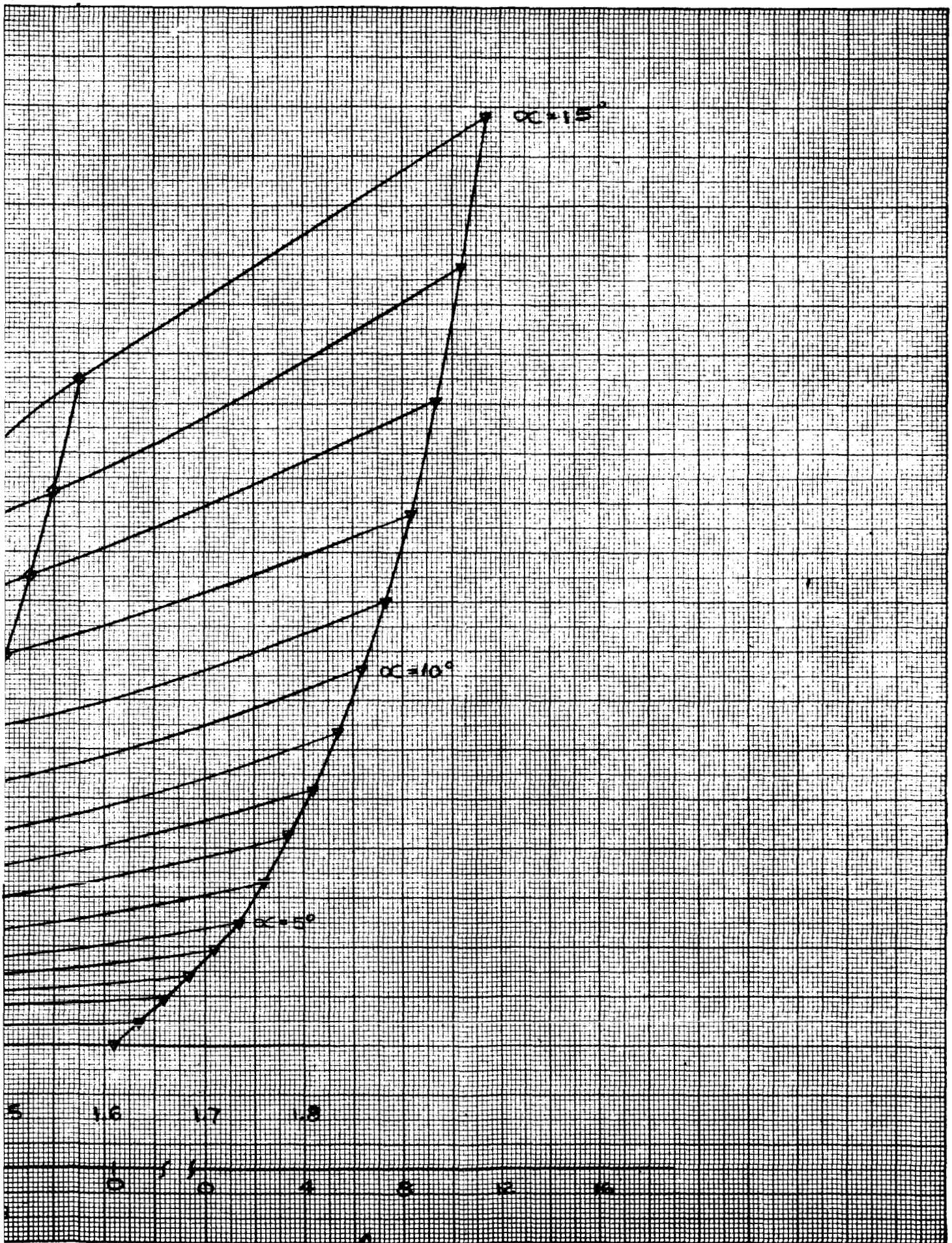
α = 15°
α = 10°
α = 5°
1.6
1.7
1.8
0
4
8
12

PITCHING MOMENT COEFFICIENTS, S-IVB STAGE
TOLERANCES OFF
SYMBOL
MACH NO.
.79
.84
.89
.94
.99
1.04
1.10
1.20
1.61
LEM ADAPTER
S-IVB STAGE
S-IVB STAGE
2.0
1.0
0.5
0
-0.5
-1.0
-1.5
-2.0
C_m

FIGURE 3

ANGLE OF ATTACK-DEGREES
16
14
12
10
8
6
4
2
0

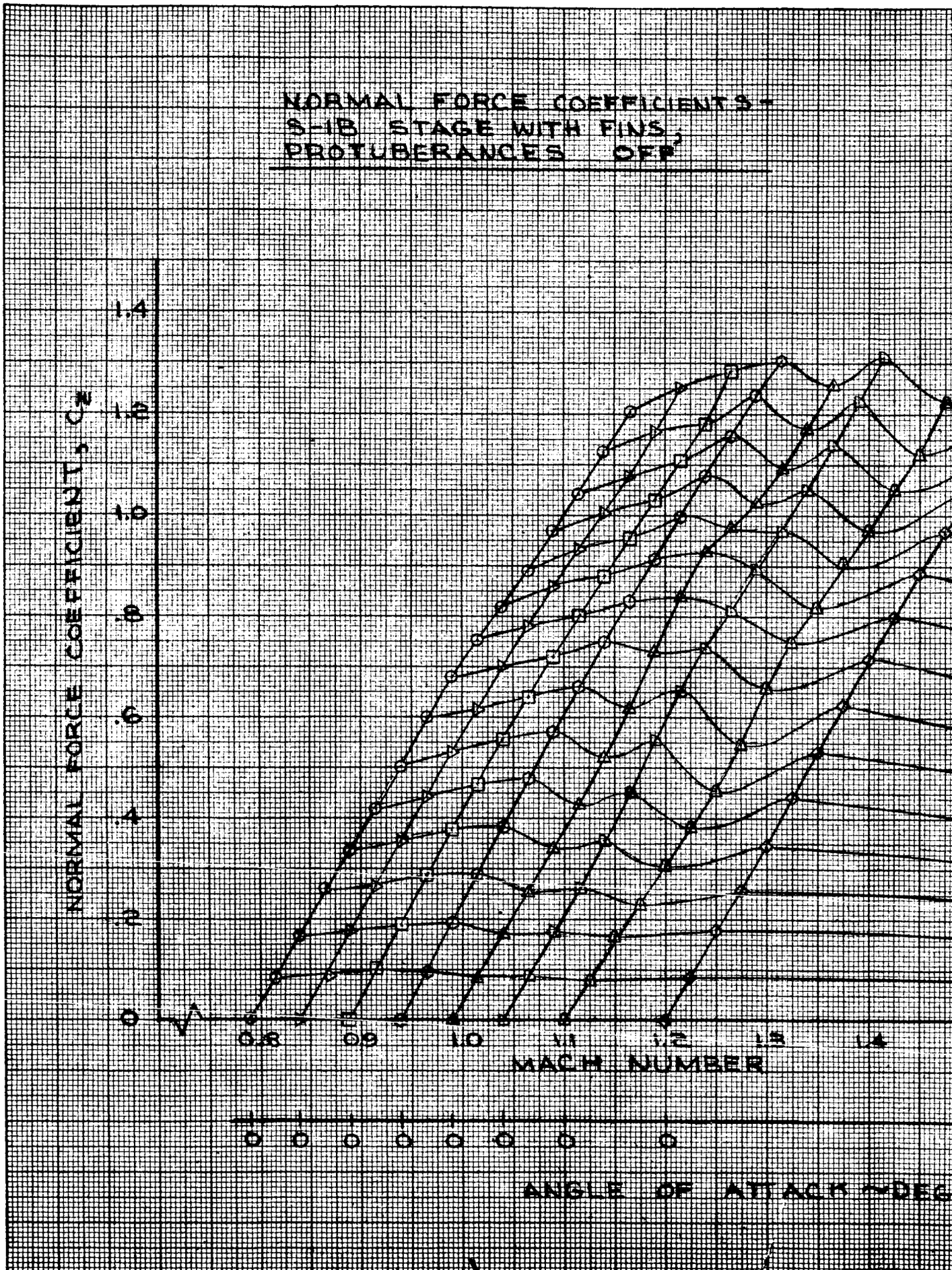
NORMAL FORCE COEFFICIENT S-1
S-IB STAGE WITH FINS, PROTUBERANCES OFF
NORMAL FORCE COEFFICIENT, C_N
1.4
1.2
1.0
.8
.6
.4
.2
0
0.8
0.9
1.0
1.1
1.2
1.3
1.4
MACH NUMBER
0 0 0 0 0 0 0 0
ANGLE OF ATTACK ~DEG

FIGURE 39

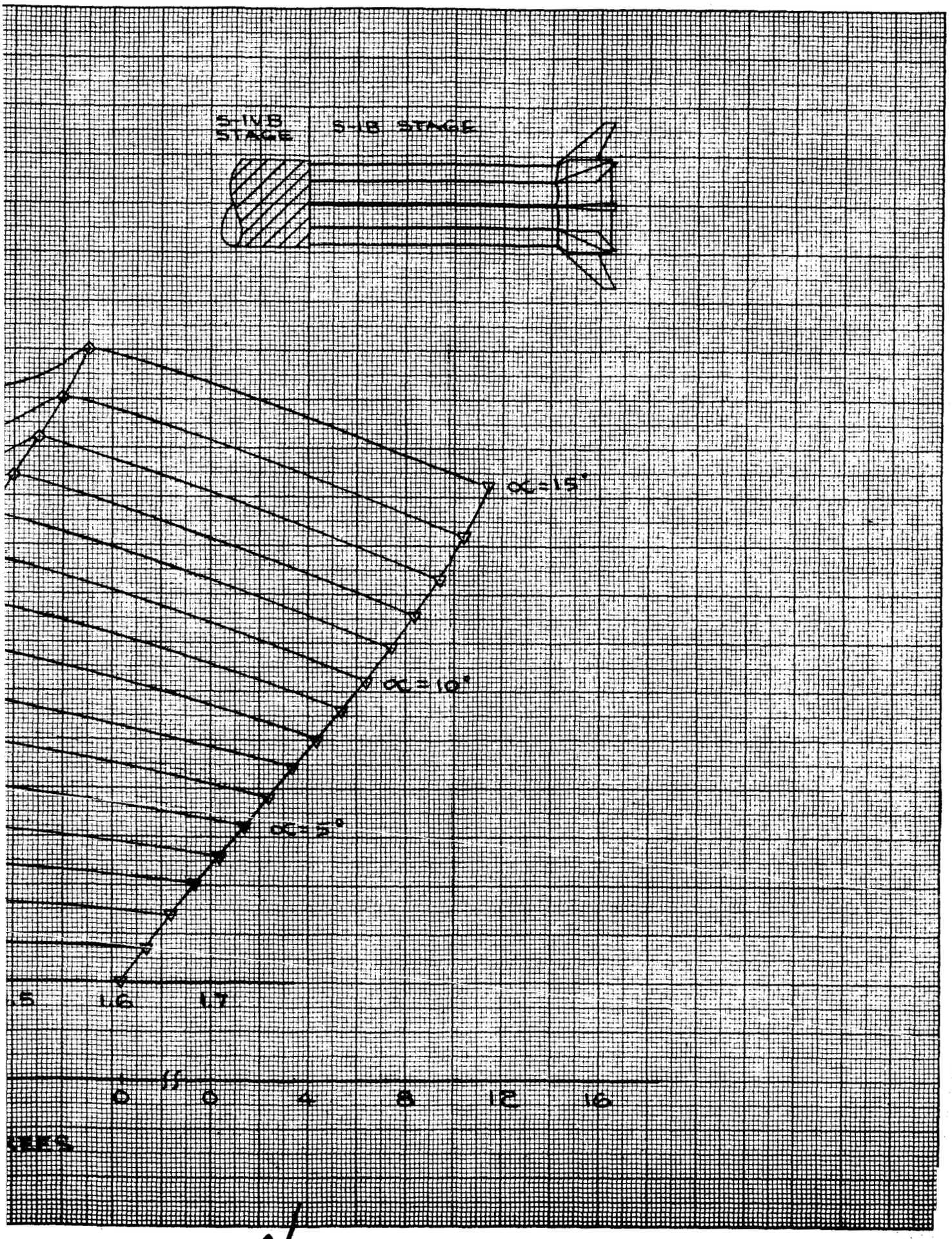
S-IVB STAGE
S-IB STAGE
α = 15°
α = 10°
α = 5°
1.5
1.6
1.7
0
4
8
12
16

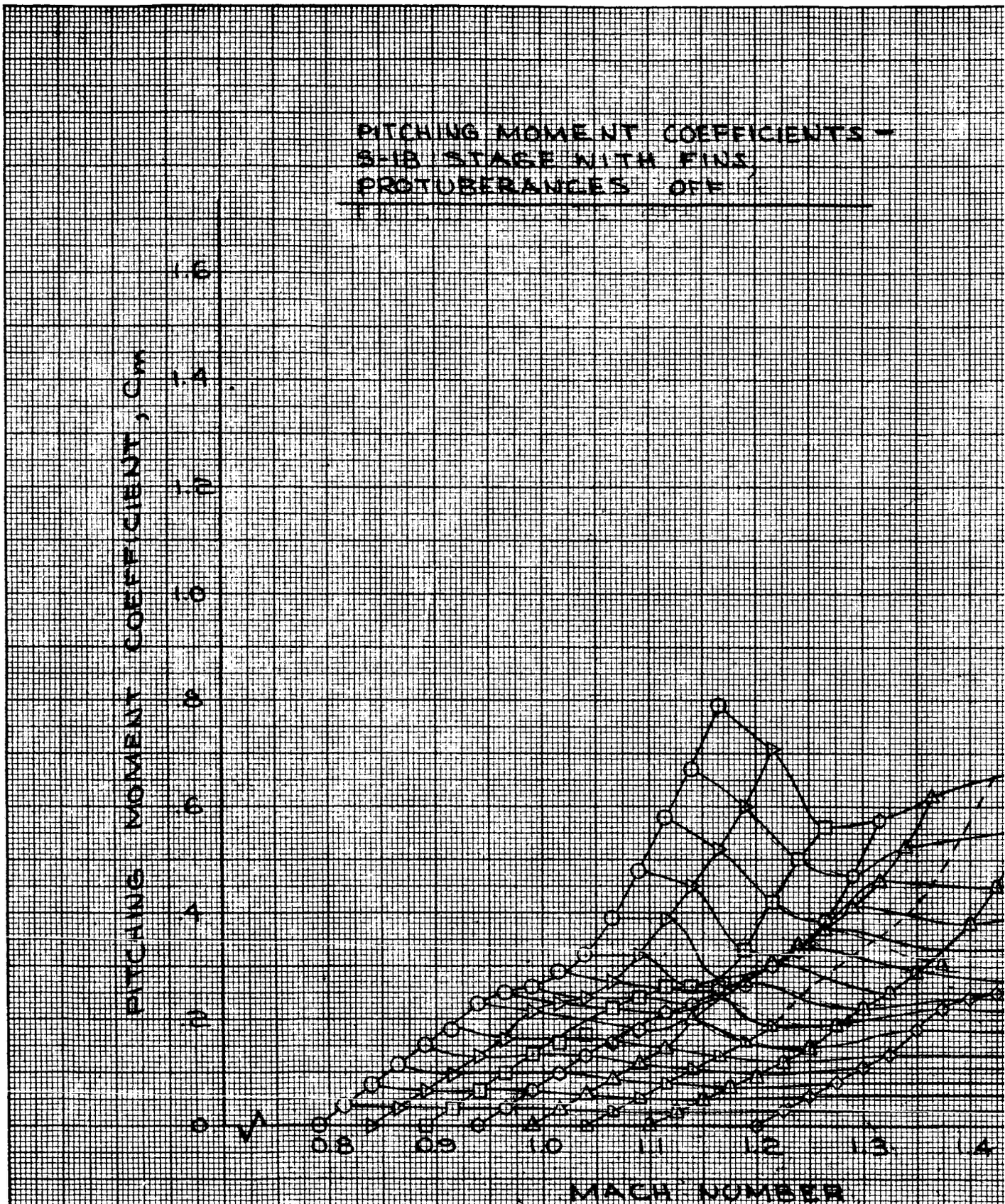
PITCHING MOMENT COEFFICIENTS -
S-IB STAGE WITH FINS,
PROTUBERANCES OFF
PITCHING MOMENT COEFFICIENT, C_m
1.6
1.4
1.2
1.0
.8
.6
.4
.2
0
.8
.9
1.0
1.1
1.2
1.3
1.4
MACH NUMBER
0 0 0 0 0 0 0 0
ANGLE OF ATTACK - DEGR

FIGURE 40

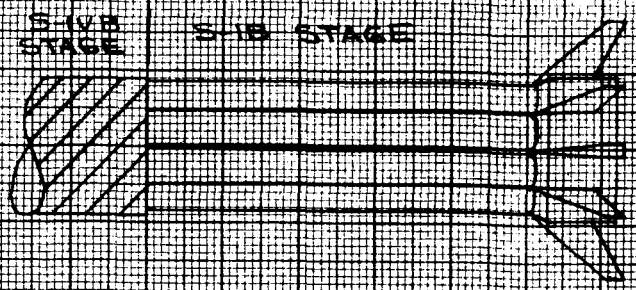
S-IVB STAGE
S-IB STAGE

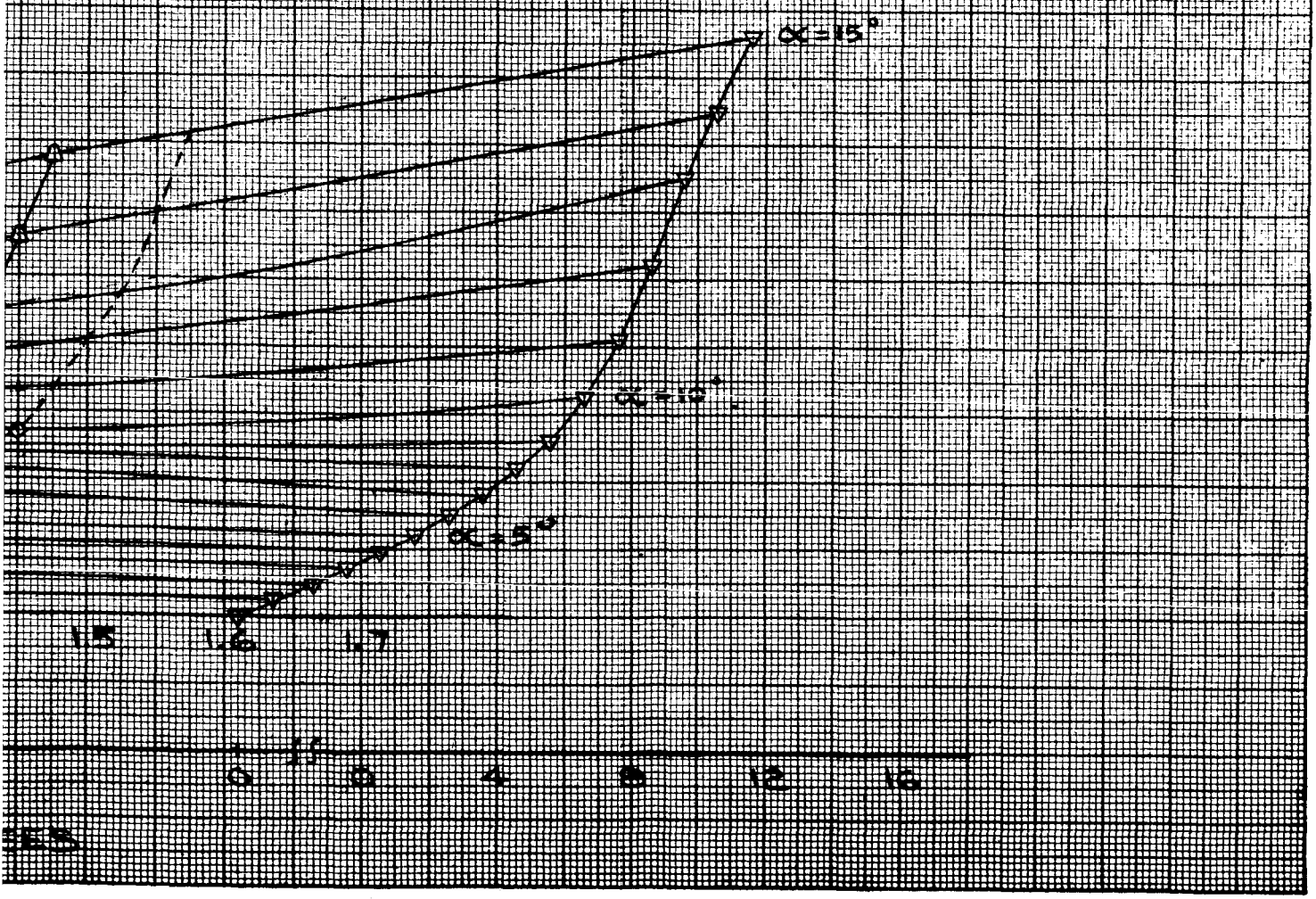
α = 15°
α = 10°
α = 5°
1.5
1.6
1.7
6
8
12
16

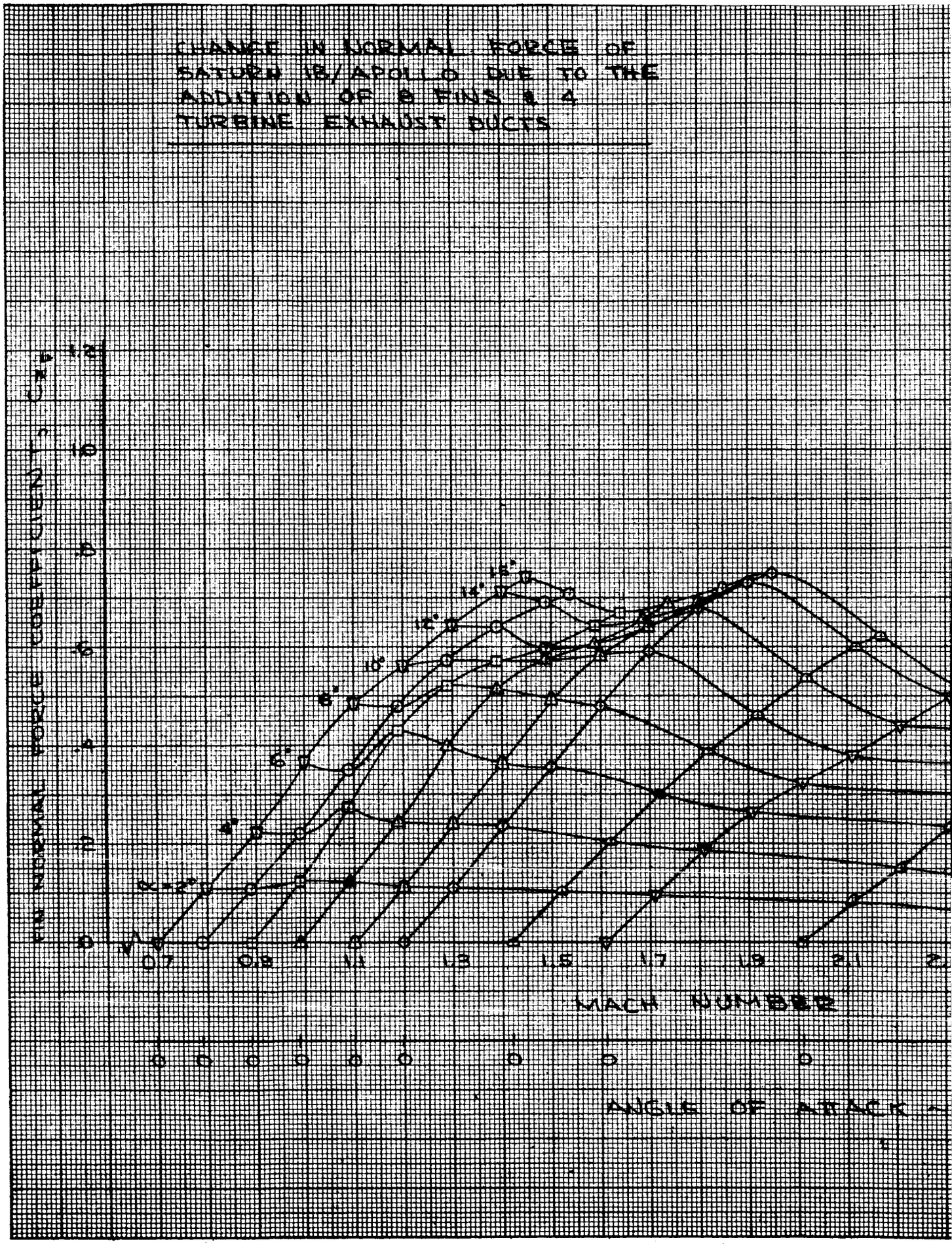
CHANGE IN NORMAL FORCE OF SATURN IB/APOLLO DUE TO THE ADDITION OF 8 FINS & 4 TURBINE EXHAUST DUCTS
INCREMENT IN NORMAL FORCE COEFFICIENT, C_{N_α}
MACH NUMBER
ANGLE OF ATTACK, α
α = 2°
4°
6°
8°
10°
12°
14°
16°
0.7
0.9
1.1
1.3
1.5
1.7
1.9
2.1

FIGURE 41

$$C_{Z_\delta} = (C_Z)_{\substack{\text{FINS TED} \\ \text{ON}}} - (C_Z)_{\substack{\text{FINS TED} \\ \text{OFF}}}$$

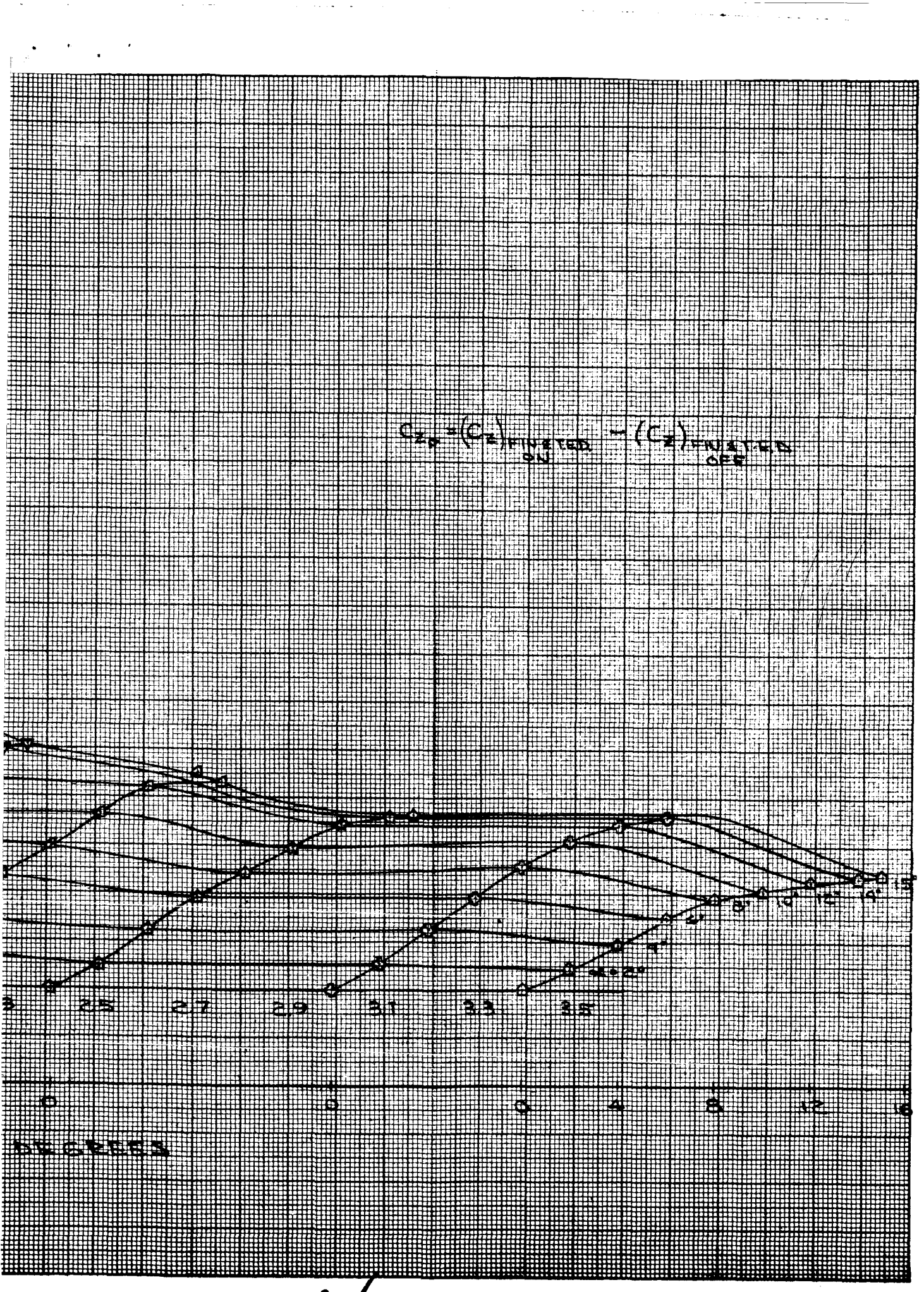

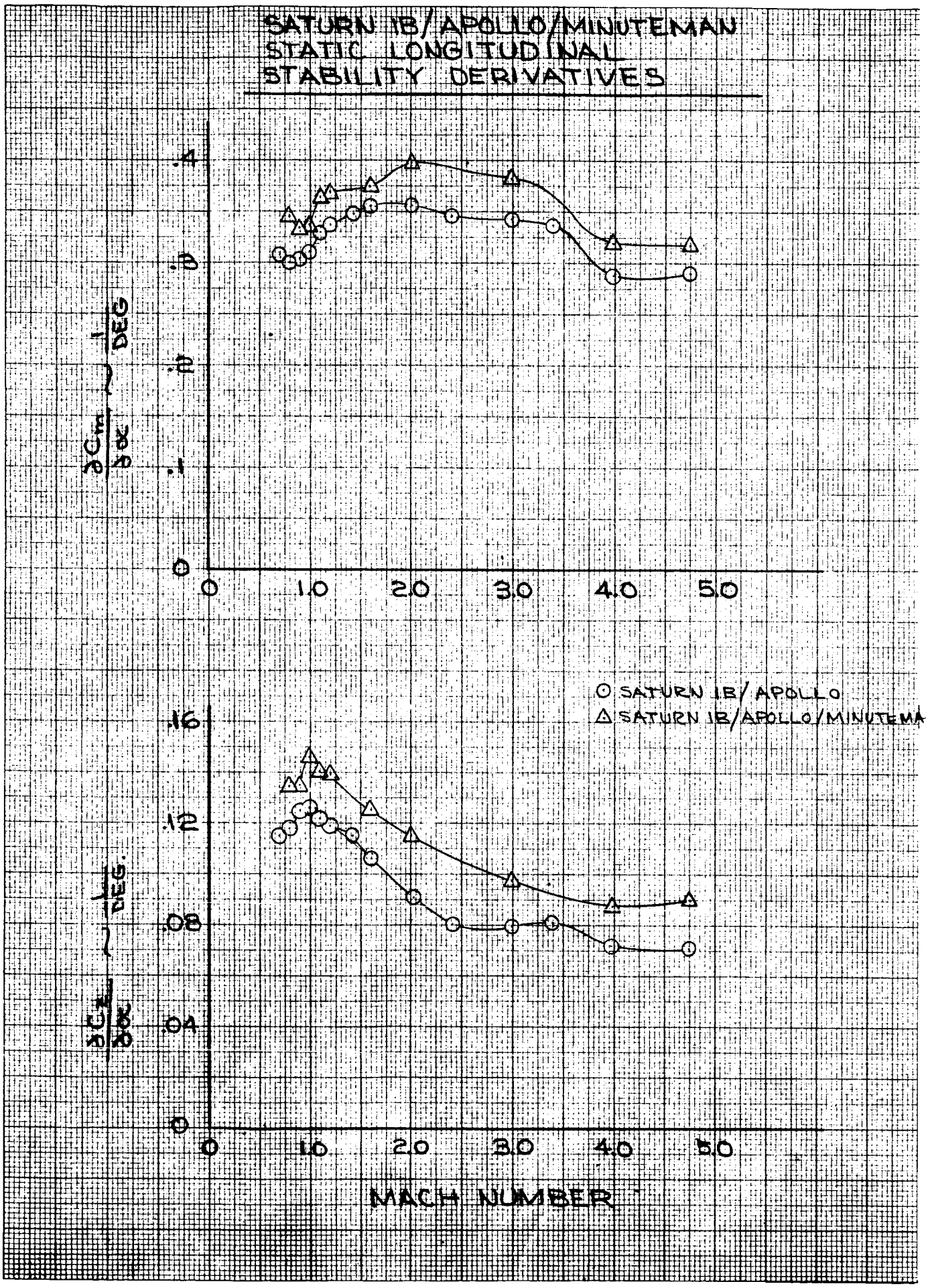
SATURN IB/APOLLO/MINUTEMAN
STATIC LONGITUDINAL
STABILITY DERIVATIVES
$\frac{\partial C_m}{\partial \alpha} \sim \frac{1}{DEG}$
.4
.3
.2
.1
0
0
1.0
2.0
3.0
4.0
5.0
⊙ SATURN IB/APOLLO
△ SATURN IB/APOLLO/MINUTEMAN
$\frac{\partial C_L}{\partial \alpha} \sim \frac{1}{DEG}$
.16
.12
.08
.04
0
0
1.0
2.0
3.0
4.0
5.0
MACH NUMBER

FIGURE 42

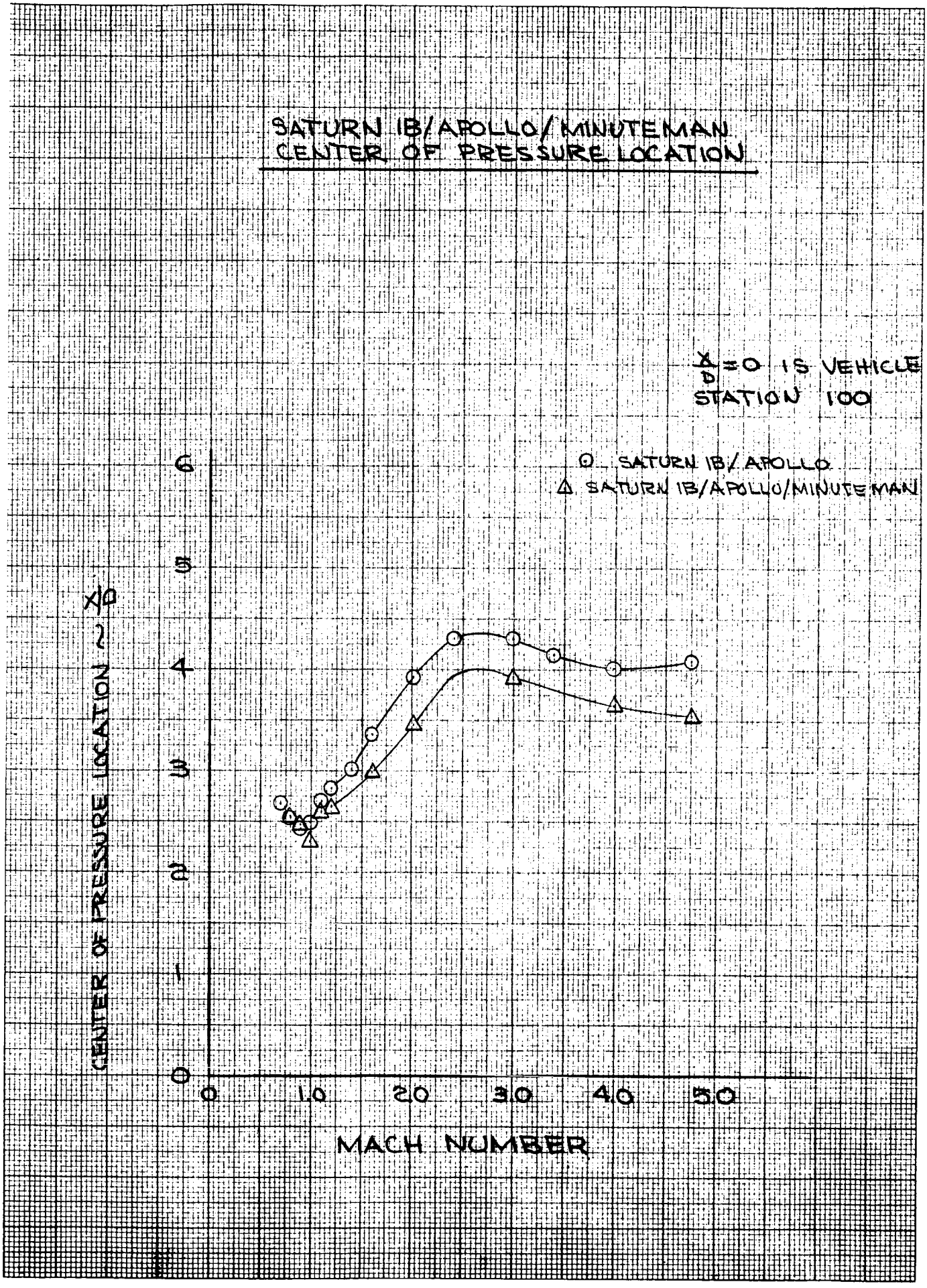
SATURN IB/APOLLO/MINUTEMAN
CENTER OF PRESSURE LOCATION
$\frac{X}{D}$=0 IS VEHICLE STATION 100
SATURN IB/APOLLO
SATURN IB/APOLLO/MINUTEMAN
CENTER OF PRESSURE LOCATION $\frac{X}{D}$
0
1
2
3
4
5
6
1.0
2.0
3.0
4.0
5.0
MACH NUMBER

FIGURE 43

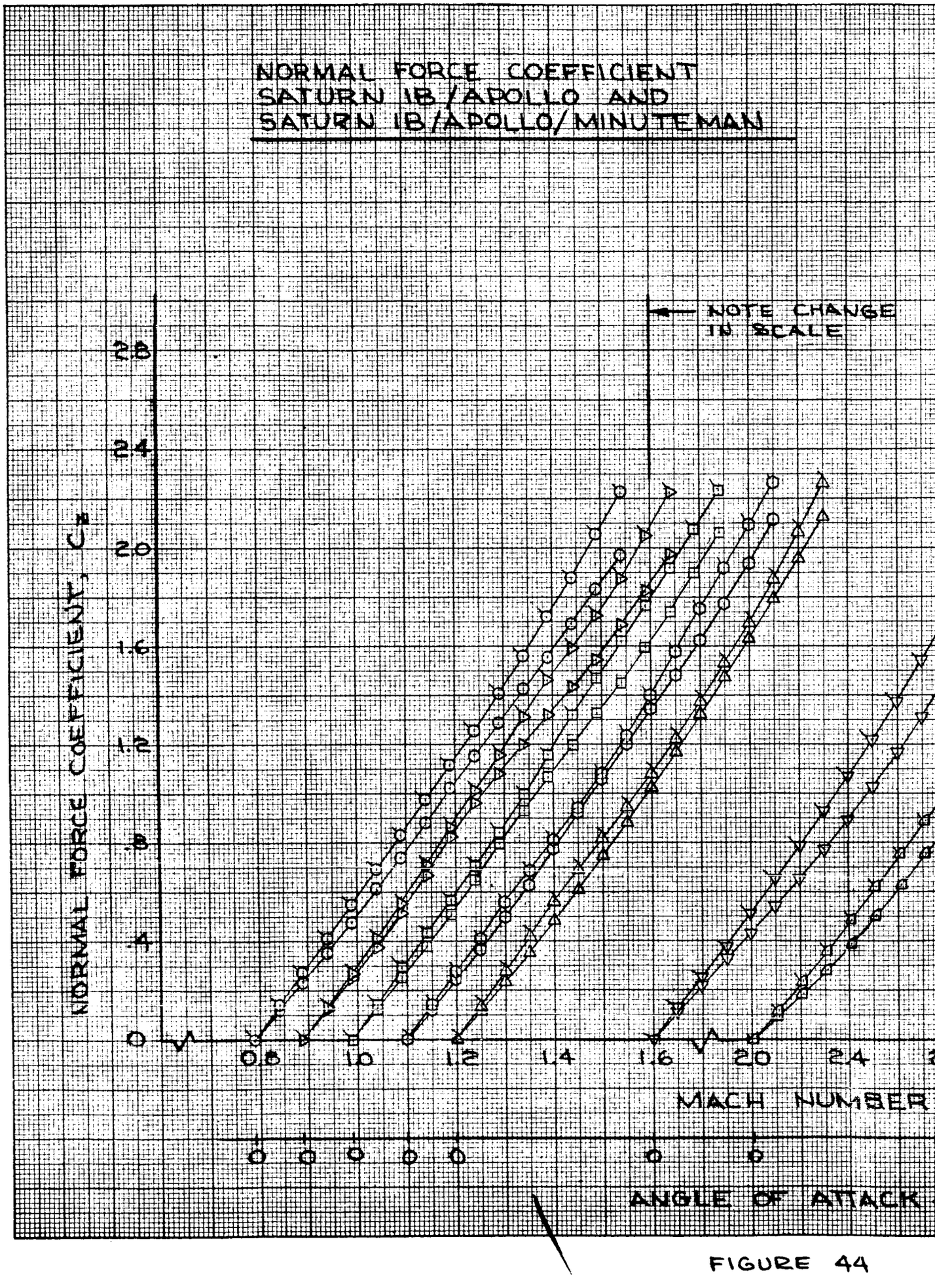
NORMAL FORCE COEFFICIENT
SATURN IB/APOLLO AND
SATURN IB/APOLLO/MINUTEMAN
NOTE CHANGE IN SCALE
NORMAL FORCE COEFFICIENT, C_N
2.8
2.4
2.0
1.6
1.2
.8
.4
0
0.8
1.0
1.2
1.4
1.6
2.0
2.4
MACH NUMBER
0 0 0 0 0 0 0
ANGLE OF ATTACK

FIGURE 44

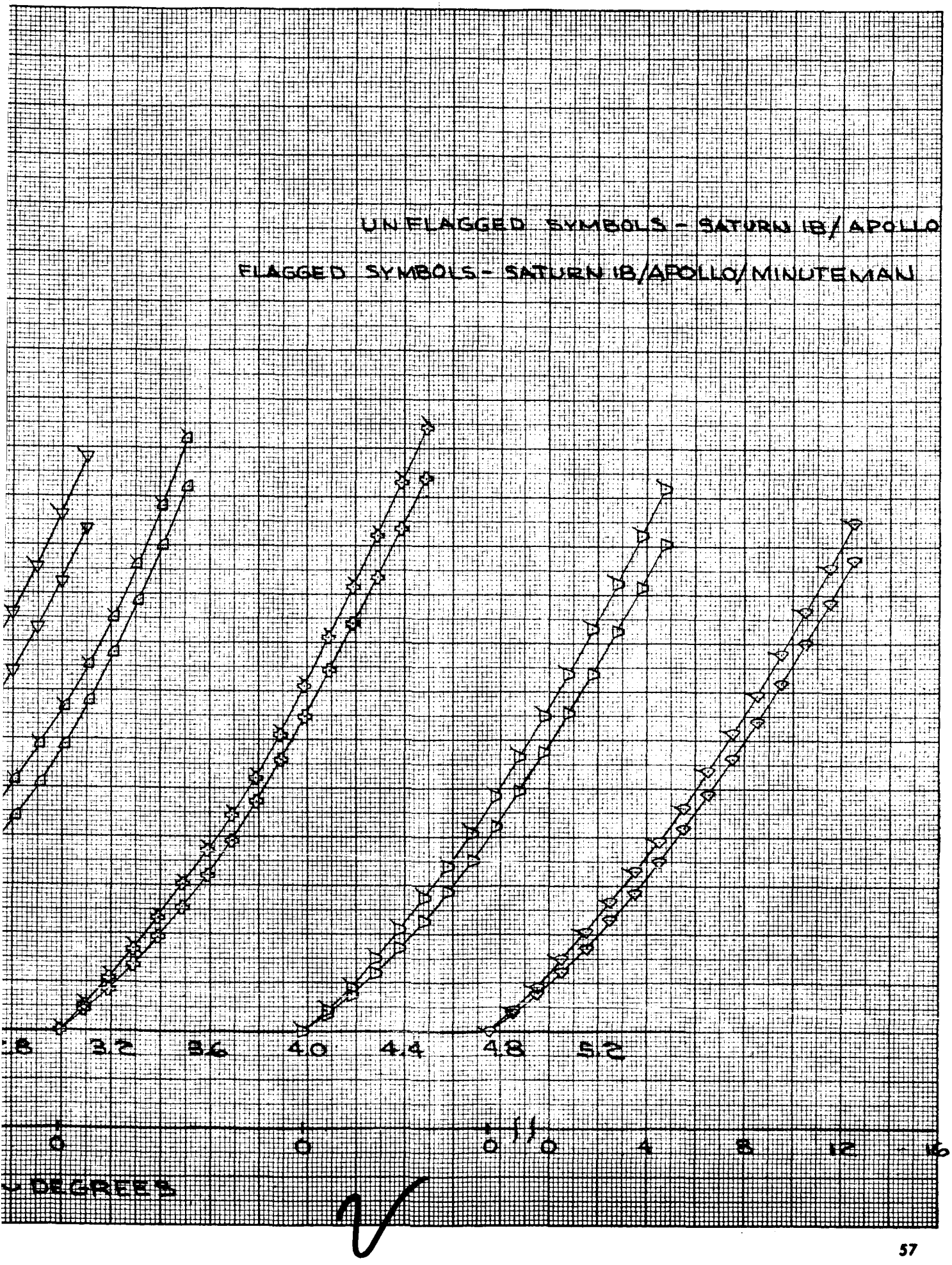
UNFLAGGED SYMBOLS - SATURN IB/APOLLO
FLAGGED SYMBOLS - SATURN IB/APOLLO/MINUTEMAN
3.2
3.6
4.0
4.4
4.8
5.2
0
0
0
4
8
12
16
DEGREES

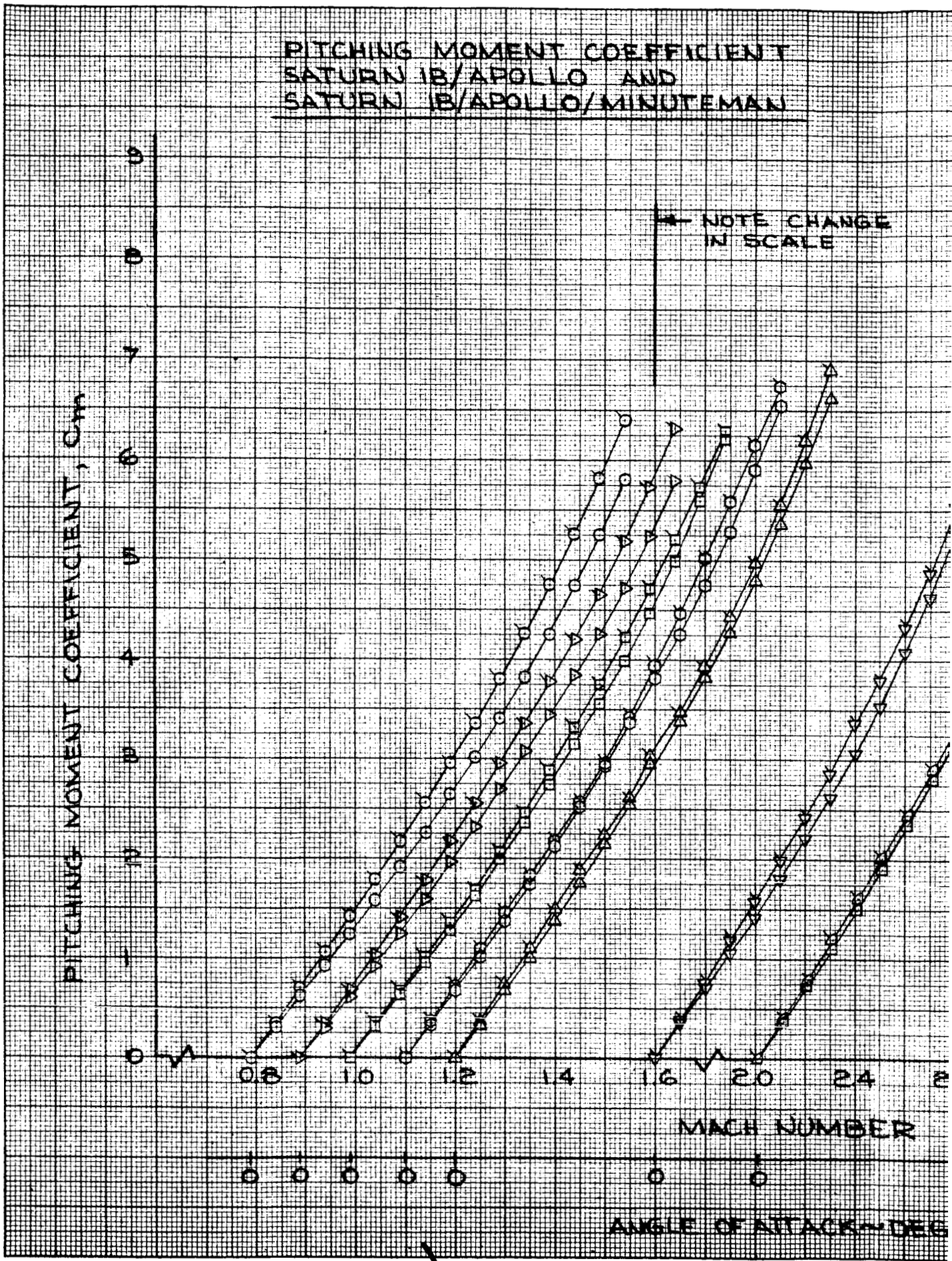
PITCHING MOMENT COEFFICIENT
SATURN IB/APOLLO AND
SATURN IB/APOLLO/MINUTEMAN
NOTE CHANGE IN SCALE
PITCHING MOMENT COEFFICIENT, Cm
9
8
7
6
5
4
3
2
1
0
0.8
1.0
1.2
1.4
1.6
2.0
2.4
MACH NUMBER
ANGLE OF ATTACK - DEG

FIGURE 45

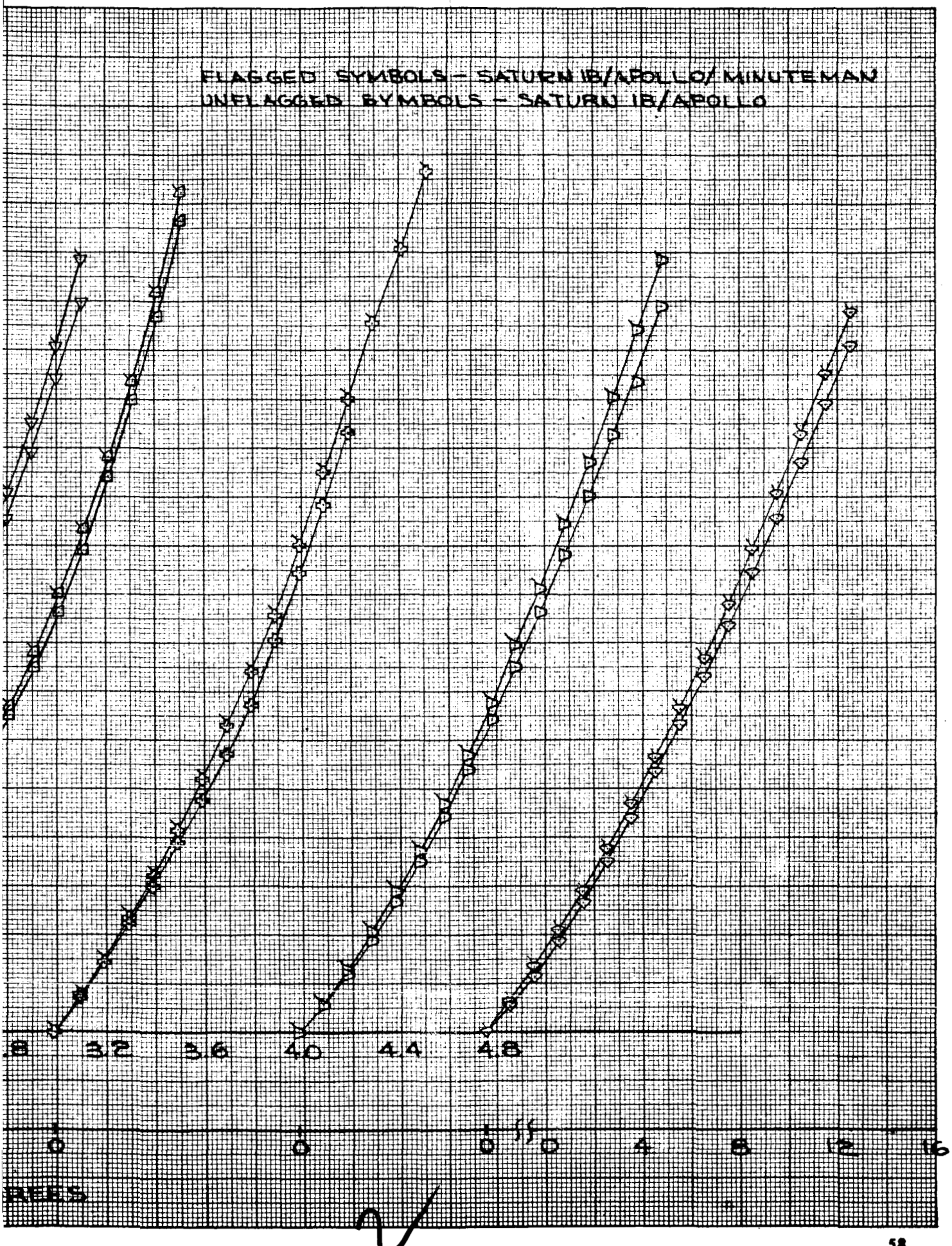
FLAGGED SYMBOLS – SATURN IB/APOLLO/ MINUTEMAN
UNFLAGGED SYMBOLS – SATURN IB/APOLLO
3.2
3.6
4.0
4.4
4.8
0
0
0
4
8
12
16
REES

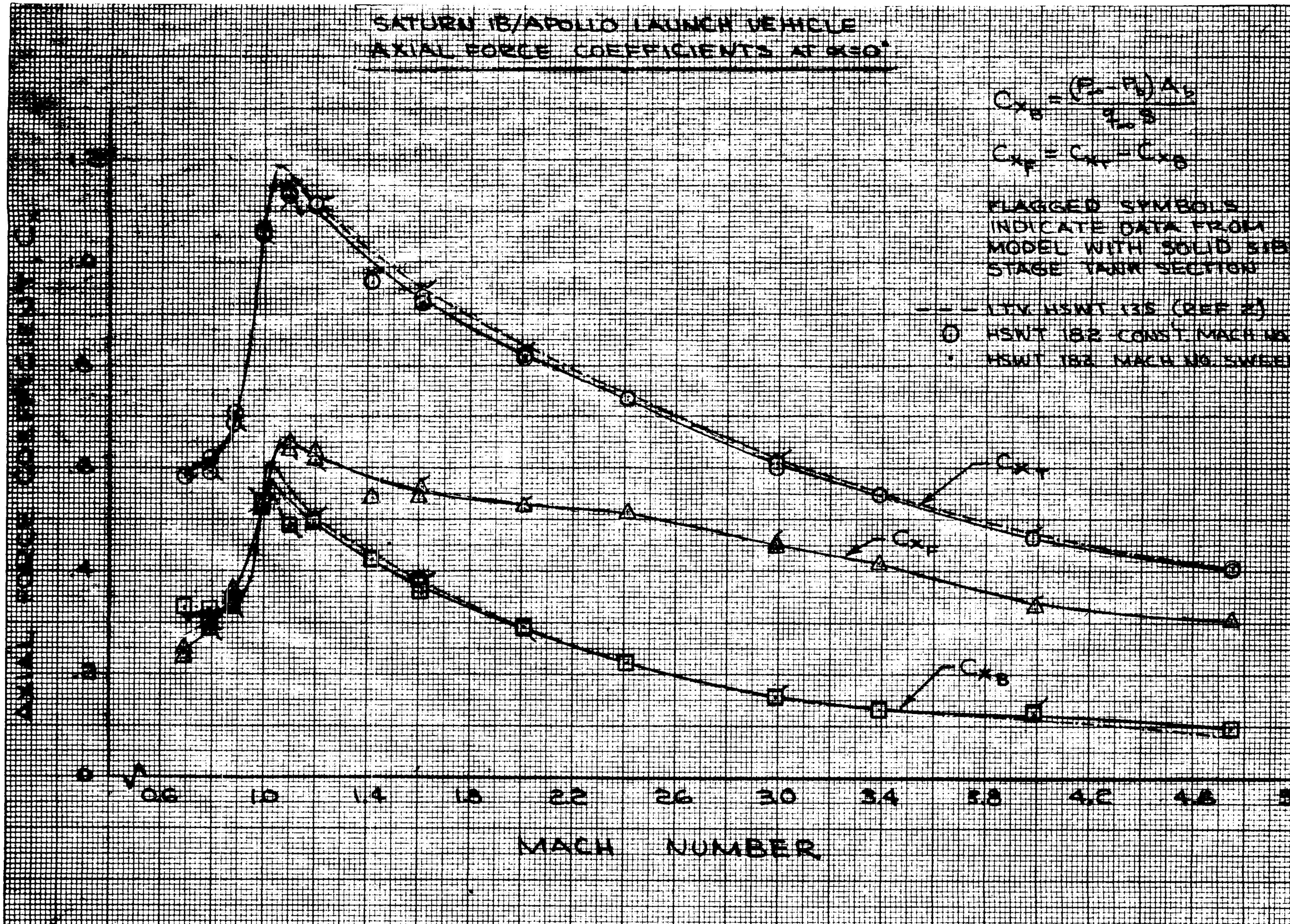
SATURN IB/APOLLO LAUNCH VEHICLE
AXIAL FORCE COEFFICIENTS AT α=0°
$C_{X_B} = \frac{(P_\infty - P_b) A_b}{q_\infty S}$
$C_{X_F} = C_{X_T} - C_{X_B}$
FLAGGED SYMBOLS INDICATE DATA FROM MODEL WITH SOLID S-IB STAGE TANK SECTION
LTV HSWT 135 (REF 2)
HSWT 182 CONST MACH NO
HSWT 182 MACH NO SWEEP
C_{X_T}
C_{X_F}
C_{X_B}
AXIAL FORCE COEFFICIENT, C_X
MACH NUMBER

FIGURE 46

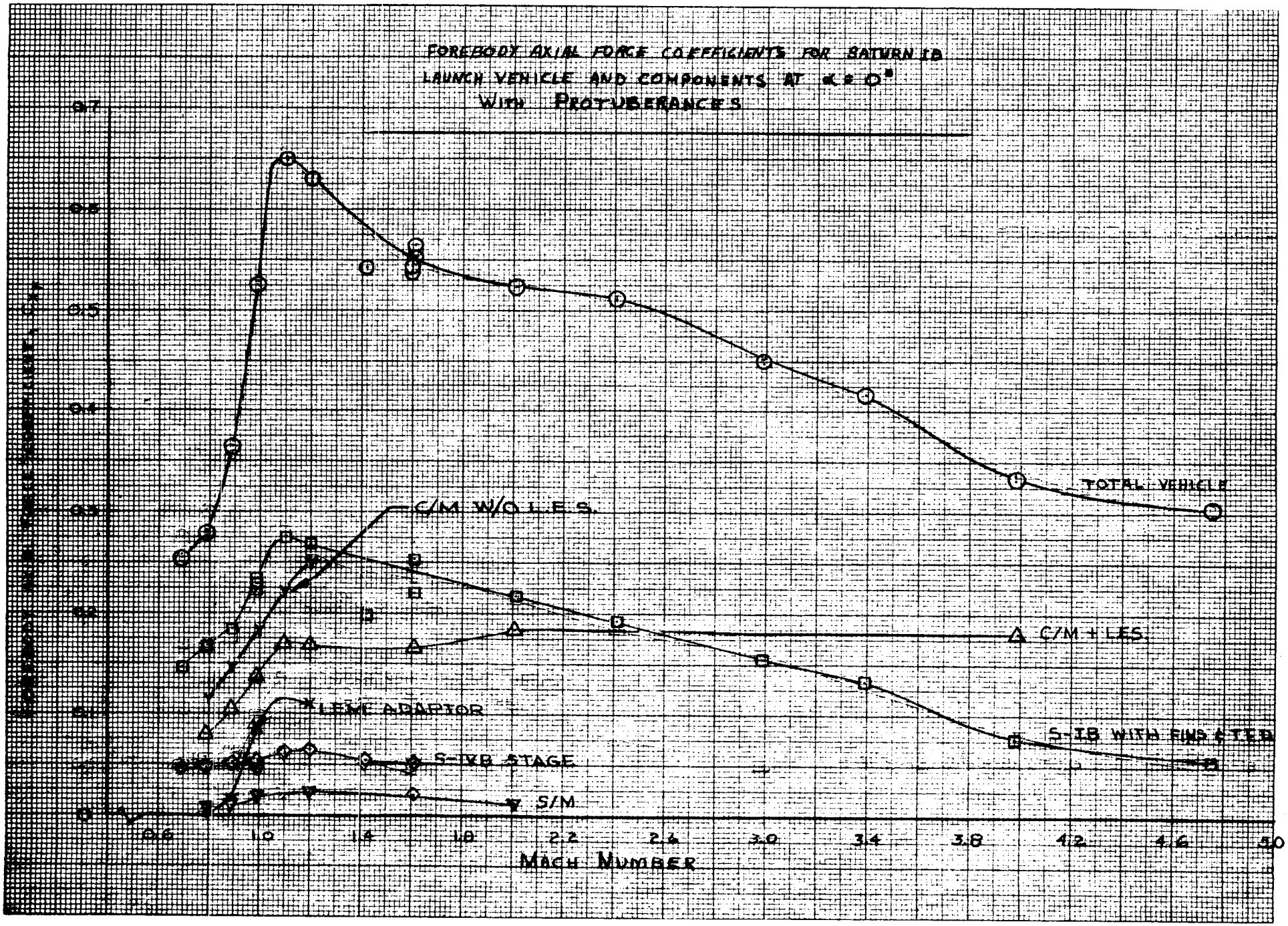
FOREBODY AXIAL FORCE COEFFICIENTS FOR SATURN IB
LAUNCH VEHICLE AND COMPONENTS AT α = 0°
WITH PROTUBERANCES
0.7
0.6
0.5
0.4
0.3
0.2
0.1
0
0.6
1.0
1.4
1.8
2.2
2.6
3.0
3.4
3.8
4.2
4.6
5.0
MACH NUMBER
TOTAL VEHICLE
C/M W/O L.E.S.
C/M + L.E.S.
L.E.M. ADAPTOR
S-IVB STAGE
S/M
S-IB WITH FINS & TEB

69

FOREBODY AXIAL FORCE COEFFICIENTS FOR SATURN IB
LAUNCH VEHICLE AND COMPONENTS AT α = 0°
WITHOUT PROTUBERANCES
TOTAL VEHICLE
RW/RT = 8.51 - 7.0 x 10⁻⁶
RW/RT = 8.5 - 9.1 x 10⁻⁶
S-IB WITH FINS
LUNAR EXCURSION MODULE ADAPTOR
S-IVB
S/M
FOREBODY AXIAL FORCE COEFFICIENT, C_{A_F}
MACH NUMBER
0
0.2
0.8
1.0
1.2
1.4
1.6
1.8
2.0
.47
.48
.49
.50
.51

FIGURE 48

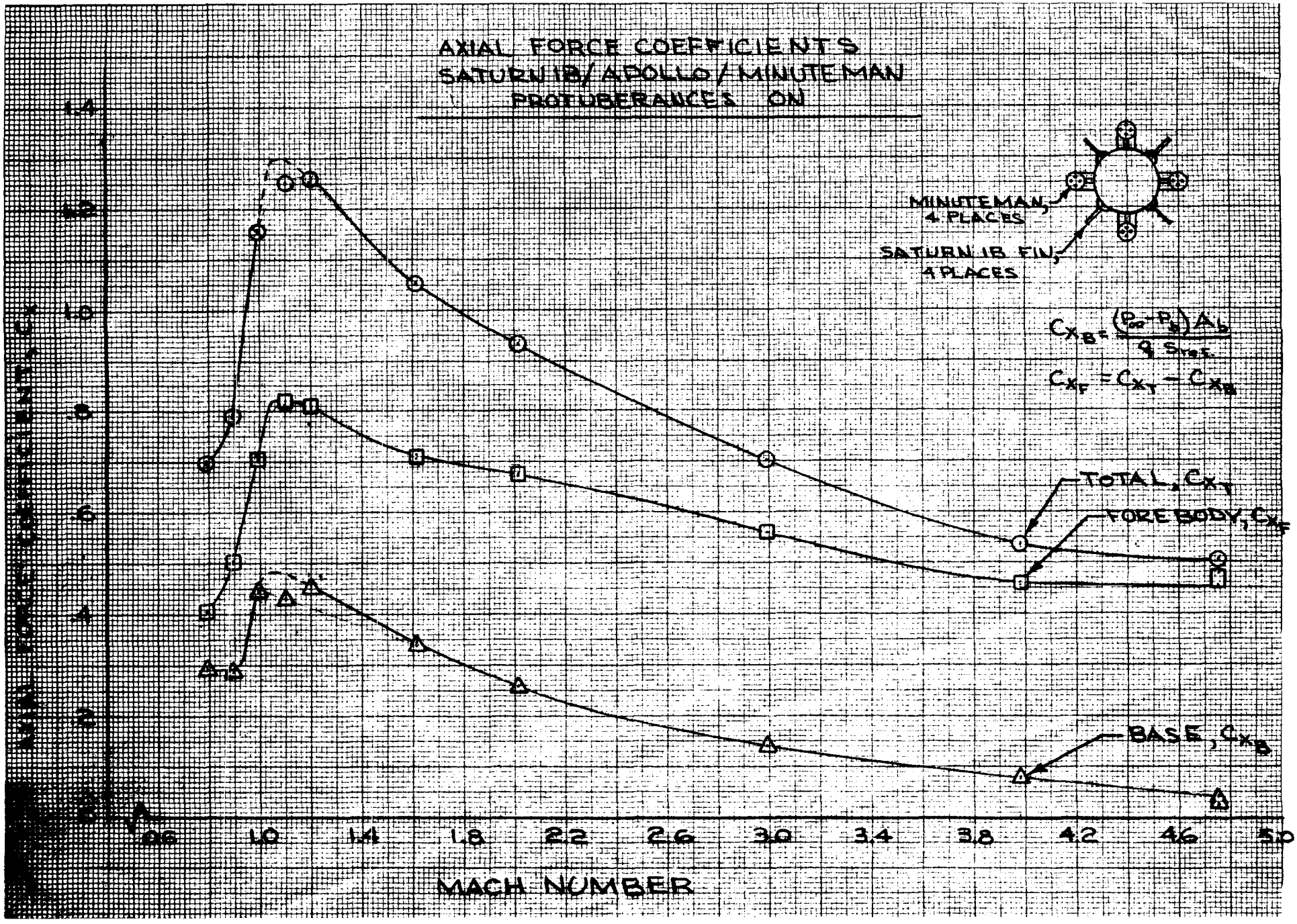
AXIAL FORCE COEFFICIENTS
SATURN IB/APOLLO/MINUTEMAN
PROTUBERANCES ON
MINUTEMAN, 4 PLACES
SATURN IB FIN, 4 PLACES
$C_{X_B} = \frac{(p_\infty - p_b) A_b}{q S_{ref.}}$
$C_{X_F} = C_{X_T} - C_{X_B}$
TOTAL, C_{X_T}
FOREBODY, C_{X_F}
BASE, C_{X_B}
AXIAL FORCE COEFFICIENT, C_X
MACH NUMBER
.6
1.0
1.4
1.8
2.2
2.6
3.0
3.4
3.8
4.2
4.6
5.0
.4
.8
1.2
1.6
2.0
2.4
2.8

DISTRIBUTION LIST

Chrysler Corporation Space Division

T. E. Ballinger	1
G. T. Boyd	1
F. Chianese	10
N. D. Kemp	1
J. B. Misner	1
E. A. Rawls	1
G. F. Romberg	1
Technical Files	5
Technical Information Center	1

DISTRIBUTION LIST

George C. Marshall Space Flight Center

L. L. McNair	R-AERO-P	1
W. K. Dahm	R-AERO-A	1
T. G. Reed	R-AERO-AU	1
H. B. Wilson	R-AERO-AT	1
E. B. May	R-AERO-AD	1
C. D. Andrews	R-AERO-ADE	1
B. G. Dunn	R-AERO-ADD	4
R. C. Callaway	I-I/IB-E	1

GOVERNMENT FIELD PRINTING PLANT
(Under Contract NAS 8-14017)
NASA – MICHOUD OPERATIONS – 1965
NEW ORLEANS 26, LOUISIANA